

**VARIABILITY OF ORGANIC CARBON ACCUMULATION
ON A TIDAL WETLAND COAST**

by

Kaitlin Joy Tucker

A thesis submitted to the Faculty of the University of Delaware in partial fulfillment of the requirements for the degree of Master of Science in Marine Studies

Winter 2016

© 2016 Kaitlin J. Tucker
All Rights Reserved

ProQuest Number: 10055516

All rights reserved

INFORMATION TO ALL USERS

The quality of this reproduction is dependent upon the quality of the copy submitted.

In the unlikely event that the author did not send a complete manuscript and there are missing pages, these will be noted. Also, if material had to be removed, a note will indicate the deletion.



ProQuest 10055516

Published by ProQuest LLC (2016). Copyright of the Dissertation is held by the Author.

All rights reserved.

This work is protected against unauthorized copying under Title 17, United States Code
Microform Edition © ProQuest LLC.

ProQuest LLC.
789 East Eisenhower Parkway
P.O. Box 1346
Ann Arbor, MI 48106 - 1346

**VARIABILITY OF ORGANIC CARBON ACCUMULATION
ON A TIDAL WETLAND COAST**

by

Kaitlin Joy Tucker

Approved: _____
Christopher K. Sommerfield, Ph.D.
Professor in charge of thesis on behalf of the Advisory Committee

Approved: _____
Mark A. Moline, Ph.D.
Director of the School of Marine Science and Policy

Approved: _____
Mohsen Badiy, Ph.D.
Acting Dean of the College of Earth, Ocean, and Environment

Approved: _____
Ann L. Ardis, Ph.D.
Interim Vice Provost for Graduate and Professional Education

ACKNOWLEDGMENTS

I would like to thank my family, mainly my parents Roy and Karen and my fiancé Raymond, for their encouragement and support of my goals. They have continued to give me the confidence I need and taught me to believe in myself.

I would also like to thank my committee members Dr. Bill Ullman, Dr. David Velinsky, and Dr. Wei-Jun Cai for their helpful guidance and inputs to my research. My advisor, Dr. Chris Sommerfield, has always encouraged me and made me a better scientist. I am greatly appreciative to have worked in his lab. The University of Delaware and the Delaware Sea Grant funded this research and I am grateful for their financial support.

I would also like to acknowledge my lab mates Brandon Boyd, Conor Mcdowell, Katie Pijanowski, and Zac Duval for their help in the lab and field. Kyra Kim also provided assistance in sample collection and Erin Landis helped in sample processing. It was truly a pleasure to work with all of them. I thank all of my friends at the University of Delaware for their support and friendship over the last three years.

TABLE OF CONTENTS

| | |
|-----------------------|------|
| LIST OF TABLES | vi |
| LIST OF FIGURES | viii |
| ABSTRACT | xiii |

Chapter

| | | |
|-------|--|----|
| 1 | INTRODUCTION | 1 |
| 1.1 | Organic Carbon Production and Storage in Tidal Marshes..... | 1 |
| 1.2 | Marsh Soil Formation and Carbon Accumulation | 3 |
| 1.3 | Sedimentary Influences on Carbon Accumulation..... | 7 |
| 1.4 | Research Goals and Hypotheses..... | 9 |
| 1.5 | Geographic Setting of the Delaware Estuary | 11 |
| 2 | METHODS..... | 13 |
| 2.1 | Core Collection..... | 13 |
| 2.1.1 | Short Cores | 13 |
| 2.1.2 | Long Cores | 14 |
| 2.2 | Physical Properties Measurements | 14 |
| 2.3 | Organic Carbon and Total Nitrogen Analysis..... | 16 |
| 2.4 | Radionuclide Geochronology..... | 17 |
| 2.5 | Size Fractionation of Soil Material | 20 |
| 2.6 | Organic Carbon Accumulation Rates..... | 22 |
| 2.7 | Statistical Analysis | 24 |
| 3 | RESULTS..... | 25 |
| 3.1 | Marsh Soil Physical Properties..... | 25 |
| 3.2 | Total Organic Carbon and C/N Ratios | 26 |
| 3.3 | Stable Carbon Isotope Values | 28 |
| 3.4 | ¹⁴ C age dates and $\Delta^{14}\text{C}$ Values | 28 |
| 3.5 | Marsh Accretion Rates | 30 |
| 3.6 | Soil Bulk Carbon Accumulation Rates | 30 |
| 3.7 | Carbon Accumulation Rates For Soil Size Fractions..... | 31 |

| | | |
|----------|---|-----|
| 4 | DISCUSSION..... | 35 |
| 4.1 | Spatial Variability of Organic Carbon Accumulation in Tidal Marshes. | 35 |
| 4.2 | Time-Dependent Carbon Accumulation in Marshes..... | 38 |
| 4.3 | Geologic Influences on Carbon Accumulation Rates | 40 |
| 4.4 | Size-Specific Soil Carbon Accumulation..... | 42 |
| 4.5 | Sources and Pathways of Marsh Soil Carbon | 44 |
| 5 | REGIONAL AND GLOBAL VARIABILITY IN TIDAL MARSH CARBON ACCUMULATION | 47 |
| 5.1 | Soil Carbon Accumulation Rates | 47 |
| 5.2 | Marsh Carbon Storage..... | 49 |
| 6 | CONCLUSIONS | 51 |
| | TABLES | 53 |
| | FIGURES | 60 |
| | REFERENCES | 87 |
| Appendix | | |
| A | CARBON ACCUMULATION RATES AND RADIOCARBON DATA | 95 |
| B | NITROGEN DATA..... | 103 |

LIST OF TABLES

| | | |
|-----------|---|----|
| Table 1: | Information for the 24 short cores and five long cores used for this study. Asterisks indicate cores collected specifically for this study. The other cores were collected for prior research by C. Sommerfield and D. Velinsky. | 53 |
| Table 2: | Radiocarbon data for the dated root material from soil cores. $\Delta^{14}\text{C}$ and $\delta^{13}\text{C}$ values are also shown. | 55 |
| Table 3: | Short-term rates of marsh accretion, organic accumulation, mineral accumulation, and carbon accumulation discussed in the text. | 56 |
| Table 4: | Long-term rates of marsh accretion, organic accumulation, mineral accumulation, and carbon accumulation discussed in the text. Calibrated radiocarbon ages used to compute these rates are also shown. | 57 |
| Table 5: | Comparison of marsh accretion rates, mineral accumulation rates (MAR), and organic accumulation rates (OAR) average over different timescale using radionuclide chronometers. | 58 |
| Table 6: | Global comparisons of carbon accumulation rate (CAR), marsh area, and storage in tidal marshes. Table modified from Ouyang and Lee (2014) to include results from this study. Asterisk indicates data from Tiner et al. (2011). | 59 |
| Table A1: | Physical property data, C/N ratios, and total organic carbon concentrations for bulk material of long cores. | 96 |
| Table A2: | C/N ratios and total organic carbon concentrations for size fractions of the Great Marsh long core. | 97 |
| Table A3: | C/N ratios and total organic carbon concentrations for size fractions of the Mispillion River long core. | 98 |
| Table A4: | C/N ratios and total organic carbon concentrations for size fractions of the Kelly Island long core. | 99 |

| | | |
|-----------|---|-----|
| Table A5: | C/N ratios and total organic carbon concentrations for size fractions of the Blackbird Creek long core..... | 100 |
| Table A6: | C/N ratios and total organic carbon concentrations for size fractions of the St. Georges long core. | 101 |
| Table A7: | Total carbon concentration and carbon concentrations of soil size fractions for long cores..... | 102 |
| Table B1: | Nitrogen accumulation rates for short cores..... | 104 |
| Table B2: | Total nitrogen concentrations for bulk material of long cores. | 105 |
| Table B3: | Long-term nitrogen accumulation rates. Rates were calculated based on ages shown. | 106 |
| Table B4: | Total nitrogen concentrations for size fractions of the Great Marsh long core. | 107 |
| Table B5: | Total nitrogen concentrations for size fractions of the Mispillion River long core. | 108 |
| Table B6: | Total nitrogen concentrations for size fractions of the Kelly Island long core. | 109 |
| Table B7: | Total nitrogen concentrations for size fractions of the Blackbird Creek long core. | 110 |
| Table B8: | Total nitrogen concentrations for size fractions of the St. Georges long core. | 111 |
| Table B9: | Total nitrogen concentrations and nitrogen concentrations of soil size fractions for long cores..... | 112 |

LIST OF FIGURES

| | | |
|------------|--|----|
| Figure 1: | Carbon budget for Sweet Hall Marsh, USA from Megonigal and Neubauer (2009). Rates are reported in $\text{g m}^{-2} \text{ yr}^{-1}$. Pathways represent conceptual model of carbon cycling in tidal marsh sediments..... | 60 |
| Figure 2: | Map of the Delaware Estuary showing the marsh locations referred to in the text. Wetland areas shown in grey are delineations by the U.S. Fish and Wildlife Service..... | 61 |
| Figure 3: | Short- and long-coring sites at the marsh locations shown in Figure 2. . | 62 |
| Figure 4: | Soil fractionation scheme used for this study. The bold boxes denote the size fraction subjected to organic carbon analysis. See text for details..... | 63 |
| Figure 5: | Depth profiles of dry bulk density for the short cores examined in this study. | 64 |
| Figure 6: | Depth profiles of loss on ignition for the short cores examined in this study. | 65 |
| Figure 7: | a) Total organic carbon (TOC) concentrations and b) C/N ratios for the short cores examined in this study. Solid and dashed lines are the median and mean of all samples, respectively. Black circles indicate outliers. The total number (n) of subsamples analyzed per core is noted. | 66 |
| Figure 8: | Depth profiles of total organic carbon (TOC) concentration for the short cores examined in this study. | 67 |
| Figure 9: | Depth variations in C/N ratio for the short cores examined in this study. | 68 |
| Figure 10: | Regression analysis of total organic carbon (TOC) concentration versus loss on ignition (LOI) for the short cores examined in this study. | 69 |

| | | |
|------------|--|----|
| Figure 11: | a) Total organic carbon (TOC) concentration and b) C/N ratio data for the long cores examined in this study. Solid and dashed lines are the median and mean of all samples, respectively. The total number of samples (n) analyzed for each core is shown. | 70 |
| Figure 12: | Depth profiles of $\Delta^{14}\text{C}$ for the long cores examined in this study. Depths corresponding to the years 1954 and 1963 are noted..... | 71 |
| Figure 13: | Organic carbon accumulation rates for the marsh sites based on ^{137}Cs or ^{210}Pb chronology. The mean and range of accumulation rates averaged for n coring sites are shown by the vertical bars and error bars, respectively. | 72 |
| Figure 14: | Depth profiles of organic carbon accumulation rate for the long cores examined in this study..... | 73 |
| Figure 15: | Box plots showing the weight percentages for the soil-size fractions examined for long cores (n=34 for all fractions). Solid and dashed lines within the boxes are the median and means of n samples, respectively, and the closed circles are individual outliers. | 74 |
| Figure 16: | Box plots showing a) total organic carbon (TOC) concentrations and b) C/N ratios for bulk and size-fractioned soils from long cores examined in this study. Solid and dashed lines within the boxes are the median and means of n samples, respectively, and the closed circles are individual outliers..... | 75 |
| Figure 17: | Down-core profiles for the Great Marsh vibracore showing a) variations in dry bulk density, organic matter density, and mineral matter density; and b) variations in total carbon concentration and the carbon concentration of individual size fractions..... | 76 |
| Figure 18: | Down-core profiles for the Mispillion River vibracore showing a) variations in dry bulk density, organic matter density, and mineral matter density; and b) variations in total carbon concentration and the carbon concentration of individual size fractions..... | 77 |
| Figure 19: | Down-core profiles for the Kelly Island vibracore showing a) variations in dry bulk density, organic matter density, and mineral matter density; and b) variations in total carbon concentration and the carbon concentration of individual size fractions..... | 78 |

| | | |
|------------|---|----|
| Figure 20: | Down-core profiles for the Blackbird Creek vibracore showing a) variations in dry bulk density, organic matter density, and mineral matter density; and b) variations in total carbon concentration and the carbon concentration of individual size fractions..... | 79 |
| Figure 21: | Down-core profiles for the St. Georges vibracore showing a) variations in dry bulk density, organic matter density, and mineral matter density; and b) variations in total carbon concentration and the carbon concentration of individual size fractions..... | 80 |
| Figure 22: | Stacked bar chart showing the relative contributions of the four soil size fractions to the long-term carbon accumulation rate determined for the five long cores. The age range over which these rates were averaged is noted in calibrated yr B.P. Note the significant contribution of the silt- and clay-sized carbon fractions of the total rate. | 81 |
| Figure 23: | Correlation between a) carbon accumulation rate and mineral accumulation rate, and b) carbon accumulation rate and organic accumulation rate for the short cores examined in this study. Rates and inventories are calculated relative to 1963. See text for further discussion. | 82 |
| Figure 24: | Comparison of short-term and long-term carbon accumulation rates. Black bars represent rates determined from ^{137}Cs or ^{210}Pb dating of the short cores; gray bars represent rates based on ^{14}C dating of the long cores. 83 | |
| Figure 25: | Scatter plots showing the dependence of a) carbon accumulation rate, b) mass accumulation rate (organic matter plus mineral sediment), and c) carbon concentration on soil age (cal yr B.P.). Red and black circles denote rates for short cores and long cores collected at the same locations..... | 84 |
| Figure 26: | Relationship between C/N ratio and total organic carbon (TOC) concentration for the four size fractions of soil samples from the long cores examined in this study. | 85 |
| Figure 27: | Depth variations in C/N ratio for bulk material and size fractions examined in long cores..... | 86 |

| | | |
|-------------|---|-----|
| Figure B1: | Total nitrogen concentrations for the short cores examined in this study. Solid and dashed lines are the median and mean of all samples, respectively. Black circles are outliers. The total number (n) of subsamples analyzed per core is noted..... | 113 |
| Figure B2: | Depth profiles of total nitrogen concentration for the short cores examined in this study..... | 114 |
| Figure B3: | Total nitrogen concentrations for the long cores examined in this study. Solid and dashed lines are the median and mean of all samples, respectively. The total number (n) of subsamples analyzed per core is noted | 115 |
| Figure B4: | Nitrogen accumulation rates for the marsh sites based on ¹³⁷ Cs and ²¹⁰ Pb chronology. The mean and range of accumulation rates average for n coring sites are shown by the vertical bars and error bars, respectively..... | 116 |
| Figure B5: | Depth profiles of nitrogen accumulation rates for the long cores examined in this study..... | 117 |
| Figure B6: | Box plot showing total nitrogen concentrations for bulk and size-fractionated soils from long cores examined in this study. Solid and dashed lines within the boxes are the median and means of n samples, respectively, and the closed circles are individual outliers. | 118 |
| Figure B7: | Down-core profiles for the Great Marsh vibracore showing variations in total nitrogen concentration and the nitrogen concentration of individual size fractions..... | 119 |
| Figure B8: | Down-core profiles for the Mispillion River vibracore showing variations in total nitrogen concentration and the nitrogen concentration of individual size fractions. | 120 |
| Figure B9: | Down-core profiles for the Kelly Island vibracore showing variations in total nitrogen concentration and the nitrogen concentration of individual size fractions..... | 121 |
| Figure B10: | Down-core profiles for the Blackbird Creek vibracore showing variations in total nitrogen concentration and the nitrogen concentration of individual size fractions. | 122 |

Figure B11: Down-core profiles for the St. Georges vibracore showing variations in total nitrogen concentration and the nitrogen concentration of individual size fractions..... 123

Figure B12: Stacked bar chart showing the relative contributions of the four soil size fractions to the long-term nitrogen accumulation rate determined for the five long cores. The timespan over which these rates were averaged is noted in calibrated yr B.P. 124

Figure B13: Comparison of short-term and long-term nitrogen accumulation rates. Black bars represent rates determined from ^{137}Cs or ^{210}Pb dating of the short cores; gray bars represent rates based on radiocarbon dating of the long cores..... 125

Figure B14: Scatter plots showing the dependence of a) nitrogen accumulation rate and b) nitrogen concentration on soil age (cal yr B.P.). Red and black circles denote rates for short cores and long cores collected at the same locations. 126

ABSTRACT

Organic carbon burial in tidal wetlands has been proposed to be an important means to mitigate the impacts of greenhouse gas emissions on climate change, given that coastal marshes and mangroves are a major sink for atmospheric carbon dioxide globally. Among the different types of wetland ecosystems, carbon accumulation in tidal marshes (tidal fresh, brackish, and salt marshes) is particularly high with a global average of $244.7 \text{ g C m}^{-2} \text{ yr}^{-1}$ (Ouyang and Lee, 2014). In these ecosystems high primary production rates coupled with slow rates of decomposition cause organic matter to accumulate in sediments and soils. It is crucial to understand the processes governing carbon burial to address how marsh ecosystems will respond to climate change. If marsh accretion and landward migration keeps pace with sea level rise, then marshes may continue to function as a carbon sink.

This study investigated the spatial variability of carbon accumulation on the tidal wetland coast of western Delaware Estuary. The following three specific objectives were addressed: (1) patterns and rates of marsh carbon accumulation along the estuarine salinity gradient; (2) the time-dependence of carbon accumulation averaged over timescales ranging from several decades to millennia; and (3) variations in carbon accumulation associated with different soil organic matter size fractions. While it is generally known that organic carbon accumulates in marsh soils through a combination of plant primary production and inputs of allochthonous particulate organic matter and mineral sediment, there are many unanswered questions concerning the mechanisms of soil formation and carbon burial. Understanding

variations in carbon accumulation rates both spatially and temporally in Delaware Estuary tidal wetlands will provide important geological context for assessments of carbon sequestration regionally.

Radionuclide chronometry (^{137}Cs , ^{210}Pb , ^{14}C) for 24 short cores and five long cores was used in this study along with measurements of organic carbon concentration from core subsamples to compute carbon accumulation rates. Total organic carbon and total nitrogen concentration was determined for a total of 613 soil samples. A soil fractionation procedure was developed to isolate the specific contributions of plant biomass, particulate organic and inorganic (mineral sediment) sedimentary materials. Using a combination of sieving and centrifugation, four soil carbon size fractions were isolated and analyzed for organic carbon and nitrogen content: $>125\mu\text{m}$, $63\text{--}125\mu\text{m}$, $4\text{--}63\mu\text{m}$ (silt size), and $<4\mu\text{m}$ (clay size).

Results indicated significant spatial variation in carbon accumulation rates along the tidal wetland coast. Short term rates (~ 50 -year average) determined using ^{137}Cs or ^{210}Pb chronology were generally higher ($246.4 \pm 101.8 \text{ g C m}^{-2} \text{ yr}^{-1}$) for the brackish marshes than the salt marshes sampled for this study ($147.8 \pm 66 \text{ g C m}^{-2} \text{ yr}^{-1}$). The higher rates of carbon accumulation can be explained by higher rates of mineral sediment accumulation in the brackish marshes, perhaps because of the closer proximity of the brackish marshes than the saltmarshes to the estuarine turbidity maximum zone of Delaware Estuary. As a whole, rates of carbon accumulation determined for this study fall within the range of rates reported for a wide range of tidal marshes dominated by *Spartina* vegetation.

As expected, short-term rates of marsh carbon accumulation (overall mean= $172.4 \pm 85.9 \text{ g C m}^{-2} \text{ yr}^{-1}$) were higher than longer-term rates ($72.8 \pm 24.3 \text{ g C$

$\text{m}^{-2} \text{yr}^{-1}$) determined using radiocarbon dating (200–1500 year averages). Carbon accumulation rates varied inversely with the period of averaging even though soil carbon concentrations did not exhibit decreases over the same time span. This suggests that non-steady-state sediment accumulation of the soil column exerts a control on long-term burial of marsh carbon.

A major finding of this research is that fine-grained particulate organic matter and (or) mineral-associated carbon delivered by the tides comprises a significant (>40%) proportion of the total soil carbon buried in Delaware Estuary marsh soils. Although plant biomass carbon (>125 μm and 63–125 μm fractions) had the highest organic carbon concentrations among the four size fractions, the silt- and clay-sized fractions were large and dominated the soil carbon inventory in four out of the five marshes investigated. The silt- and clay-sized carbon samples were compositionally distinct from plant biomass carbon accumulating at the same soil depth. Specifically, C/N ratios for the fine-grained carbon fractions were suggestive of degraded C-4 plant matter or a mixture of C-3 plant matter and terrestrial soil organic matter. The source of this fine-grained, allochthonous carbon is presumably aged marsh deposits, including particulate organic matter and mineral-associated carbon, reintroduced to the surface by marsh edge erosion and perhaps particle bioturbation. Identifying the composition, provenance, and mineral associations of this fine-grained carbon will require further research.

Chapter 1

INTRODUCTION

1.1 Organic Carbon Production and Storage in Tidal Marshes

Vegetated wetlands such as mangroves and tidal marshes (freshwater, estuarine, and coastal) are effective at sequestering atmospheric carbon dioxide (CO₂), because of their high rates of primary production and carbon fixation in plant biomass. Marsh plant biomass and particulate organic matter supplied by the tides are the two most important sources of organic carbon in wetland soils. High rates of plant primary production combined with inefficient decomposition results in accumulation and storage of soil organic carbon. Among the world's terrestrial ecosystems, carbon storage in coastal wetlands accounts for about 15% of the total despite comprising only 2–6% of the land area (Post et al., 1982). This is partly due to the high densities of organic carbon present in tidal wetland soils (10s to 100s of kg C m⁻²), which can be an order of magnitude greater than carbon densities for terrestrial soils (Post et al., 1982). Carbon sequestered in coastal waters, including tidal wetlands, is frequently referred to as "blue carbon" (Nellemann et al., 2009). Because tidal wetlands are quantitatively important sinks for atmospheric CO₂, it has been proposed that marsh preservation and restoration may help mitigate rising CO₂ concentrations in the atmosphere (McLeod et al., 2011).

The amount of organic carbon stored in wetland soils is controlled by rates of above and belowground organic matter production, decomposition by microbial activity, and accumulation (Connor et al., 2001). These processes are depicted in

Figure 1 (after Megonigal and Neubauer 2009). *In situ* primary production by marsh plants (above and belowground) and algae assimilate CO₂ from the atmosphere. The majority of this fixed carbon is used in plant and microbial respiration and re-enters the atmosphere or surrounding waters as CO₂, CH₄, or dissolved inorganic carbon. The remaining fixed organic carbon is buried in sediments, where microbial decomposition is slow. Incoming inorganic sediments from tidal exchange with their associated adsorbed organic matter also supply particulate carbon to marsh soils. Although the carbon pathways shown schematically in Figure 1 are specific to a tidal freshwater marsh (Sweet Hall Marsh, USA), they are similar in brackish and salt marsh; however, the fluxes will vary among different types of marsh depending on the local hydrogeomorphic setting.

Coastal and estuarine marshes dominated by *Spartina* vegetation are perhaps the best studied type of tidal marsh. Total net primary production of *Spartina alterniflora* ranges from 1100 to 7600 g dry mass m⁻² yr⁻¹, with belowground production accounting for 68% of the total production (Schubauer and Hopkinson, 1984). Carbon accumulation rates for *Spartina* marshes ranges from 18 to 1713 g C m⁻² yr⁻¹ (Chmura et al., 2003; Ouyang and Lee, 2014). Much of the organic material produced aboveground decomposes *in situ* or is exported by the tides, particularly carbon associated with plant stem and leaf litter.

Differences in physical and biotic conditions among different types of tidal marshes influence organic carbon accumulation and storage in soils. Tidal freshwater marshes have a mean salinity of less than 0.5 ppt whereas salt marshes have salinities of 15–18 ppt. Odum and Hoover (1987) suggest that total system production is greater in tidal freshwater marshes than in salt marshes due to high production across the

entire marsh surface (from the creek bank to the high marsh), which may not occur in salt marshes. Salt marshes are harsh environments and few plant species are adapted to salt stress, whereas species diversity is high in tidal freshwater marshes (Odum and Heywood, 1978). Marsh plants uptake and respire atmospheric CO₂ through the process of photosynthesis. Salt stress reduces primary production in salt marshes relative to that in tidal freshwater marshes (Odum and Hoover, 1987). Within a given salt marsh, rates of primary production are generally higher in the low marsh than in the high marsh as a consequence of tidal flushing and soil drainage (King et al., 1982). Relatively poor flushing in high marsh soils causes salt and sulfide concentrations to build up in pore water, limiting plant biomass production (King et al., 1982).

1.2 Marsh Soil Formation and Carbon Accumulation

Organic carbon accumulates in marsh soils through *in situ* biomass production along with accumulation of allochthonous particulate organic matter and mineral-associated organic carbon delivered by the tides (see Figure 1). Rates of carbon accumulation therefore vary spatially with rates of primary production, microbial decomposition, and mineral sediment input. While organic matter reactivity is a factor in decomposition rates (Valiela et al., 1985), decomposer control of organic matter also depends on the chemical composition of the organic matter, as well as the relationship between mineral and organic compounds. For example, tidal freshwater marsh plants undergo decomposition at a significantly higher rate than salt marsh vegetation (Odum and Heywood, 1978) and could be related to the fact that freshwater marsh plants have high nitrogen and low lignin and cellulose content, allowing them to decompose more quickly. By comparison, salt marsh plant species

have more refractive tissues than tidal freshwater marsh plants and are more resistant to decomposition (Odum and Heywood, 1978).

Plant biomass production along with deposited mineral sediment creates soil volume and causes the marsh to accrete vertically at a rate that approximates the local rate of relative sea-level rise. The relative importance of aboveground biomass (plant stems and leaves) versus belowground biomass (plant roots and rhizomes) in the accretion process varies within and among different types of tidal marshes and dominant vegetation. For example, in *Spartina* salt marshes belowground biomass is greater than that of aboveground (Schubauer and Hopkinson, 1984). Because most of the aboveground biomass decomposes before burial, belowground biomass is the chief source of organic matter in accumulated soils. In contrast, aboveground biomass and litterfall contribute significantly to vertical accretion in brackish and freshwater *Phragmites* marshes (Rooth et al. 2003). Across a wide range of tidal marsh types, the lower and upper limits of marsh accretion rates are driven by the rate of organic matter accumulation and mineral sediment accumulation, respectively (Nyman et al., 2006).

Under aerobic conditions, decomposition of organic matter in wetland soils is rapid as compared to anaerobic conditions (Megonigal and Neubauer, 2009). Decomposition with oxygen as the electron acceptor occurs across the full range of tidal wetland types at rates that depend on tidal hydroperiod, drainage, and soil saturation. Under anaerobic conditions, the decomposition pathway depends largely on the available electron acceptors in the wetland source waters. For example, tidal freshwater marshes typically do not exhibit high rates of sulfate reduction because the concentration of sulfate in source waters is low. Hence, whereas methanogenesis is

the dominant pathway regulating organic matter decomposition in freshwater marshes, sulfate reduction is the dominant pathway in salt marshes where sulfate is abundant in surface waters (Megonigal and Neubauer, 2009; Tobias and Neubauer, 2009). Consequently, tidal freshwater wetlands produce more methane than their saline counterparts. For example, in North America, estimated annual methane fluxes for freshwater marshes and salt marshes are $7.1 \text{ g CH}_4 \text{ m}^{-2} \text{ yr}^{-1}$ and $1.3 \text{ g CH}_4 \text{ m}^{-2} \text{ yr}^{-1}$, respectively (Bridgham et al., 2006). Production of methane, a greenhouse gas, is one reason why there are uncertainties concerning the role of tidal wetlands as carbon sources or sinks (Whiting and Chanton, 2001).

Partly because of these differences in organic matter decomposition pathways, it is sometimes observed that carbon accumulation rates averaged over decadal timescales (using ^{137}Cs chronometry) are higher for tidal freshwater and brackish marshes than for salt marshes (Craft, 2007; Loomis and Craft, 2010). This has been attributed to relatively high plant production rates and slower rates of organic matter decomposition in tidal freshwater marshes (Craft, 2007). In a laboratory study Weston et al. (2006) found that increasing salinity in tidal freshwater marsh sediments by 10 ppt produced a doubling of organic matter mineralization rates. This demonstrates that salinity changes in estuarine environments have potential to modify rate of organic carbon decomposition and burial in wetland soils.

For a wide range of tidal marshes, short-term carbon accumulation rates, averaged over years to decades, have been observed to be higher than long-term rates, averaged over decades to millennia (e.g., Neubauer et al., 2002). This is partly related to changes in the reactivity and perhaps microbial accessibility of organic matter in the sediment column over time (Morris and Bradley, 1999; Neubauer et al., 2002).

Given that organic carbon decomposition rates decrease with time and burial depth, and considering that marsh accretion rates are generally higher within the living root zone than in the underlying strata, it is intuitive that carbon accumulation rates should vary with averaging time span (or depth scale). In other words, accumulation rates averaged over living root zone of soil column should be higher than rates averaged over several meters, because the deeper strata contain relatively aged and degraded organic matter due to the previous decomposition of more reactive fractions. This type of time dependence is predicted by numerical models of marsh carbon accumulation (Mudd et al., 2009) and is apparent from studies of some tidal marshes. For example, for a range of San Francisco Bay tidal marshes, Callaway et al. (2012) reported rates of $72\text{--}144.3 \text{ g C m}^{-2} \text{ yr}^{-1}$ averaged over the upper 40 cm of the sediment column using ^{137}Cs and ^{210}Pb geochronology (50–100 yr time scale). For the same geographic region, Drexler (2011) reported lower carbon accumulation rates of $38\text{--}79 \text{ g C m}^{-2} \text{ yr}^{-1}$ averaged over 6–9 meter depths using ^{14}C dating (2300–5500 years). For a southern tidal marsh, Brevik and Homberg (2004) reported a relatively low rate of $3 \text{ g C m}^{-2} \text{ yr}^{-1}$ averaged over the past 5000 years.

Differences in short- versus long-term rates of carbon accumulation may also be related to increases in primary production over the last century as a result of increases in relative sea level rise (Morris et al., 2002). Relative sea level, and allochthonous sediment inputs may influence plant primary production and sediment burial. With rising sea level over recent decades, plants may have increased their aboveground and belowground production to maintain their elevation with the tidal frame, which would have led to enhanced sediment trapping and an accretion feedback loop (Morris et al., 2002). This increase in primary productivity may have

resulted in increased carbon accumulation rates over more recent timescales compared to longer timescales when primary production may not have been as high.

1.3 Sedimentary Influences on Carbon Accumulation

Solid-phase organic carbon in wetlands is associated mostly with plant biomass (living and dead), particulate organic carbon, mineral-associated carbon, and microbial biomass. As shown for terrestrial soils and marine sediments, organic matter can accumulate in soil by reacting with mineral particles and thereby become protected from further decomposition (Baldock and Skjemstad, 2000; Christensen, 2001; Dungait et al., 2012; Torn et al. 1997; Wakeham et al., 2009). Because fine silt and clay particles display flocculation behavior, organic matter can become associated with mineral particles during transport in the water column. In general, as particle size decreases the area of reactive mineral surface increases as this provides more space for organic matter adsorption. As the clay content increases, the concentration of small pores (<0.5 μm) increases, perhaps protecting organic matter from larger decomposers (Mayer, 1994). Although organic matter in mineral complexes can be protected from rapid decomposition, it is not completely immune to breakdown by microbes—decomposition is just slower than it would be without protection (Baldock and Skjemstad, 2000). Consequently, loss of soil organic matter in wetland soils is ultimately controlled by its capability to resist decomposition partly through interactions between soil morphology and microbial processes (Torn et al., 1997).

Limited work on the size dependence of organic carbon accumulation in tidal marsh soils has been undertaken, but it is intuitive that small particles will contribute to the total carbon pool to an extent that depends on the hydrogeomorphic setting of the marsh. It is well known that allochthonous particulate organic matter and mineral

sediment (silt and clay) are deposited on the marsh surface and buried over time through vertical accretion. These sediments are composed of sands, silts, and clays and presumably will have different concentrations of organic matter associated with them, similarly to terrestrial soils (Anderson, 1979; Anderson et al., 1981; Christensen, 2001). Thus, it is important to consider both autochthonous and allochthonous carbon sources when investigating carbon burial to further understand how material from different sources are contributing to carbon accumulation through time.

Marsh vertical accretion is a consequence of soil volume formation through organic matter and mineral sediment accumulation, and over time responds to feedback between physical and biotic factors (French, 2006). Not surprisingly, direct relationships between accretion rate (length/time) and mass accumulation rate (mass/area/time) have been observed for a wide range of tidal marshes (e.g., Callaway et al., 2012; Chmura and Hung, 2004; Neubauer, 2008; Turner et al., 2000). Craft (2007) found that accretion rates based on ^{137}Cs dating were higher in Georgia tidal marshes along a freshwater-dominated river ($3.4 \pm 0.6 \text{ mm yr}^{-1}$) than along rivers that were marine-dominated ($1.1 \pm 0.3 \text{ mm yr}^{-1}$, $1.3 \pm 0.3 \text{ mm yr}^{-1}$). In a review by Neubauer (2008), accretion rates were concluded to be generally higher in tidal freshwater marshes than in brackish and salt marshes, which the author interpreted to reflect proximity of tidal freshwater marshes to riverine sediment sources, and the reactivity of freshwater versus salt marsh plant production. As described below, relationships between marsh accretion and organic carbon accumulation in tidal freshwater, brackish, and salt marsh were explored in this study.

1.4 Research Goals and Hypotheses

To develop a mechanistic understanding of organic carbon accumulation in estuarine marshes, this study investigated patterns and rates of organic carbon accumulation on the tidal wetland coast of the Delaware River and Bay (Delaware Estuary). The Delaware Estuary is a 215-km long coastal plain estuary composed of a tidal (freshwater) river, a weakly stratified central estuary, and a well-mixed bay (Fletcher et al., 1992). During the Holocene, tidal freshwater, brackish, and salt marshes developed around the estuary and today comprise an area of 308 km² in the state of Delaware (Tiner et al., 2011). Brackish and salt marshes on the western side of the estuary were the specific focus of this study (Figure 2).

Tidal marshes of the Delaware Estuary are presumably an important organic carbon sink regionally, although estimates of carbon accumulation and storage have yet to be reported. To this end, a goal of this research was to quantify carbon accumulation rates for selected marsh locations within the estuary, with a specific focus on the time dependence of carbon accumulation and the influence of soil composition on computed accumulation rates. Tidal marshes that fringe Canary Creek, Great Marsh, Mispillion River, St. Jones, and Kelly Island fall within mesohaline (5–18 ppt) to polyhaline (18–30 ppt) waters of Delaware Estuary (Figure 3), and in this thesis are referred to as “salt marsh”. Marshes sampled in Blackbird Creek and St. Georges marsh fall within mesohaline to oligohaline (0–5 ppt) waters and are referred to as “brackish” marsh.

At the outset of the study it was hypothesized that carbon accumulation rates are higher in brackish marshes than in salt marshes of the Delaware Estuary. This was based on observations for tidal marshes in general (e.g., Callaway et al., 2012; Craft, 2007; Loomis and Craft, 2010), and local observations that tidal freshwater marshes

in estuary have higher mineral sediment accumulation rates than the salt marshes (Sommerfield and Velinsky, 2010), perhaps due to their proximity to the estuarine turbidity maximum, a large source of fine-grained mineral sediment (Sommerfield and Wong, 2011). To test this hypothesis, carbon accumulation at selected sites within tidal marshes along the salinity gradient of Delaware Estuary was quantified.

It was also hypothesized that carbon burial rates would be lower over longer timescales (100–1000s yr) compared to shorter timescales (<100 yr). The basis for this hypothesis stems from the combined work of Callaway et al., (2012) and Drexler (2011) as described above. To test this hypothesis, carbon accumulation rates were determined for the same marsh sites but averaged over different time scales using nested ^{137}Cs , ^{210}Pb , and ^{14}C chronometry. Although understanding the time-dependence of carbon accumulation in wetlands is fundamental in regional and global estimates of coastal blue carbon sequestration, surprisingly there is little information on longer-term (millennial) carbon accumulation in U.S. estuarine and coastal wetlands.

Understanding the sources and types of organic carbon (i.e., plant biomass, particulate organic matter, mineral-associated carbon) incorporated in tidal marsh soils is fundamental to the understanding of wetland carbon burial. However, compared to terrestrial soils, little is known about the relative contribute of wetland soil carbon pools to carbon sequestration rates and storage. In particular, mineral-associated organic carbon is frequently overlooked as a source of carbon in tidal marsh soils, presumably because it contributes a small amount compared to plant biomass. As noted previously, for terrestrial soils it has been shown that carbon associated with different size and density fractions has widely different decomposition

rates and thus contributes to soil carbon storage in different ways (Trumbore, 2009). To advance our understanding of soil-size-dependent carbon accumulation in tidal marshes, detailed studies of the mass and composition of soil size fractions were conducted on core samples obtained from the tidal wetland coast of Delaware Estuary.

To summarize, the hypotheses of this study are stated below:

1. Carbon accumulation rates will be higher in brackish marshes compared to salt marshes
2. Carbon accumulation rates will be lower over longer timescales
3. Carbon accumulation rates will vary with the amount of incoming allochthonous sediment

1.5 Geographic Setting of the Delaware Estuary

Much of what is known about the geological history of Delaware Estuary's wetland coast stems from research by Fletcher et al. (1990) and Fletcher et al. (1992). Around 10 ka, low-lying regions surrounding the ancestral Delaware River became flooded by rising sea levels. Between 9 ka and 7 ka, fine-grained sediments (estuarine mud) started to accumulate at the mouth of present-day Delaware Bay, providing substrate required for plant growth. Tidal marshes then emerged from tidal flats at the edges of the former estuary. Around 6 ka, the mud depocenter migrated to today's central Delaware Bay. As the estuary enlarged, the depocenter continued to move northwest due to sea level rise and basin submergence, which decreased the amount of sediment available to lower Delaware Bay (Fletcher et al., 1992). Today, estuarine mud accumulation occurs mostly landward of Delaware Bay in the turbidity maximum zone of the estuary, extending from Christina River to Artificial Island (Sommerfield and Wong, 2011). As sea level continued to rise, marshes that occupied

the fringe of estuaries were able to migrate landward and transgress into terrestrial systems. Through this process marshes accrete vertically by accumulating peat and trapping allochthonous mineral sediments from tidal input (Kraft et al., 1992).

In general, if tidal marshes can accrete at a rate equaling or exceeding the local rate of relative sea level rise, then they will continue their role as a sink for CO₂ (Morris et al., 2002). However, landward transgression of marshlands worldwide is currently hindered by coastal development and agriculture, and, along with erosion at their seaward boundaries, has caused marshes to shrink in spatial extent, reducing the carbon sequestration potential (Hopkinson et al., 2012). In the Delaware Estuary region, tidal wetlands have been losing ground to sea-level rise and shore erosion for millennia (Kraft et al., 1992), and there is evidence to suggest that the rates of marsh loss have increased in recent decades (Tiner et al., 2011). Currently, the rate of relative sea level rise in the Delaware Estuary region is ~3 mm yr⁻¹ (Zervas, 2009).

Chapter 2

METHODS

2.1 Core Collection

To obtain marsh soil samples for analysis, two different types of cores were used in this study: (1) push-piston cores, and (2) vibracores. These cores are respectively referred to as “short cores” and “long cores” in this thesis. Most of the short cores (0.75–1.0 m in length) had been collected by C. Sommerfield and D. Velinsky in prior sampling campaigns in the Delaware Estuary region. The archived core material, previously dried or maintained in cold storage, were used for this study. Additional short cores were collected during the present study, as described below. A smaller number of long cores, 1.5–2.5 m in length, were collected for this study at several of the reoccupied short-coring sites to obtain overlapping short-term (short cores) and long-term (long cores) soil records for selected marsh locations. The locations and sampling dates for the cores used in this study are listed in Table 1, and the coring sites are shown in Figures 2 and 3.

2.1.1 Short Cores

The short cores were collected using 4-inch diameter PVC pipe and a tripod-winch device designed to minimize core shortening as the pipe was advanced into the marsh soil. Three cores were collected at each marsh site, and an attempt was made to core at locations spanning the full range of vegetation type and elevation. The short cores were vertically extruded and subsampled in 2-cm thick, alternating increments

downcore. The archived marsh soils were analyzed for bulk density, loss-on-ignition (LOI), and radionuclide content. Core samples and chronologies for GM-2, GM-3, GM-4, BC-2, and SG-3 were processed for this study; all other short cores were previously analyzed through the work of Sommerfield and Velinsky (2010). Sediment accumulation and marsh accretion rates determined by Sommerfield and Velinsky (2010) using ^{137}Cs and ^{210}Pb chronology were made available for the present study of carbon accumulation.

2.1.2 Long Cores

In five of the six marsh systems targeted for this study, one long core was collected using a portable vibratory coring system and aluminum irrigation pipe 3-inches in diameter. The vibracores were extracted from the marsh using a tripod-winch system and stored cold until lab analysis. In the lab, the core tubes were split lengthwise, visually described, photographed, and subsampled in 5-cm thick increments at 30-cm intervals from top to bottom. One half of the core was subsampled for bulk soil analyses and physical properties measurements, whereas the other half was used for the soil carbon size fractionation work and radiocarbon dating.

2.2 Physical Properties Measurements

Soil physical properties including water content, porosity, dry bulk density, and loss on ignition were determined for each sample. Bulk soil material from the cores was weighed wet (WW), dried at 105°C , and reweighed (DW_{105}) to determine the gravimetric water content (WC) as follows:

$$WC = \frac{WW - DW_{105}}{WW}$$

1

Once dry the soil material was homogenized and ground using a mortar and pestle and further using an IKA electric soil mill. Water content and loss-on-ignition (*LOI*) data were used to calculate soil porosity as follows:

$$\phi = \frac{(WC)(1-LOI)(\rho_{min})}{(WC)(1-LOI)(\rho_{min})+(LOI)(\rho_{org})+(1-WC)(\rho_{pw})} \quad 2$$

where:

ϕ = porosity

ρ_{min} = mineral solids density (2.650 g/cm³)

ρ_{org} = organic solids density (1.200 g/cm³)

ρ_{pw} = pore water density (1.025 g/cm³)

Soil dry bulk density is composed of organic and mineral density subcomponents described by $LOI * \rho_{org}$ and $(1 - LOI) * \rho_{min}$, respectively. It was computed from porosity according to:

$$\rho_d = (1 - \phi)((1 - LOI)(\rho_{min}) + (LOI * \rho_{org})) \quad 3$$

where:

ρ_d = dry bulk density (g/cm³)

Loss on ignition was determined by combusting 4 grams of material following methods described in Heiri et al. (2001). The following equation was used to calculate *LOI*:

$$LOI = \left(\frac{DW_{105} - DW_{550}}{DW_{105}} \right) * 100 \quad 4$$

where:

LOI = weight percentage of organic material (%)

DW_{105} = dry weight of sample before combustion (g)

DW_{550} = dry weight of sample after combustion at 550°C for 4 hours (g)

Based on sample triplicates, the relative uncertainty of the dry bulk density measurements is 6.2%. As discussed below, this uncertainty is propagated with other sources of error to estimate uncertainties in the organic carbon accumulation rates.

2.3 Organic Carbon and Total Nitrogen Analysis

Organic carbon and total nitrogen content of the bulk and size-fractionated marsh soils were determined following methods described by Komada et al. (2008). First, homogenized soil was weighed into silver capsules and moistened with 50 μL of deionized water to enhance acidification (Harris et al., 2001). Weighed silver capsules were then placed in a glass desiccator with 30 mL concentrated HCl for 8 hours. After fumigation, capsules were placed in an oven at 60°C overnight. Due to the brittle nature of silver capsules after acid exposure, they were placed inside tin capsules. Organic carbon and total nitrogen concentrations were determined (613 samples total) using a Costech ECS 4010 elemental analyzer using acetanilide ($\text{C}_6\text{H}_5\text{NH}(\text{COCH}_3)$) and atropine ($\text{C}_{17}\text{H}_{23}\text{NO}_3$) standards. Errors associated with instrument accuracy ranged from 0.02–9.98% for total nitrogen (average=1.22%) and 0.01–6.81% for organic carbon (average=0.91%). Triplicates were run on every fifth sample to determine the precision of the instrument. Relative uncertainty in carbon concentrations based on triplicate analysis ranged from 0.29–23.57% (average

4.58%). Relative uncertainty in nitrogen concentrations based on triplicate analysis ranged from 0.09–28.28% (average 4.37%).

2.4 Radionuclide Geochronology

Cesium-137 and ^{210}Pb are useful radionuclides for dating marsh soils and calculating accretion and mass accumulation rates (Brenner and Kenney, 2013). Cesium-137, a product of nuclear fission with a half-life of 30.70 years, was released to the atmosphere during nuclear testing in the 1950s with maximum fallout by precipitation in 1963 (Ritchie and McHenry, 1990). Cesium-137 is an effective sediment tracer for measuring sediment accretion rates because it is globally distributed and strongly adsorbed to clay and organic particles some of which become buried in marshes.

Lead-210 is a naturally occurring radionuclide produced through the ^{238}U decay series with a half-life of 22.26 years. Through the ^{238}U decay series, ^{222}Rn gas is produced and enters the atmosphere where it further decays to ^{210}Pb . Lead-210 is then deposited by rainfall or dry fallout and incorporated into sediments. In the sediment column, ^{210}Pb activity unsupported by *in situ* decay of ^{222}Rn in the soil column is known as excess activity, and activity-depth profiles of $^{210}\text{Pb}_{\text{xs}}$ provide the chronology information used to compute accretion rates (Brenner and Kenney, 2013).

Gamma spectrometry is a widely used, non-destructive method for measuring radionuclide activity in support of sediment chronometry (Wallbrink et al., 2002). In this study, high-purity germanium detectors were used to detect gamma photons emitted at known energies (662 keV for ^{137}Cs and 46 keV for ^{210}Pb) by radionuclides in homogenized core subsamples. Importantly, in gamma spectrometry $^{210}\text{Pb}_{\text{xs}}$ activity

can be determined from the total ^{210}Pb activity using measured activities of parent nuclides ^{214}Bi (609 keV) and/or ^{214}Pb (352 keV) for the same sample.

For this study, soil samples from the 24 short cores were counted for 24 hours on a Canberra Instruments low-energy germanium detector and analyzed for ^{137}Cs and ^{210}Pb activity. The corrected radionuclide activities were used to construct depth profiles for calculation of vertical accretion (cm yr^{-1}) and mass accumulation rates ($\text{g cm}^{-2} \text{yr}^{-1}$). Errors related to detector use range from 5–8% for ^{137}Cs and ^{210}Pb . With the exception of cores from St. Georges marsh, $^{210}\text{Pb}_{\text{ex}}$ activity was not detected far below the first occurrence depth of ^{137}Cs (~1954) and thus was incapable of providing a significantly longer history of soil accumulation. Hence, for simplicity, only the ^{137}Cs -based rates of accretion and accumulation were used in this study with the exception of St. Georges marsh. For this marsh site ^{210}Pb chronology was used instead, because two out of the three ^{137}Cs core profiles did not exhibit an activity peak consistent with the year 1963.

Radiocarbon (^{14}C) has a half-life of 5,730 years and has been used in studies of wetland soil sequestration of atmospheric CO_2 (Choi and Wang, 2004) and long-term accumulation of organic carbon (Brenner and Kenney, 2013; Drexler, 2011). In this study, ^{14}C was employed as a chronometer to compute long-term carbon accumulation rates. Marsh plant macrofossils for ^{14}C dating were subsampled from the $>125\mu\text{m}$ soil fraction under a microscope. Root rhizomes were picked as this material has been shown to yield ^{14}C dates with the most representative stratigraphic ages (Törnqvist et al., 1992). Thirty-four carefully selected samples from the five long cores were sent to the National Ocean Science Accelerator Mass Spectrometry (NOSAMS) facility in Woods Hole, Massachusetts, for analysis. Accelerator mass

spectrometry (AMS) has an advantage over radiocarbon analysis by beta counting because it does not require long counting times or large sample sizes.

At NOSAMS the samples underwent an acid-base-acid pretreatment to remove contaminating carbonate, humic, and fulvic compounds. A portion of each treated sample was analyzed for ^{13}C content, which is required to correct for isotopic fractionation of ^{14}C when calculating the conventional ^{14}C age of a sample. NOSAMS determines ^{13}C values by mass spectrometry during the ^{14}C analytical process.

Conventional age is expressed in years before present (^{14}C yr BP) where “present” is the reference year of 1950. Conventional ages reported by NOSAMS were later calibrated to calendar years (cal yr BP) using the CALIB program (Stuiver et al., 2015) with the INTCAL13 calibration dataset (Reimer et al., 2013). Calibration is required to account for natural changes in the atmospheric reservoir of $^{14}\text{CO}_2$, and is required to assign calendar year age dates to a stratigraphic column. The relative uncertainty in the calibrated ^{14}C ages is $\pm 4.1\%$. Calibrated radiocarbon ages were used to calculate the long-term accretion and carbon accumulation rates reported in this thesis.

NOSAMS also reports results as $\Delta^{14}\text{C}$, the ratio of the sample activity to the activity of a standard, adjusted to account for the time between sample collection and 1950, and corrected for isotopic fractionation using the ^{13}C content of the sample. $\Delta^{14}\text{C}$ data are expressed in parts per thousand (‰), decreasing from the reference value by 1‰ for every 8.1 years of radioactive decay. Nuclear weapons testing greatly increased the atmospheric reservoir of ^{14}C , thus organic materials that incorporated $^{14}\text{CO}_2$ during the bomb era have ^{14}C activities that are many times the standard reference activity. Positive and negative $\Delta^{14}\text{C}$ values represent atmospheric $^{14}\text{CO}_2$

fixed in organic matter after and before 1950, respectively. Significantly, elevated $\Delta^{14}\text{C}$ values can serve as a tracer of recent $^{14}\text{CO}_2$ sequestration in terrestrial and tidal marsh soils (Trumbore, 2009; Choi and Wang, 2004).

2.5 Size Fractionation of Soil Material

A wide range of procedures for separating sediments and soils into size and density fractions for organic carbon analysis have been proposed (Cambardella and Elliott, 1993; Elliott and Cambardella, 1991; Trumbore, 2009; Trumbore and Zheng, 1996). After reviewing the available literature, it was determined that the methodology described by Cambardella and Elliott (1993) was the most practical and informative method for the tidal marsh soils collected for this study. The general approach described by these authors was used to fractionate subsamples from the long cores for determination of organic carbon concentrations and carbon accumulation rates for specific soil size fractions.

The soil separation procedure is shown schematically in Figure 4. Using a combination of mechanical sieving and centrifugation, four size fractions were obtained: $>125\mu\text{m}$, $63\text{--}125\mu\text{m}$, $4\text{--}63\mu\text{m}$ (silt size), and $<4\mu\text{m}$ (clay size). The $>125\mu\text{m}$ size fraction consisted of living or dead plant biomass, the $63\text{--}125\mu\text{m}$ fraction was mostly dead plant biomass, and the silt- and clay-sized fractions were a combination of organic and inorganic (mineral sediment) particles. First, bulk samples were wet sieved through $125\mu\text{m}$ and $63\mu\text{m}$ sieves using sodium hexametaphosphate. Material retained on the sieves ($>125\mu\text{m}$ and $63\text{--}125\mu\text{m}$) was dried at 60°C . Next, material that passed through both sieves was separated into silt and clay fractions by centrifugation for 10 minutes at 600 RPM and 3000 RPM, respectively. Centrifugation was repeated for the clay fraction until all clay was settled out of suspension. Finally, the silt and

clay size fractions were dried at 105°C. Centrifugation speeds for the silt- and clay-sized material were calculated using the following equation derived by Genrich and Bremner (1974):

$$T = \frac{(63 \times 10^8) n (\log_{10} R/S)}{N^2 D^2 (S_p - S_l)} \quad 5$$

where:

T = time for sedimentation (minutes)

N = viscosity of water (poises)

R = radius of rotation to top of sediment (cm)

S = radius of rotation to top of suspension (cm)

N = speed of centrifuge (RPM)

D = particle diameter (microns)

S_p = specific gravity of particles (g cm^{-3})

S_l = specific gravity of water (g cm^{-3})

The actual size of organic carbon associated with the silt- and clay-sized particles, and the manner in which carbon was associated with mineral grains, could not be determined in this study. Given that these size fractions were separated by centrifugation (density), it could only be assumed that the carbon was strongly associated with mineral surfaces or grain interstices. Hence, these are operational definitions for different size fractions of carbon present in marsh soils. Note that size separation of the fine-grained fractions (4–63 μm and <4 μm) by centrifugation is partly a function of particle density, thus the separation procedure used for this study has elements of density separation using heavy liquids (e.g., Wakeham et al., 2009).

2.6 Organic Carbon Accumulation Rates

For the short cores, organic matter accumulation rates (OAR in $\text{g m}^{-2} \text{yr}^{-1}$) averaged since 1963 were determined as follows:

$$OAR = \sum_{i=0cm}^{1963 \text{ depth}} (OM_i \cdot \rho_{di} \cdot x_i \cdot 10,000) / t \quad 6$$

where OM_i is the mass concentration (g organic matter/g soil sample) of combustible organic matter (LOI/100) for the i th depth interval, ρ_d is the soil dry bulk density (g cm^{-3}), x_i is the interval thickness (cm), and t is the time between core collection and 1963 (yr). Alternating 2-cm intervals of the short cores were subsampled and analyzed. Because these cores were not sampled continuously from top to bottom, OM_i and ρ_d were interpolated as needed between the analyzed intervals.

Mineral sediment accumulation rates (MAR in $\text{g m}^{-2} \text{yr}^{-1}$) were calculated according to:

$$MAR = \sum_{i=0cm}^{1963 \text{ depth}} (MM_i \cdot \rho_{di} \cdot x_i \cdot 10,000) / t \quad 7$$

where MM_i is the mass concentration (g mineral matter/g soil sample) of incombustible solids ($1 - \text{LOI}/100$) for the i th depth interval, and the other terms are described above. Short-term organic carbon accumulation rates (CAR in $\text{gC m}^{-2} \text{yr}^{-1}$) were calculated as follows:

$$CAR = \sum_{i=0cm}^{1963 \text{ depth}} (C_i \cdot \rho_{di} \cdot x_i \cdot 10,000) / t \quad 8$$

where C_i is the bulk organic carbon concentration (g C/g soil sample) for the i th depth interval, determined by elemental analysis. The other terms are described above. Note that the product of C and ρ is the concentration of organic carbon per unit volume of

soil (g C cm^{-3}) herein. Nitrogen accumulation rates were calculated using the equation above, substituting carbon concentration with nitrogen concentration.

For the long cores, long-term carbon accumulation rates were calculated using ^{14}C dates as follows:

$$\sum_{i=0}^{z_i} (C_i \cdot \rho_{di} \cdot x \cdot 10,000) / {}^{14}\text{C}_i \quad 9$$

where z_i is the depth (cm) of the i th ^{14}C age date in cal yr BP. Equation 9 was solved iteratively using successive age dates to construct a depth profile of carbon accumulation rate. Because the cores were not sampled continuously from top to bottom, C and ρ_d were interpolated as needed between ^{14}C -dated intervals to account for the intervening carbon inventory. The same approach was used to compute long-term nitrogen, organic, and mineral accumulation rates.

Carbon accumulation rates calculated for the four soil size fractions were computed following Equation 9 above, but substituting the bulk carbon concentration per unit soil volume ($C \cdot \rho_d$) with carbon volume concentration associated with the specific size fraction. This was calculated according to:

$$CD_i = \frac{C_i \rho_d}{DW} \quad 10$$

where:

CD_i = carbon concentration of the i th size fraction (g cm^{-3})

C_i = carbon concentration of the i th size fraction (g/g)

DW = total mass of dry soil (g)

ρ_d = dry bulk density of soil (g cm^{-3})

Following Equation 10, the sum of the fractional carbon concentrations equal the total carbon concentration (CD_T) as follows:

$$CD_T = CD_{>125} + CD_{63-125} + CD_{silt} + CD_{clay} \quad 11$$

Based on core-sample splits, CD_T was determined to be nearly identical to the bulk carbon density computed as $C \cdot \rho_d$. This important result verifies that soil material was not lost during the size-segregation procedures. Uncertainties associated with carbon and nitrogen accumulation rates calculated using ^{137}Cs or ^{210}Pb chronology are below $\pm 11\%$, and for rates computed using ^{14}C dates are below $\pm 9\%$. Carbon concentration data for size fraction samples are given in Appendix A.

2.7 Statistical Analysis

Differences were considered statistically significant when $p < 0.05$. ANOVA's were completed using SigmaPlot version 13 with the SigmaStat package and t-tests were performed using RStudio version 3.0.1.

Chapter 3

RESULTS

3.1 Marsh Soil Physical Properties

Results of the physical property measurements for the short and long cores are listed in Appendix A. Dry bulk density measurements for short core soils ranged from 0.0982 to 1.852 g cm⁻³ with the lowest values in St. Jones marsh and the highest in Canary Creek marsh (Figure 5). Some of the high dry bulk densities in the lower sections of the Canary Creek cores CC-1 and CC-5 are a result of coring through the marsh sequence into sandy, pre-marsh strata. The overall average dry bulk density for all short cores was 0.433 ± 0.282 g cm⁻³ (1 σ , n=441). Core samples from Mispillion River had the lowest dry bulk density on average (0.272 ± 0.121 g cm⁻³, n=56), and St. Georges marsh had the highest (0.640 ± 0.125 g cm⁻³, n=70). Overall, dry bulk density fluctuated down-core with variations in organic matter and mineral sediment content, and there were no consistent trends with depth for individual marshes.

Loss on ignition co-varied with the amount of organic material within the short core samples (n=439). Overall, LOI ranged from 0.0174 to 0.950 and averaged 0.268 ± 0.138 (1 σ , n=441) for all short core samples (Figure 6). St. Jones marsh soils had the highest LOI values on average (0.341 ± 0.186 , n=62), and St. Georges marsh had the lowest LOI measurements on average (0.143 ± 0.0352 , n=70). Again, Canary Creek short cores CC-1 and CC-5 penetrated a layer with sand, the source of the very low LOI values near the bottom of the profiles. As per the bulk density profiles, LOI

was variable with soil depth. One exception were profiles for the cores from St. Georges marsh, which exhibited relatively uniform depths profiles of LOI.

3.2 Total Organic Carbon and C/N Ratios

Total organic carbon (TOC) concentration and C/N data for soils subsampled from the short cores are presented in Figure 7. Overall, TOC and C/N ratios varied widely among the marsh sampling sites as well as within a given soil profile. Values of TOC ranged from 0.079% to 38.014% with an overall mean of $9.62 \pm 5.87\%$ (1σ , $n=444$). Among the marsh sites Mispillion River marsh had the highest TOC concentrations ($13.19 \pm 3.62\%$, $n=56$) whereas the St. Georges marsh had the lowest ($5.40 \pm 1.22\%$, $n=70$). ANOVA analysis indicated that the means for this marsh sites were statistically different ($p<0.001$).

C/N ratios ranged from 6.33 to 37.38 with an overall mean of 20.43 ± 3.45 (1σ , $n=444$). Kelly Island marsh and St. Georges marsh had the highest (22.20 ± 3.55 , $n=55$) and lowest (18.35 ± 2.25 , $n=70$) C/N ratios, respectively. Again, ANOVA analysis indicated that the means for this marsh sites were statistically different ($p<0.001$). Soils from Canary Creek marsh had very low TOC and low C/N ratios overall, presumably because one of the cores penetrated into sandy strata of low organic carbon content.

Within a given core, profiles of TOC and C/N ranged from nearly uniform to highly variable down core (Figure 8, Figure 9). TOC concentrations varied with depth in almost all cores collected (Figure 8). There were no consistent pattern of TOC content with depth within individual marshes except for Great Marsh and St. Georges marsh. In Great Marsh, TOC concentrations were higher at the surface and then decrease with depth. Lastly, in St. Georges marsh TOC content remained constant

with depth for all three short cores. Increases in TOC content with depth were present in some cores from Mispillion River, St. Jones, and Blackbird Creek marshes, although trends with depth were not consistent among the cores from these locations. Generally, C/N ratios were highest at the surface and decreased slightly with depth in cores, although in other cases C/N increased with depth (CC-2, SJBM-1, BC-1, SG cores).

The relationship between LOI and TOC for the short-core marsh soils is shown in Figure 10. As expected, LOI increases with increasing TOC content and soils from the brackish marshes (Blackbird Creek, St. Georges) had lower values of LOI and TOC. There is a strong correlation between LOI and TOC content but some data for Canary Creek and Great Marsh are clustered below the overall trend line. This could be due to LOI and TOC values that are much lower than those from the other cores. Canary Creek and Great Marsh cores captured pre-marsh sandy mud (as mentioned previously), resulting in a different relationship between LOI and TOC than for marsh soils at other locations.

Organic carbon concentration and C/N data for the long cores are presented in Figure 11. Core VCBC had the highest TOC values on average ($21.85 \pm 9.95\%$, $n=7$), whereas VCSG had the lowest ($5.28 \pm 2.23\%$, $n=7$), similar to the short core results. C/N ratios for soils from VCBC have the highest C/N ratios (24.83 ± 2.99 , $n=7$) as shown in Figure 11b. Lastly, VCSG had the lowest C/N ratios with an average of 19.65 ± 2.22 ($n=7$). Overall, the mean TOC content and C/N ratios for long cores are $12.94 \pm 8.42\%$ ($n=34$) and 21.91 ± 9.50 ($n=34$), respectively.

3.3 Stable Carbon Isotope Values

Stable carbon isotope ($\delta^{13}\text{C}$) values ranged from -24.46 to -9.93 ‰ (Table 2). Samples from cores VCGM, VCMR, and VCKI had $\delta^{13}\text{C}$ values between -13.81 and -9.93 ‰, consistent with the composition of fresh *Spartina alterniflora* (Haines, 1976; Ember et al., 1987). Some samples from core VCBC and VCSG were relatively depleted in ^{13}C (-14.33 to -24.46 ‰). These more depleted samples may be partially decomposed *Spartina alterniflora* roots (Ember et al., 1987; Middelburg et al., 1997) or roots from C-3 marsh plants such as *Juncus gerardii*. None of the soil profiles exhibited depth trends in $\delta^{13}\text{C}$ suggestive of major changes in marsh vegetation type.

3.4 ^{14}C age dates and $\Delta^{14}\text{C}$ Values

The results of the ^{14}C analyses are listed in Table 2, including the uncorrected conventional ^{14}C ages reported by the laboratory. The ^{14}C data presented in the figures are expressed as calibrated age before present (cal yr BP) and $\Delta^{14}\text{C}$ (‰) following standard conventions (Stuiver and Polach, 1977). As mentioned previously, age calibration corrects for variations in atmospheric $^{14}\text{CO}_2$ concentrations over time and is necessary to assign calendar age dates to the soil column. Radiocarbon data expressed as $\Delta^{14}\text{C}$ conveys the amount of “modern” ^{14}C incorporated into the dated organic material, as $^{14}\text{CO}_2$ fixed in plant tissue after 1955 is elevated with ^{14}C produced by nuclear weapons testing. Although weapons testing ceased in 1964, atmospheric $^{14}\text{CO}_2$ concentrations are still elevated above those prior to the bomb era, and contemporary marsh plants continue to sequester legacy $^{14}\text{CO}_2$.

Calibrated ^{14}C age dates ranged from 178 to 1459 cal yr B.P. and generally increased with depth in cores (Table 2). In cores VCBC and VCSG, some ^{14}C ages were inverted with older dates above younger ones by several 100s of years. Age

inversions may be more common in tidal marshes than aquatic environments and these inverted ages are most likely a result of downward extension and sloughing of relatively young roots and rhizomes into older soil horizons, which can introduce relatively young CO₂ and plant biomass carbon to older (deeper) soils (Nilsson et al., 2001; Turetsky et al., 2004). This is further complicated by subsurface redistribution and uptake of dissolved organic carbon produced during decomposition and from root exudation (Waddington and Roulet, 1997).

Samples from all of the cores contained modern ¹⁴C ($\Delta^{14}\text{C}$ values greater than 0 ‰) in the uppermost soil column, which demonstrates that the marsh plants have been actively fixing atmospheric ¹⁴CO₂ since about 1954 (Figure 12). Samples from cores VCGM, VCMR, and VCKI contained modern ¹⁴C down to a depth of about 35 cm, just below the bottom of the living root zone. In cores VCBC and VCSG, modern ¹⁴C was detected down to 122.5 cm and 152.5 cm, respectively, with intervening non-modern $\Delta^{14}\text{C}$ values.

Because both ¹³⁷Cs and modern ¹⁴C activity are a consequence of nuclear weapons testing, their depth distributions in marsh soils should be comparable provided the source function is not altered post-deposition. In the case of cores VCGM, VCMR, and VCKI, the depth of modern (bomb-produced) ¹⁴C is broadly consistent with the first occurrence and peak of ¹³⁷Cs activity. As shown in Figure 12, the lowermost modern $\Delta^{14}\text{C}$ value fell within the 1954-1963 date range in these cores. In cores VCBC and VCSG, two modern ¹⁴C samples fell below the 1954 age horizon, suggesting downward transport by root extension. This is consistent with the visual examinations of these cores, which indicated a relatively deep root zone.

3.5 Marsh Accretion Rates

Short-term marsh accretion rates based on ^{137}Cs and ^{210}Pb chronology ranged from 0.11 to 1.20 cm yr^{-1} among the sampled marshes (Table 3). The highest and lowest accretion rates were observed for St. Georges marsh ($0.89 \pm 0.27 \text{ cm yr}^{-1}$; 1σ , $n=3$) and Canary Creek marsh ($0.29 \pm 0.18 \text{ cm yr}^{-1}$; $n=5$), respectively. Overall, the average short-term accretion rate for all of the sites is $0.49 \pm 0.21 \text{ cm yr}^{-1}$ ($n=24$); removing the brackish marsh data, the mean salt marsh accretion rate is $0.42 \pm 0.21 \text{ cm yr}^{-1}$, $n=18$.

Long-term (700-1500 years) accretion rates were computed for the long cores by dividing the depth of the ^{14}C -dated root material by the corresponding calibrated age date. Repeating this for all of the pre-modern ^{14}C age dates resulted in a total of 20 accretion rates, ranging from 0.13 to 0.50 cm yr^{-1} with an overall mean of $0.25 \pm 0.10 \text{ cm yr}^{-1}$, $n=20$ (Table 4). These accretion rates are generally lower than those determined for the same sampling sites by ^{210}Pb and ^{137}Cs chronology (Table 5), which is often the case since ^{14}C averages over longer time spans and a wider range of sedimentation conditions.

3.6 Soil Bulk Carbon Accumulation Rates

Short-term carbon accumulation rates computed using Equation 8 are shown in Figure 13 and listed in Table 3 (see Appendix B for the corresponding nitrogen data). Carbon accumulation rates ranged from 28.3 $\text{g C m}^{-2} \text{ yr}^{-1}$ (core CC-1) to 439.9 $\text{g C m}^{-2} \text{ yr}^{-1}$ (core SG-3) with an overall mean of $172.4 \pm 85.9 \text{ g C m}^{-2} \text{ yr}^{-1}$, $n=24$. There was a general down-estuary decrease in marsh-averaged carbon accumulation rates from the tidal freshwater zone to saline region, which may reflect differences in burial conditions (Figure 13) and marsh-mean rates are significantly different between St.

Georges and Canary Creek ($p=0.006$), as well as St. Georges and Great Marsh ($p=0.019$).

Long-term carbon accumulation rates (calculated using Equation 9) and ^{14}C calibrated age dates were overall lower than the short-term rates (Figure 14). All long-term carbon accumulation rates ($n=20$) ranged from 45.1 to 160 $\text{g C m}^{-2} \text{ yr}^{-1}$ with an overall mean carbon accumulation rate of $93.3 \pm 35.5 \text{ g C m}^{-2} \text{ yr}^{-1}$. Rates decreased over all depths in cores VCGM, VCMR, and within the upper portion of VCBC. Rates increased with depth for VCSG ($n=2$) and at the bottom-most sample of VCBC, corresponding to the previously noted age inversions. Overall, there was no consistent trend in carbon accumulation rates with depth for the long cores.

3.7 Carbon Accumulation Rates For Soil Size Fractions

As described previously, marsh soil samples from long cores were separated into four size fractions representing plant biomass ($>125\mu\text{m}$ and $63\text{--}125\mu\text{m}$) and particulate organic material ($4\text{--}63$ and $<4\mu\text{m}$). Together these four size fractions make up the total weight of the bulk soil. For all of the long core subsamples ($n=136$), the $>125\mu\text{m}$ size fraction was variable and ranged from 0.16–49.20 weight % of the bulk soil with an average of 12.56% (Figure 15). The $63\text{--}125\mu\text{m}$ size fraction did not contribute much weight to the bulk soil, ranging from 0.10 to 7.90% and averaging of 1.32%. In contrast, silt-sized ($4\text{--}63\mu\text{m}$) particles comprised a large percentage of the soil, ranging from 32.31 to 84.73% and averaging 67.10%. The clay-size fraction ($<4\mu\text{m}$) contributed 7.68–37.63% and averaged 18.99%. In sum, the soil samples by weight were composed of organic matter mostly $>125\mu\text{m}$ in size and silt-sized particles.

Results of the size-specific TOC and C/N analyses are presented in Figure 16. As expected, TOC concentrations were highest for the $>125\mu\text{m}$ and $4\text{--}63\mu\text{m}$ size fractions with overall means of $37.84 \pm 8.75\%$ and $33.76 \pm 9.38\%$ by weight (Figure 16a). Silt- and clay-sized particles had lower overall mean TOC concentrations of $8.94 \pm 6.44\%$ and $9.93 \pm 7.28\%$, respectively. The average bulk TOC concentration was $12.94 \pm 8.42\%$. Generally, silt and clay TOC concentrations are more similar to the bulk material TOC content than to the $>125\mu\text{m}$ and $4\text{--}63\mu\text{m}$ size fractions. This could be because the finer size fractions made up more of the bulk sample by mass (see Figure 15), whereas the $>125\mu\text{m}$ and $4\text{--}63\mu\text{m}$ size fractions (plant material) had a smaller weight contribution.

C/N ratios were highest for the $>125\mu\text{m}$ size fraction and generally decreased with decreasing particle size (Figure 16b). The $>125\mu\text{m}$ material had a mean C/N value of 38.06 ± 11.26 , whereas the $4\text{--}63\mu\text{m}$ fraction had a mean of 28.42 ± 8.91 . The silt- and clay-sized particles had overall mean values of 17.79 ± 2.86 and 15.45 ± 3.99 , respectively. Bulk C/N ratios averaged 21.91 ± 3.95 and fell between those for individual size fractions, reflecting mixing among them.

To gain insight on the relationship between soil physical properties and organic carbon content, profiles of dry bulk density (Equation 4), organic matter density ($\rho_d \times LOI$) and mineral sediment density ($\rho_d \times (1 - LOI)$) were constructed for the long cores and compared to corresponding profiles of size-specific carbon concentration (Equation 10) and total carbon concentration (Equation 11). These profiles are presented in Figures 17–21. In all cases, organic density remained fairly constant with depth, and variations in dry bulk density corresponded to depth changes in mineral density. In most cases soil mineral density was greater than the organic

density. The only exception to this was observed in VCBC at 122.5 and 152.5 cm depth, where organic density was slightly higher than mineral density (Figure 20).

The >125 μm size fraction had the highest carbon concentration (expressed as g C cm^{-3}) in VCMR and VCKI in the upper depths of the cores. In the lower depths of these cores, silt-sized material had the highest carbon concentrations. Additionally, the >125 μm size fraction contributed most to the total carbon concentration for the VCGM core. For VCBC and VCSG, silt-sized particles had the highest carbon concentrations at almost all depths compared to the other size fractions. Clay-sized particles had the second highest carbon concentrations in VCSG and the >125 μm fraction had the second highest carbon concentrations in VCBC. For all cores, the 4–63 μm fraction had the lowest carbon concentrations and did not contribute much to the total carbon concentration. Lastly, carbon concentrations for silt- and clay-sized particles remained relatively constant with depth in VCGM, VCMR, and VCKI, but were more variable in VCBC and VCSG. On average, total carbon concentrations were highest in VCGM ($0.044 \pm 0.012 \text{ g C cm}^{-3}$; $n=5$) and lowest in VCSG ($0.028 \pm 0.0053 \text{ g C cm}^{-3}$; $n=7$).

The relative contributions of the soil size fractions to the total, long-term carbon accumulation rate was computed by depth-integrating the carbon concentration profiles shown in Figures 17–21 and dividing by the bottommost ^{14}C age date (Figure 22). Interestingly, the silt-sized fraction contributed most (18.3–47.9 $\text{g C m}^{-2} \text{ yr}^{-1}$) to the total carbon accumulation rate at sites VCMR, VCBC, and VCSG, whereas the >125 μm fraction contributed most (7.1–32.6 $\text{g C m}^{-2} \text{ yr}^{-1}$, $n=5$) at sites VCGM and VCKI (Figure 22). The clay-sized fraction contributed less (6.4–18.9 $\text{g C m}^{-2} \text{ yr}^{-1}$) and the 4–63 μm size fraction the least overall (1.3–3.7 $\text{g C m}^{-2} \text{ yr}^{-1}$). In summary, at four

of the five tidal marsh sites sampled for this study, silt- and clay-sized particulate organic carbon, in some manner associated with mineral sediment, contributed more to the long-term carbon accumulation rate than plant biomass fractions, as much as 44–88% of the total CAR. The implications of this finding are explored in Chapter 4.

Chapter 4

DISCUSSION

4.1 Spatial Variability of Organic Carbon Accumulation in Tidal Marshes

Rates of organic carbon accumulation in tidal marshes vary with a variety of factors including plant productivity rates, decomposition rates, allochthonous mineral sediment and particulate organic matter inputs (Megonigal and Neubauer, 2009; Tobias and Neubauer, 2009). These factors are ultimately a function of wetland hydrogeomorphic setting, including the salinity and nutrient content of source waters and tidal sedimentary processes. Results of this study demonstrate that carbon accumulation rates vary along the salinity gradient of Delaware Estuary, generally increasing with decreasing salinity as observed in other estuarine systems (Callaway et al., 2012; Craft, 2007; Loomis and Craft, 2010; Neubauer et al., 2002; Neubauer, 2008). The brackish marshes (n=6) sampled had an average short-term carbon accumulation rate of $246.4 \pm 101.8 \text{ g C m}^{-2} \text{ yr}^{-1}$, whereas the salt marshes (n=18) averaged $147.8 \pm 65.9 \text{ g C m}^{-2} \text{ yr}^{-1}$. ANOVA analysis indicated that the means of this ranges are not significantly different ($p=0.066$). As these rates were computed as the product of mass accumulation rate and organic carbon concentration, spatial variations in these two variables can explain much of the along-estuary variability in organic carbon accumulation, as elaborated below.

Previous work on marsh accretion and sediment accumulation in Delaware Estuary by Sommerfield and Velinsky (2010) has demonstrated that accretion rates generally decrease seaward from tidal freshwater segment to the brackish and saline

segments of the estuary. This pattern partly reflects the proximity of fringing wetlands to the resident suspended sediment load of the estuary, and fluxes of suspended sediment from the estuary to the wetlands. Suspended sediment concentrations in Delaware Estuary are intermediate (25–50 mg L⁻¹) in the tidal freshwater river, highest in the brackish estuary (50–250 mg L⁻¹), and lowest in the saline bay (<25 mg L⁻¹); concentrations are especially high (200–500 mg L⁻¹) in bottom waters of the turbidity maximum zone, which extends from about Wilmington southward to Bombay Hook (Cook et al., 2007; Sommerfield and Wong, 2011). Wetlands in the upper and middle estuary, i.e., proximal to the turbidity maximum zone, have the highest potential to capture suspended sediment transported landward from the estuary. Below Bombay Hook where suspended sediment concentrations are lower, sediment transported landward to the salt marshes is sourced mostly from marsh edge erosion, a relatively small source of sediment. Hence, from the head to mouth of Delaware Estuary, there should be a general decrease in the net estuary-to-wetland flux of suspended sediment.

Sedimentation rates are important in controlling carbon burial in Delaware Estuary. St. Georges has lower surface organic carbon concentrations than the other six marshes (Figure 8), but has higher surface dry bulk density (Figure 5) and the highest accretion rates among the seven marshes. The latter factor leads to higher rates of carbon accumulation in St. Georges than the other six marshes. This supports the idea that sediment accumulation rate may be more important than TOC concentration in moderating rates of carbon accumulation among the marsh sites investigated. Higher rates of mineral sediment deposition have potential to bury

organic carbon and remove it from the oxic zone quicker than locations with lower deposition rates.

Similar spatial gradients in organic carbon accumulation have been observed for other U.S. tidal marshes. In a study of three coastal plain estuaries in Georgia, Loomis and Craft (2010) found that mineral sediment accumulation rates (based on ^{137}Cs dating) were highest in brackish marshes ($1191 \pm 256 \text{ g m}^{-2} \text{ yr}^{-1}$), intermediate in tidal freshwater marshes ($856 \pm 105 \text{ g m}^{-2} \text{ yr}^{-1}$), and lowest in salt marshes ($537 \pm 103 \text{ g m}^{-2} \text{ yr}^{-1}$). Similarly, they found higher rates of organic carbon accumulation in tidal freshwater ($124 \pm 10 \text{ g C m}^{-2} \text{ yr}^{-1}$) and brackish marshes ($93 \pm 17 \text{ g C m}^{-2} \text{ yr}^{-1}$) compared to salt marshes ($40 \pm 7 \text{ g C m}^{-2} \text{ yr}^{-1}$). They interpreted this trend to reflect marsh proximity to the estuarine turbidity maximum and riverine sediment sources. The apparent relationship between carbon accumulation rate and mineral sediment accumulation rate identified by Loomis and Craft (2010) is supported by the present results in Delaware Bay.

Regression analysis of the short core data indicates a strong positive relationship between measured rates of organic carbon accumulation rates and both organic matter and mineral sediment inventory, the depth-integrated organic and sediment density above the 1963 reference depth. As shown in Figure 23, 59% of the variation in carbon accumulation rates can be explained by variation in the mineral inventory and 83% by the organic matter inventory. Because marsh plant production and allochthonous organic inputs are necessary for carbon accumulation in soils, low rates of production and input lead to low carbon inventories (note the zero intercept of the trendline in Figure 23a). In contrast, it is possible for organic carbon to accumulate even when mineral sediment inputs are low (Figure 23b). Hence, inputs of

organic matter and mineral sediment set the minimum and maximum rates of carbon accumulation in tidal marsh soils. The apparent function of rapid mineral sedimentation is to transport labile carbon from the oxic zone into deeper, anoxic soils and thereby reduce the rate of decomposition (Connor et al., 2001).

4.2 Time-Dependent Carbon Accumulation in Marshes

Results of this study demonstrate that rates of organic carbon accumulation in Delaware Estuary marshes are temporally variable, but further that they are dependent on the averaging period. As shown in Figure 24, short-term accumulation rates based on ^{137}Cs and ^{210}Pb chronology (50–100 year average) were consistently higher than the longer-term rates determined by ^{14}C dating (centuries to millennia) for the same coring site. Similarly, rates of marsh vertical accretion, organic matter accumulation, and mineral sediment accumulation were found to be lower when averaged over longer timespans (Table 5).

Time-dependent organic carbon accumulation is apparent from research of other tidal marsh systems. For example, for a San Francisco Bay tidal marsh Callaway et al. (2012) measured carbon accumulation rates of $156 \text{ g C m}^{-2} \text{ yr}^{-1}$ and $107 \text{ g C m}^{-2} \text{ yr}^{-1}$ at sites using ^{137}Cs and ^{210}Pb methods, respectively. For the same location, Drexler (2011) reported a carbon accumulation rate of $79 \pm 46.1 \text{ g C m}^{-2} \text{ yr}^{-1}$ averaged over 6150 cal yr BP based on ^{14}C dating. For tidal marshes in St. Marks National Wildlife Refuge, northwest Florida, Choi and Wang (2004) report carbon accumulation rates of $130 \pm 9 \text{ g C m}^{-2} \text{ yr}^{-1}$ averaged over the last 100 years, but significantly lower rates of $13 \pm 2 \text{ g C m}^{-2} \text{ yr}^{-1}$ averaged over several 1000s of years. Choi and Wang (2004) attributed this difference to decomposition with time.

Although there are a number of possible interpretations for time-dependent carbon accumulation in tidal marshes, two overarching factors include (1) continual organic matter decomposition and decrease in carbon concentration over time, and (2) stratigraphic incompleteness produced by periodic hiatuses in organic and mineral sediment accumulation. The relative influences of these factors can be assessed by plotting composite depth profiles of carbon accumulation rate, carbon concentration, and mass accumulation rate as a function of timespan. As shown in Figure 25, both carbon accumulation and mass accumulation rates decrease with increasing age. On the other hand, carbon concentration does not vary over the same timespans. Hence, it is unlikely that progressive decomposition of organic matter over time explain the difference between short- and long-term rates of carbon accumulation.

It is likely that stratigraphic incompleteness has a major influence on time-dependent carbon accumulation in Delaware Estuary tidal marshes. In estuarine and marine sedimentary environments, stratigraphic incompleteness results from periods of non-deposition or erosion (McKee et al., 1983; Sommerfield, 2006). As more time is incorporated into a sediment column, it is liable to include gaps in the record known as hiatuses. Hiatuses are evidenced by the general inverse relationship between sediment accumulation rates and the timespan over which these rates are averaged, as shown for other sedimentary environments (Neubauer et al., 2002; Sommerfield, 2006). This is why sediment accumulation rates determined using ^{137}Cs and ^{210}Pb chronology (50–100 average) are generally higher than rates based in ^{14}C dating (centuries to millennia). Because tidal marsh sedimentation is not a steady-state process, it stands to reason that the soil column should be less than 100% complete

and that sediment (and carbon) accumulation rates will vary inversely with the averaging period.

4.3 Geologic Influences on Carbon Accumulation Rates

Geologic history is a frequently overlooked consideration in wetland carbon accumulation studies. Tidal marshes undergo many changes throughout their lifetime due to variations in sea level, salinity, and sediment inputs, which influence patterns and rates of marsh horizontal expansion, marsh loss by edge erosion, and successional changes in marsh types. These changes influence carbon accumulation in marshes by moderating rates of plant growth and vertical accretion, and sources of allochthonous particulate organic matter and mineral sediment.

In Delaware Estuary, estuarine mud became available to the present-day mouth of the estuary between 9 ka and 7 ka (Fletcher et al., 1990; Fletcher et al., 1992), allowing tidal marshes to develop in this area. Although salt marshes currently occupy the mouth of Delaware Estuary, at 9-7 ka the tidal marshes were likely tidal freshwater or brackish. As the mud depocenter moved up-estuary towards its current location, the tidal marshes would have moved inland with rising sea level and/or transitioned to salt marshes as salinities increased. Because the sediment source moved up-estuary, accretion rates presumably decreased over time in the present-day salt marshes. As the marshes transgressed landward, wave erosion along the estuary coast began to rework older marsh strata and produce organic and mineral-sediment particulates. Some of this material is available to be tidally transported to the wetland interior where it is re-deposited on tidal flats and marsh platforms.

Effects of coastal environmental change on wetland carbon accumulation were described in a study by Brevik and Homburg (2004). They estimated carbon

accumulation over 5000 years in the Ballona wetlands of Southern California, using a suite of sediment cores that captured different wetland paleo-environments. An average of $39 \text{ g C m}^{-2} \text{ yr}^{-1}$ was sequestered in salt marsh sediments, $41 \text{ g C m}^{-2} \text{ yr}^{-1}$ in intertidal sediments, $20 \text{ g C m}^{-2} \text{ yr}^{-1}$ in freshwater marsh sediments, $9 \text{ g C m}^{-2} \text{ yr}^{-1}$ in aeolian deposits, and $52 \text{ g C m}^{-2} \text{ yr}^{-1}$ in lagoonal sediments (Brevik and Homburg, 2004). The spatially and temporally (5000 years) averaged rate of carbon accumulation the wetland was determined to be $33 \text{ g C m}^{-2} \text{ yr}^{-1}$. Hence, because different paleo-environments of wetlands sequester carbon at different rates, recent geologic history is an important consideration in carbon sequestration studies.

On the tidal wetland coast of Delaware Bay, Pizzuto and Rogers (1992) identified four different depositional environments over $11,480 \pm 150 \text{ yr BP}$ at Duck Creek, DE, including a fluvial channel, freshwater palustrine wetland, oligohaline estuarine wetland, and a tidal river channel. They suggested that that Duck Creek did not become an estuarine or riverine wetland until 1000 yr BP. The Leipsic River had three former depositional environments identified over $8,020 \pm 100 \text{ yr BP}$: non-tidal fluvial channel, palustrine wetland, and floodplain. Apparently, oceanic tides did not impact these areas until about 1000-2000 years ago (Pizzuto and Rogers, 1992); hence, some of the present-day marshes of the estuary only recently converted to tidal marshes. Pizzuto and Rogers (1992) showed that these depositional environments changed throughout the Holocene, evolving into different environments under changing environmental conditions and relative sea level. Again, it is probable that these changing conditions resulted in differences in carbon accumulation rates on the wetland coast of Delaware Estuary.

4.4 Size-Specific Soil Carbon Accumulation

It is well known that tidal marsh soils consist of plant biomass carbon (living and dead) produced *in situ* by plants, allochthonous detrital carbon, and mineral-bound carbon delivered by the tides, along with carbon associated with microorganisms. However, little is known about the relative importance of these carbon pools on soil formation and measured rates of carbon accumulation. This is so because virtually all of what is known about marsh soil diagenesis and belowground carbon cycling has been based on studies of bulk soil material, which is an amalgam of locally produced plant biomass and externally derived particulate carbon. In reality, different components of the soil will have different reactivities and mineralization rates depending on the carbon composition and availability to microbes. Hence, although most workers recognize the existence of labile and refractory carbon pools associated with fresh plant biomass and degraded particulate carbon, respectively (e.g., Morris and Bradley, 1999), the relative influence of these pools on mineralization has been treated only conceptually and qualitatively. For example, Connor et al. (2001) observed that live roots contribute to the total soil carbon pool only in the upper depths of the marsh, whereas dead roots and fine particulate carbon contribute at all depths. However, they did not address the provenance (local production versus import) or reactivity of the soil carbon components.

It is intuitive that plant biomass should be the dominant source of organic carbon in marsh soils, but as shown in this study fine-grained organic and inorganic particles may be quantitatively important in allochthonous marsh systems (Figure 22). A significant quantity of organic carbon associated with clay-sized (<4 μm) and silt-sized (4–63 μm) mineral solids were found to accumulate along with larger (>125 μm and 63–125 μm) plant biomass carbon. This result is consistent with the work of

Elsy-Quirk et al. (2011), who in a study of a Delaware coastal marsh found that most (64–93%) of the total soil carbon pool was associated with <1 mm diameter particles with the balance composed of living and dead plant biomass. Although plant biomass had the highest *concentration* of soil carbon in samples examined for the study, the *mass* of silt-sized carbon was large enough (and the carbon concentration high enough) for it to comprise the largest component of the total carbon concentration in four of the five long cores examined. Clay-sized particles contributed more carbon to the soil overall than the 63–125 μ m fraction, which had relatively larger carbon concentrations but lower weight percentages.

Differences in the contribution of each individual soil size fraction to the total carbon concentration are apparent for tidal marshes of Delaware Estuary. At the most saline site (Great Marsh), the >125 μ m fraction had the highest carbon concentration for all depths above the bottommost interval, where silt carbon concentration was the highest of all the size fractions (Figure 17). At Mispillion River and Kelly Island, the >125 μ m fraction had the highest carbon concentration above about 100 cm, below which carbon concentration was dominated by the silt and clay fractions (Figure 18 and Figure 19). At Blackbird Creek and St. Georges (brackish marsh sites) the highest carbon concentration was associated with the silt fractions (Figure 20 and Figure 21). Overall, it would appear that the >125 μ m size fraction of the total carbon concentration increases in importance down-estuary from the brackish to salt marshes, and that silt-associated carbon is most important component in at least some of the brackish marshes.

Based on the long-core profiles of carbon concentrations, temporal (down-core) variations in the amount of carbon associated with soil size fractions reflects

some combination of marsh depositional conditions and post-depositional organic matter decomposition. Only the uppermost profiles for the >125 μm size fraction (plant biomass) exhibited a distribution that could be explained by depth decreases in carbon concentration related to mineralization processes. The smaller size fractions had depth profiles characterized by uniform (63–125 μm and clay) or moderately variable (silt) depth profiles of carbon concentration. Depth distributions for these size fractions suggest that deposition conditions such as tidal flooding, suspended sediment concentration, and particulate organic carbon concentration have not changed over the time span captured by the long cores (732–1459 cal yr BP).

4.5 Sources and Pathways of Marsh Soil Carbon

The soil fractionation procedure employed in this study helps clarify the origin and cycling of different organic carbon pools in tidal marsh soils. The organic carbon composition (C/N and $\delta^{13}\text{C}$) of tidal marsh soils has traditionally been explained in two ways: (1) preferential decomposition of labile, isotopically heavy (^{13}C -rich) carbon substrates and selective preservation of refractory, isotopically light substrates (e.g., Benner et al., 1991; Wang et al., 2003); and (2) tidal input of particulate organic matter, including non-locally produced plant matter, phytoplankton, microphytobenthos, and mineral-associated carbon (Middelburg et al., 1997; Neubauer et al., 2002; Zhou et al., 2006; Zhou et al., 2007). Knowing that Delaware Estuary marshes trap tidally imported particles and are dominated by deposition, some of carbon present in the marsh soil column is presumably sourced in adjacent waters.

Measurements of stable carbon isotope ($\delta^{13}\text{C}$) were not made in this study to constrain carbon sources, but C/N ratios can be used as a proxy. Results indicate that C/N ratios for the >125 μm soil fraction are highest (average= 38.06 ± 11.26) and

generally decrease with decreasing particle size (Figure 15). These highest ratios are consistent with C-3 and C-4 plant sources (Meyers, 1994), which is expected since the $>125\mu\text{m}$ material was exclusively living or dead plant biomass. The C/N ratios for the $63\text{--}125\mu\text{m}$ fraction were slightly lower (average= 28.42 ± 8.91), indicating a higher ratio of decomposed plant material. The C/N ratios for the silt- and clay-sized particles averaged 17.79 ± 2.86 and 15.49 ± 3.99 , respectively. These values, which are consistent with C/N ratios reported for fine-grained sediment in minerogenic tidal marshes (Middelburg et al., 1997), reflect mixing of some combination of decomposed marsh plant material, algal organic carbon, and perhaps terrestrial soil carbon associated with mineral grains.

In a scatter plot of C/N versus TOC concentration, coarse ($>63\mu\text{m}$) and fine ($<63\mu\text{m}$) sample size fractions cluster at either ends of the data continuum (Figure 26). Hence, while the soils are bound to contain a mixture of carbon sources, coarse and fine particulates are somewhat distinct in terms of carbon composition. This distinction is clear from depth profiles of C/N ratio for the long cores. As shown in Figure 27, there is little to no overlap of C/N profiles for the coarse and fine soil fractions, suggesting that these carbon pools are more or less stable and separate on timescales of several centuries to just over a millennium. The general decrease in C/N ratios from the coarse to fine soil fractions (Figure 26) reflects differences in particulate carbon sources and transport pathways prior to deposition rather than belowground decomposition and preferential preservation. In the case of the silt- and clay-sized particles, the lack of change in C/N over time may be a consequence of carbon stabilization associated with grain morphology as observed for terrestrial soils and marine sediments (Baldock and Skjemstad, 2000; Dungait et al., 2012; Mayer,

1994; Wakeham et al., 2009.). Organic matter associated with fine mineral particles is stable and more resistant to mineralization, and this fraction may be more important to long-term carbon accumulation and preservation than plant-derived organic matter.

Results of this study demonstrate that detrital silt- and clay-sized particles are quantitatively important in bulk rates of carbon accumulation for tidal marshes, contributing 30–70% of the total. The C/N ratios for the silt- and clay-sized soil fractions are not consistent with estuarine-marine planktonic (4–10; Meyers, 1994) or terrestrial carbon sources (>20; Meyers, 1994), thus it is more likely that this carbon is sourced within the marsh itself, perhaps associated with the decay of *Spartina* litter and roots. However, a more detailed compositional study is required to confirm this idea.

Marsh edge erosion and redeposition of fine particles, and perhaps bioturbation, are likely sources of aged, fine-grained carbon in Delaware Estuary. The existence of large quantities of aged carbon has implications for conceptual views of carbon cycling in tidal wetlands, as the role of this material is not explicitly addressed in carbon budgets (e.g., Bridgham et al., 2006). It is likely that aged marsh carbon must be considered in model budgets from some wetland systems. A related issue is the fate of particulate and mineral-associated carbon sourced by marsh edge erosion, a ubiquitous process on transgressive coasts. Results of this research suggest that at least some of this material is redeposited on the marsh platform, influencing rates of carbon accumulation and perhaps the overall carbon budget for the wetland coast of Delaware Estuary.

Chapter 5

REGIONAL AND GLOBAL VARIABILITY IN TIDAL MARSH CARBON ACCUMULATION

5.1 Soil Carbon Accumulation Rates

As noted previously, rates of short- and long-term soil carbon accumulation determined for Delaware Estuary marshes are comparable to rates reported for similar U.S. tidal marshes. More broadly, it is instructive to compare these rates to those reported for tidal marshes worldwide. In a review of the literature, Ouyang and Lee (2014) synthesized carbon accumulation rate data for 143 sampling sites and subdivided them into seven geographic regions with three U.S. subregions. These short-term rates (based on ^{137}Cs or ^{210}Pb geochronology) were determined following similar methods to those employed in this study. As shown in Table 6 the globally averaged rate is $244.7 \pm 26.1 \text{ g C m}^{-2} \text{ yr}^{-1}$ ($n=143$). In the U.S., rates are highest in the Tropical Western Atlantic Region (Gulf Coast states), intermediate in the Northeast Pacific Region (West Coast), and lowest in the Northwest Atlantic region (North and South Atlantic coasts). By comparison, the mean rate for the brackish and salt marshes sampled in this study was $172.4 \pm 35.2 \text{ g C m}^{-2} \text{ yr}^{-1}$ ($n=24$), which is nearly identical to the Northwest Atlantic regional rate determined by Ouyang and Lee (2014).

Marsh carbon accumulation rates for the U.S. East Coast fall below the global average presumably because of differences in vegetation type, tidal range, sediment availability, latitude, and temperature. Firstly, marsh zonation (low, mid, high) is

classified by frequency of tidal inundation and changes in vegetation type. It is known that low marsh environments often have higher carbon accumulation rates than high marsh environments (Connor et al., 2001; Ouyang and Lee, 2014) because of higher rates of mineral sediment accumulation in low marsh zones (Chmura and Hung, 2004). Also, it is important to note that changes in salinity, elevation, and nutrient inputs to a marsh system will influence vegetation productivity (Kirwan et al., 2009) and subsequent carbon burial.

Different types of marsh vegetation will have different carbon burial efficiencies. Of five genera of halophytes, *Spartina* had an average carbon accumulation rate of the 200.9 g C m⁻² yr⁻¹ (Ouyang and Lee, 2014), which was the highest rate compared to four other genera of halophytes (*Distichlis*, *Halimione*, *Juncus*, *Phragmites*). In contrast, *Distichlis* had the lowest carbon accumulation rates with an average rate of 107.5 g C m⁻² yr⁻¹ (Ouyang and Lee, 2014). Vegetation type may be an important factor in carbon accumulation since different types of vegetation have different rates of decomposition (Hopkinson et al., 1978; Valiela et al., 1985; Windham, 2001). On the other hand, in their review, Ouyang and Lee (2014) found no significant relationship between vegetation type and carbon accumulation rates. It is more likely that tidal influences and sediment availability are more important controls on carbon accumulation rates (Connor et al., 2001).

Ouyang and Lee (2014) found that carbon accumulation rates in salt marshes are highest in mid-latitudes (48.5-58.5° N), likely due to the length of the growing season and possibly sediment salinity changes influenced by rain and evaporation trends. Carbon accumulation rates are highest within these latitudes because there is an optimum balance between primary productivity and decomposition rates since

decomposition rates are influenced by temperature (Chmura et al., 2003; Kirwan et al., 2014). These latitudes would incorporate the European salt marshes, which as mentioned previously have the highest carbon accumulation rates on average globally (Table 6). A positive relationship exists between the decay of organic matter and soil temperature (Kirwan et al., 2014), and although areas with higher temperatures may have longer vegetation growing seasons (Kirwan et al., 2009) higher temperatures would also likely be associated with higher rates of decomposition (Chmura et al., 2003; Craft, 2007). This could be the case for U.S. salt marshes and one reason why Delaware Estuary marsh has somewhat lower carbon burial rates than the global average. On the other hand, Ouyang and Lee (2014) found that mean average temperature did not significantly influence carbon accumulation rates.

5.2 Marsh Carbon Storage

Carbon accumulation rates ($\text{g C m}^{-2} \text{yr}^{-1}$) represent the burial flux of carbon into sediments, whereas carbon storage or carbon inventory (g cm^{-2}) is calculated as the summed products of carbon concentration (g C cm^{-3}) and interval thickness (cm). To estimate the carbon stock (g C) for a certain region, the at-site carbon inventory (g cm^{-2}) is multiplied by the marsh surface area (cm^2). Carbon stocks are used when assigning monetary values to tidal marshes (DeLaune and White, 2012). In Delaware Estuary marshes, the average carbon accumulation rate is $172.4 \pm 85.9 \text{ g C m}^{-2} \text{yr}^{-1}$, which equates to $0.009 \pm 0.006 \text{ Tg C km}^{-2}$ (1 gram = 10^{-12} Tg) since 1963. For the western coast of Delaware Estuary (in the state of Delaware), the area of tidal marshland is 308 km^2 (Tiner et al., 2011). Hence, the estimated carbon stock for this region is $2.9 \pm 1.9 \text{ Tg C}$.

Most studies report carbon accumulation rates ($\text{g C m}^{-2} \text{ yr}^{-1}$), but comparisons can be made across different global regions when land area is considered (Table 6). For example, Ouyang and Lee (2014) report that northern and southern Europe (which includes salt marshes of the Mediterranean) are the two regions with the highest average carbon accumulation rates, however marshes in these regions make up 2,302 km^2 and 93 km^2 of the land area, respectively (Table 6). This results in an estimated soil carbon accumulation of $0.72 \pm 0.12 \text{ Tg C yr}^{-1}$ in Europe marshes and $0.30 \pm 0.01 \text{ Tg C yr}^{-1}$ in North Africa marshes. Northwest Atlantic and northwest Pacific regions have the lowest carbon accumulation rates on average but occupy large areas of land. The northwest Atlantic region has 2,685 km^2 of marsh area and the northeast Pacific has 7,984 km^2 of marsh area, leading to soil carbon accumulation rates of $0.36 \pm 0.03 \text{ Tg C yr}^{-1}$ and $1.39 \pm 0.36 \text{ Tg C yr}^{-1}$, respectively (Ouyang and Lee, 2014). These rates are comparable, and in the case of the northeastern Pacific marshes, higher than the European/Mediterranean marshes, solely due to the tidal marsh land area.

Of the estimated $0.36 \pm 0.03 \text{ Tg C yr}^{-1}$ accumulated in northwest Atlantic marshes (Ouyang and Lee, 2014), Delaware Estuary marshes examined in this study accumulate an estimated $0.05 \pm 0.005 \text{ Tg C yr}^{-1}$. This is equivalent to ~14% of the total amount of carbon accumulated in the northwest Atlantic region as reported by Ouyang and Lee (2014). Based on these calculations, Delaware estuarine marshes are quantitatively important in the northwest Atlantic regional stock of carbon. Hence, loss of Delaware marshes by natural or human causes would significantly reduce the size of the regional stock. Although speculative, this estimate of carbon demonstrates the significance of Delaware Estuary marshes and provides further motivation for protection and restoration.

Chapter 6

CONCLUSIONS

The overarching goal of this study was to advance our understanding of the spatial, temporal, and sedimentological variations in organic carbon accumulation in Delaware Estuary tidal marshes as a means to advance our general knowledge of tidal marsh soil formation and carbon burial. These aspects of marsh carbon burial have not been previously addressed together in a prior of tidal marsh systems. The concept of size-dependent carbon accumulation has *never* been examined in previous studies, and the results reported in this thesis have implications to coastal and estuarine carbon cycles.

In terms of spatial variability, it was found that carbon accumulation rates are higher in brackish marshes ($246.4 \pm 101.9 \text{ g C m}^{-2} \text{ yr}^{-1}$) than salt marshes ($147.8 \pm 66 \text{ g C m}^{-2} \text{ yr}^{-1}$) of the estuary, and that carbon accumulation rates increased with increasing rates of mineral sediment accumulation. The higher rates of carbon burial in the brackish marshes can be explained from their closer proximity to the estuarine turbidity maximum in Delaware Bay.

Short-term carbon accumulation rates ($172.4 \pm 85.9 \text{ g C m}^{-2} \text{ yr}^{-1}$) were found to be higher than long-term carbon accumulation rates ($72.8 \pm 24.3 \text{ g C m}^{-2} \text{ yr}^{-1}$). Although this result was expected, carbon concentrations and C/N ratios did not indicate trends that could be explained by post-depositional decomposition alone. It is more likely that non-steady-state organic matter production and mineral sediment

accumulation control long-term rates of carbon accumulation in marsh soils of Delaware Estuary.

Lastly, there was a clear size-dependence of carbon accumulation when comparing four size fractions ($>125\mu\text{m}$, $63\text{--}125\mu\text{m}$, $4\text{--}63\mu\text{m}$, $<4\mu\text{m}$). Significantly, fine-grained ($<63\mu\text{m}$) fractions of the soil contributed $>40\%$ to the total carbon buried on the long term, exceeding that contributed by plant biomass in some cases. Based on C/N data, the fine grained fraction of the soil carbon appeared to be marsh-sourced rather than particulate carbon imported from adjacent estuarine waters. It is likely that some combination of marsh edge erosion and perhaps bioturbation are responsible for reintroducing this aged, fine grained carbon to the marsh surface where is redeposited with living and dead plant biomass. Given that most carbon budgets are based on bulk carbon concentrations for soils and sediments, these results have implications to our evolving understanding of carbon cycling in tidal wetlands and adjoining coastal waters.

Tidal marshes along the Delaware coast of Delaware Estuary accumulate an estimated $0.05 \pm 0.005 \text{ Tg C yr}^{-1}$, based on ^{137}Cs -derived carbon accumulation rates computed for this study. This is equivalent to $\sim 14\%$ of the total carbon sequestered in U.S. Atlantic coast marshes (Ouyang and Lee, 2014). Hence, a large sink of carbon would be lost if Delaware Estuary marshes were to disappear through edge erosion or conversion to open water under the influences of sea level rise and human pressures.

TABLES

Table 1: Information for the 24 short cores and five long cores used for this study. Asterisks indicate cores collected specifically for this study. The other cores were collected for prior research by C. Sommerfield and D. Velinsky.

| Location (Abbreviation) | Core Id | LAT | LON | Length (cm) | Collection Date |
|---------------------------------|---------|-------------|-------------|----------------|--------------------|
| Canary Creek, DE (CC) | CC-1 | 38° 46.867' | 75° 10.112' | 65 | 5/10/2007 |
| | CC-2 | 38° 46.918' | 75° 10.203' | 55 | 5/10/2007 |
| | CC-3 | 38° 46.968' | 75° 10.253' | 81 | 5/10/2007 |
| | *CC-5 | 38° 47.013' | 75° 10.398' | 50 | 7/1/2014 |
| | *CC-6 | 38° 46.978' | 75° 10.338' | 50 | 7/12/2014 |
| Great Marsh, DE (GM) | GM-1 | 38° 47.989' | 75° 11.738' | 87 | 5/10/2007 |
| | GM-2 | 38° 47.920' | 75° 11.870' | 75 | 5/10/2007 |
| | GM-3 | 38° 47.873' | 75° 11.962' | 78 | 5/10/2007 |
| | *GM-4 | 38° 47.937' | 75° 12.424' | 50 | 8/7/2014 |
| | *VCGM | 38° 47.937' | 75° 12.424' | 229.5 | 8/7/2014 |
| Kelly Island, DE (KI) | KI-1 | 39° 12.466' | 75° 24.504' | 80 | 6/21/2007 |
| | KI-2 | 39° 12.762' | 75° 24.252' | 72 | 6/21/2007 |
| | KI-3 | 39° 12.201' | 75° 24.034' | 72 | 6/21/2007 |
| | *VCKI | 39° 12.201' | 75° 24.034' | 213 | 10/9/2014 |
| Mispillion River, DE (MR) | MR-1 | 38° 56.872' | 75° 21.233' | 76 | 7/3/2007 |
| | MR-2 | 38° 56.930' | 75° 21.366' | 76 | 7/3/2007 |
| | MR-3 | 38° 56.740' | 75° 21.448' | 88 | 7/3/2007 |
| | *VCMR | 38° 56.930' | 75° 21.366' | 239.5 | 10/21/2014 |
| Blackbird Creek, DE (BC) | BC-1 | 39° 26.063' | 75° 35.014' | 72 | 5/15/2008 |
| | BC-2 | 39° 25.874' | 75° 35.818' | 80 | 5/15/2008 |
| | BC-3 | 39° 25.400' | 75° 36.108' | 94 | 5/15/2008 |
| | *VCBC | 39° 25.874' | 75° 35.818' | 185 | 11/14/2014 |

| Location (Abbreviation) | Core Id | LAT | LON | Length (cm) | Collection Date |
|----------------------------------|---------|-------------|-------------|----------------|--------------------|
| St. Georges Marsh, DE (SG) | SG-1 | 39° 32.480' | 75° 34.520' | 100 | 6/9/2008 |
| | SG-2 | 39° 32.769' | 75° 34.196' | 96 | 6/9/2008 |
| | SG-3 | 39° 32.072' | 75° 34.468' | 94 | 6/9/2008 |
| | *VCSG | 39° 32.072' | 75° 34.468' | 207 | 11/14/2014 |
| St. Jones Reserve, DE (SJ) | SJBM-1 | 39° 05.313' | 75° 26.160' | 74 | March 2012 |
| | SJBM-2 | 39° 05.046' | 75° 26.284' | 78 | March 2012 |
| | SJBM-3 | 39° 04.703' | 75° 26.322' | 110 | March 2012 |

Table 2: Radiocarbon data for the dated root material from soil cores. $\Delta^{14}\text{C}$ and $\delta^{13}\text{C}$ values are also shown.

| Lab ID | Core Id | Depth (cm) | Conventional Age (yr BP) | ^{14}C Error (yr BP) | Calibrated Age Ranges | $\Delta^{14}\text{C}$ (‰) | $\delta^{13}\text{C}$ (‰) |
|-----------|---------|------------|--------------------------|-------------------------------|-----------------------|---------------------------|---------------------------|
| OS-118074 | VCGM | 2.5 | >Modern | | | 24.50 | -12.97 |
| OS-118075 | VCGM | 32.5 | >Modern | | | -6.26 | -12.72 |
| OS-118076 | VCGM | 62.5 | 180 | 15 | 20-285 | -29.79 | -10.04 |
| OS-118077 | VCGM | 92.5 | 300 | 20 | 302-430 | -43.92 | -9.93 |
| OS-118078 | VCGM | 122.5 | 905 | 15 | 769-909 | -113.64 | -13.42 |
| OS-118079 | VCMR | 2.5 | >Modern | | | 33.21 | -13.81 |
| OS-118080 | VCMR | 32.5 | >Modern | | | 488.23 | -12.01 |
| OS-118081 | VCMR | 62.5 | 165 | 15 | 1-283 | -27.93 | -11.61 |
| OS-118082 | VCMR | 94 | 270 | 15 | 289-423 | -40.64 | -10.26 |
| OS-118083 | VCMR | 122.5 | 400 | 15 | 339-506 | -55.66 | -11.20 |
| OS-118084 | VCMR | 152.5 | 915 | 15 | 787-909 | -114.39 | -11.79 |
| OS-118085 | VCMR | 186.5 | 1170 | 15 | 1012-1174 | -142.24 | -10.14 |
| OS-118292 | VCMR | 216.5 | 1590 | 15 | 1414-1530 | -185.63 | -11.30 |
| OS-118364 | VCKI | 2.5 | >Modern | | | 46.58 | -13.26 |
| OS-118360 | VCKI | 32.5 | >Modern | | | 97.50 | -12.06 |
| OS-118293 | VCKI | 62.5 | 175 | 20 | 1-185 | -29.30 | -11.23 |
| OS-118294 | VCKI | 92.5 | 245 | 20 | 155-307 | -37.73 | -11.72 |
| OS-118295 | VCKI | 122.5 | 255 | 15 | 155-312 | -38.98 | -10.95 |
| OS-118361 | VCKI | 152.5 | 275 | 15 | 289-424 | -40.83 | -12.35 |
| OS-118296 | VCKI | 182.5 | 990 | 15 | 804-950 | -122.68 | -10.86 |
| OS-119977 | VCBC | 2.5 | >Modern | | | 18.63 | -12.71 |
| OS-119978 | VCBC | 32.5 | 190 | 15 | 1-287 | -30.70 | -11.31 |
| OS-119979 | VCBC | 62.5 | >Modern | | | 15.96 | -11.55 |
| OS-120086 | VCBC | 93 | 630 | 15 | 557-657 | -82.32 | -24.46 |
| OS-120020 | VCBC | 122.5 | >Modern | | | 89.95 | -21.98 |
| OS-120021 | VCBC | 152.5 | 1240 | 15 | 1084-1259 | -149.34 | -12.54 |
| OS-120022 | VCBC | 182.5 | 830 | 20 | 693-781 | -104.86 | -22.19 |
| OS-120025 | VCSG | 2.5 | >Modern | | | 49.92 | -13.64 |
| OS-120026 | VCSG | 32.5 | >Modern | | | 132.91 | -15.65 |
| OS-120027 | VCSG | 62.5 | >Modern | | | 53.00 | -16.23 |
| OS-120028 | VCSG | 92.5 | >Modern | | | 10.62 | -17.45 |
| OS-120029 | VCSG | 122.5 | 980 | 15 | 803-933 | -121.92 | -10.75 |
| OS-120218 | VCSG | 152.5 | >Modern | | | 59.43 | -17.18 |
| OS-120030 | VCSG | 182.5 | 845 | 15 | 709-788 | -106.81 | -14.33 |

Table 3: Short-term rates of marsh accretion, organic accumulation, mineral accumulation, and carbon accumulation discussed in the text.

| Location (Abbreviation) | Core Id | Accretion Rate (cm yr ⁻¹) | Organic Accumulation Rate (g m ⁻² yr ⁻¹) | Mineral Accumulation Rate (g m ⁻² yr ⁻¹) | Carbon Accumulation Rate (g C m ⁻² yr ⁻¹) |
|----------------------------------|---------|---|--|--|---|
| Canary Creek, DE (CC) | CC-1 | 0.11 | 130.0 | 141.1 | 28.3 |
| | CC-2 | 0.20 | 205 | 302.2 | 67.7 |
| | CC-3 | 0.57 | 632.7 | 2383.3 | 167.5 |
| | CC-5 | 0.22 | 250.9 | 772.6 | 106.1 |
| | CC-6 | 0.37 | 313.1 | 1504.8 | 136.4 |
| Great Marsh, DE (GM) | GM-1 | 0.39 | 451.3 | 1201.9 | 102.7 |
| | GM-2 | 0.39 | 393.8 | 458.4 | 98.7 |
| | GM-3 | 0.39 | 386.5 | 225.8 | 140.5 |
| | GM-4 | 0.29 | 315.8 | 338.1 | 141.9 |
| Mispillion River, DE (MR) | MR-1 | 0.39 | 443.8 | 1562.6 | 145.6 |
| | MR-2 | 0.38 | 381.2 | 763.0 | 152.9 |
| | MR-3 | 0.48 | 533.8 | 1490.9 | 187.8 |
| St. Jones Reserve, DE (SJ) | SJBM-1 | 0.43 | 309.4 | 906.3 | 115.6 |
| | SJBM-2 | 1.10 | 1020.9 | 4026.3 | 337.3 |
| | SJBM-3 | 0.59 | 610.7 | 1449.8 | 208.5 |
| Kelly Island, DE (KI) | KI-1 | 0.48 | 559.7 | 1329.7 | 204.3 |
| | KI-2 | 0.39 | 417 | 826.7 | 139.3 |
| | KI-3 | 0.47 | 430.1 | 665.8 | 178.9 |
| Blackbird Creek, DE (BC) | BC-1 | 0.48 | 525.2 | 1818.1 | 208.4 |
| | BC-2 | 0.56 | 575.3 | 1343.8 | 203.0 |
| | BC-3 | 0.38 | 369.1 | 855.4 | 147.0 |
| St. Georges Marsh, DE (SG) | SG-1 | 0.69 | 574.6 | 4126.6 | 222.7 |
| | SG-2 | 0.78 | 639.4 | 3725.5 | 262.4 |
| | SG-3 | 1.20 | 1276.8 | 6151.2 | 439.9 |

Table 4: Long-term rates of marsh accretion, organic accumulation, mineral accumulation, and carbon accumulation discussed in the text. Calibrated radiocarbon ages used to compute these rates are also shown.

| Core Id | Depth (cm) | 2-sigma Calibrated Age (Cal yr B.P.) | Accretion Rate (cm yr ⁻¹) | Organic Accumulation (g m ⁻² yr ⁻¹) | Mineral Accumulation (g m ⁻² yr ⁻¹) | Carbon Accumulation (g m ⁻² yr ⁻¹) |
|---------|------------|--------------------------------------|---------------------------------------|--|--|---|
| VCGM | 62.50 | 182 | 0.34 | 301.8 | 576.1 | 133.2 |
| VCGM | 92.50 | 397 | 0.23 | 200.2 | 340.4 | 90.9 |
| VCGM | 122.50 | 866 | 0.14 | 123.5 | 207.3 | 57.4 |
| VCMR | 62.50 | 189 | 0.33 | 284.1 | 501.5 | 137.1 |
| VCMR | 94.00 | 307 | 0.31 | 249.5 | 462.2 | 122.5 |
| VCMR | 122.50 | 487 | 0.25 | 195.1 | 423.1 | 95.5 |
| VCMR | 152.50 | 864 | 0.18 | 133.7 | 353.6 | 64.1 |
| VCMR | 186.50 | 1108 | 0.17 | 125.0 | 393.8 | 60.2 |
| VCMR | 216.50 | 1459 | 0.15 | 108.8 | 364.9 | 52.7 |
| VCKI | 62.50 | 184 | 0.34 | 291.1 | 1069.5 | 128.1 |
| VCKI | 92.50 | 296 | 0.31 | 256.3 | 881.0 | 113.3 |
| VCKI | 122.50 | 300 | 0.41 | 326.6 | 1138.4 | 144.5 |
| VCKI | 152.50 | 308 | 0.50 | 373.5 | 1563.5 | 160.0 |
| VCKI | 182.50 | 924 | 0.20 | 145.3 | 679.8 | 61.8 |
| VCBC | 32.50 | 178 | 0.18 | 180.1 | 609.4 | 83.3 |
| VCBC | 93.00 | 594 | 0.16 | 139.1 | 36.3 | 67.5 |
| VCBC | 152.50 | 1213 | 0.13 | 112.9 | 214.2 | 56.7 |
| VCBC | 182.50 | 732 | 0.25 | 220.5 | 385.9 | 112.3 |
| VCSG | 122.50 | 920 | 0.13 | 102.6 | 773.0 | 45.1 |
| VCSG | 182.50 | 753 | 0.24 | 188.0 | 1503.2 | 79.5 |

Table 5: Comparison of marsh accretion rates, mineral accumulation rates (MAR), and organic accumulation rates (OAR) average over different timescale using radionuclide chronometers.

| Location | Accretion Rate (cm/yr) | | MAR (g m ⁻² yr ⁻¹) | | OAR (g m ⁻² yr ⁻¹) | |
|--------------|---------------------------|-----------------|--|-----------------|--|-----------------|
| | ¹³⁷ Cs | ¹⁴ C | ¹³⁷ Cs | ¹⁴ C | ¹³⁷ Cs | ¹⁴ C |
| | ²¹⁰ Pb | | ²¹⁰ Pb | | ²¹⁰ Pb | |
| GM-4 VCGM | 0.29 | 0.14 | 338.1 | 207.3 | 315.1 | 123.5 |
| MR-2 VCMR | 0.38 | 0.15 | 763.0 | 364.9 | 381.2 | 108.7 |
| KI-3 VCKI | 0.47 | 0.20 | 665.8 | 679.8 | 430.1 | 145.3 |
| BC-2 VCBC | 0.56 | 0.25 | 1343.8 | 385.8 | 575.2 | 220.4 |
| SG-3 VCSG | 1.20 | 0.24 | 6151.2 | 1503.1 | 1276.7 | 188.0 |

Table 6: Global comparisons of carbon accumulation rate (CAR), marsh area, and storage in tidal marshes. Table modified from Ouyang and Lee (2014) to include results from this study. Asterisk indicates data from Tiner et al. (2011).

| Region | Soil CAR, g C m ⁻² yr ⁻¹ (mean ± SE) | Area (km ²) | Soil CAR, Tg C yr ⁻¹ (mean ± SE) |
|--------------------------|---|----------------------------|---|
| Australia | 274.8 | 13 765 | 3.78 |
| China | 223.6 | 5734 | 1.28 |
| USA | | | |
| Tropic W Atlantic region | 293.7±60.9 | 8596 | 2.52±0.52 |
| NW Atlantic region | 134.0±12.8 | 2685 | 0.36±0.03 |
| Delaware Estuary | 172.4±17.5 | 308* | 0.05±0.005 |
| NE Pacific region | 173.6±45.1 | 7984 | 1.39±0.36 |
| Europe and Scandinavia | 312.4±50.6 | 2302 | 0.72±0.12 |
| Canada | 214.3±33.7 | 328 | 0.07±0.01 |
| Northern Africa | 305.5±86 | 93 | 0.03±0.01 |
| Southern Africa | 200.9±23 | 170 | 0.03±0.004 |
| Total | 244.7±26.1 | 41 657 | 10.2±1.1 |

FIGURES

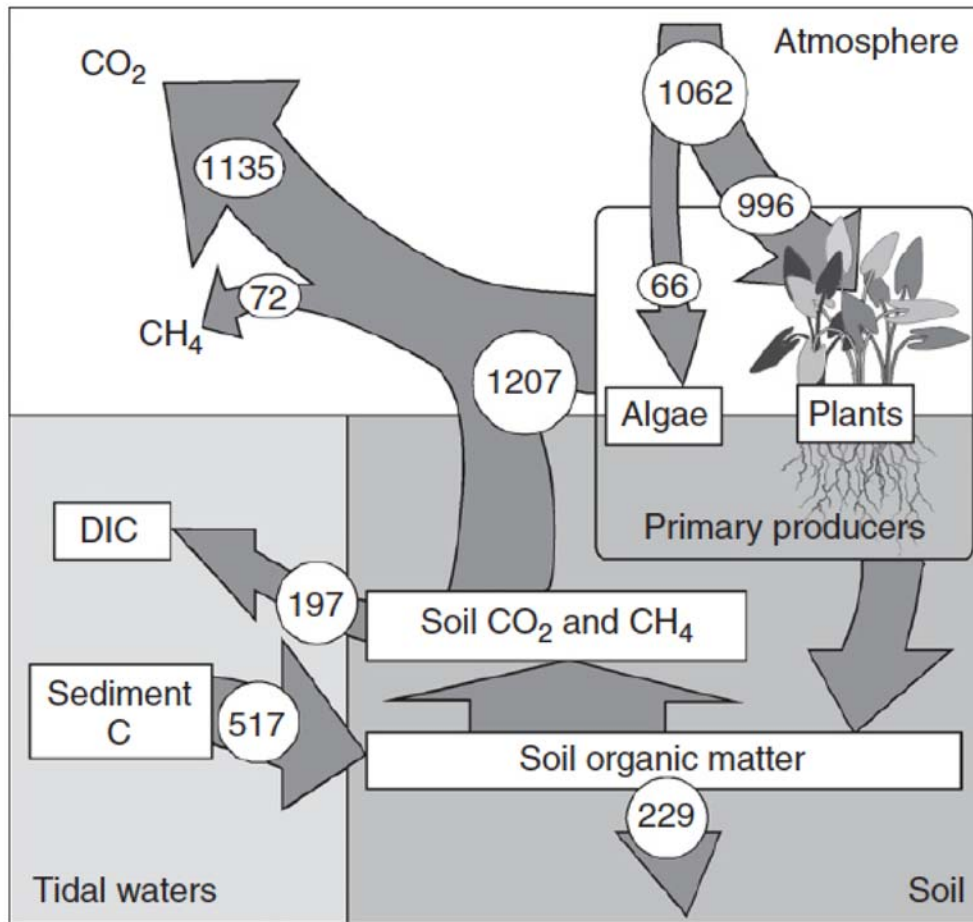


Figure 1: Carbon budget for Sweet Hall Marsh, USA from Megonigal and Neubauer (2009). Rates are reported in $\text{g m}^{-2} \text{ yr}^{-1}$. Pathways represent conceptual model of carbon cycling in tidal marsh sediments.

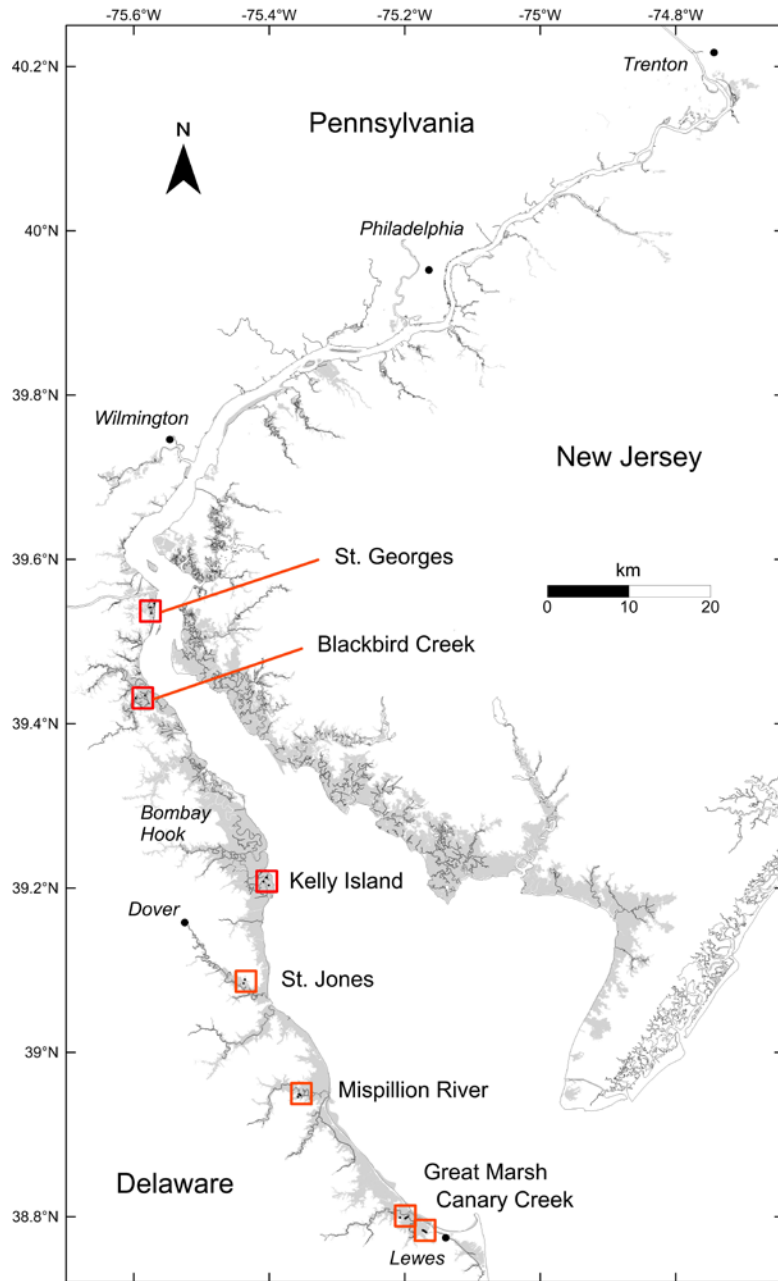


Figure 2: Map of the Delaware Estuary showing the marsh locations referred to in the text. Wetland areas shown in grey are delineations by the U.S. Fish and Wildlife Service.

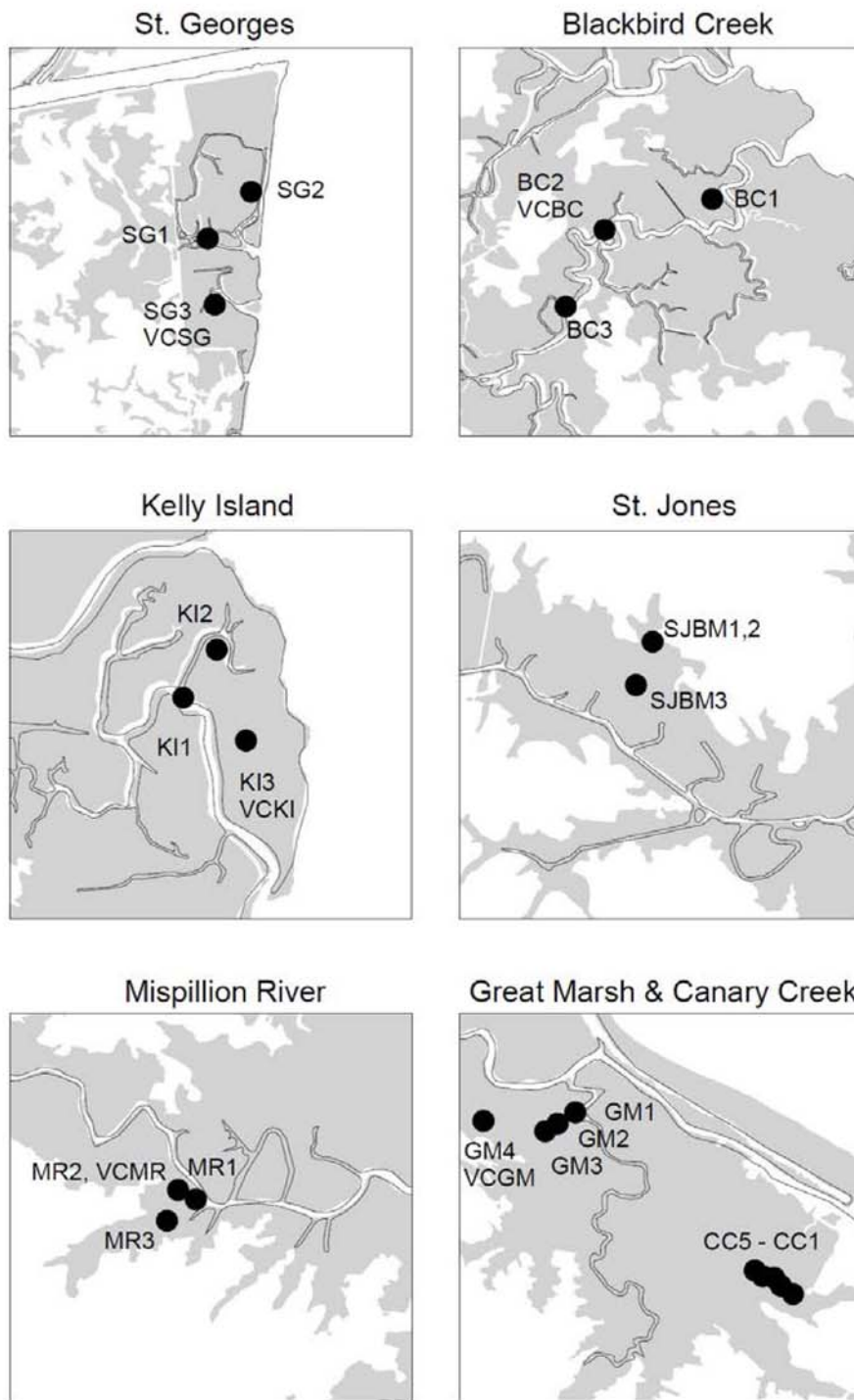


Figure 3: Short- and long-coring sites at the marsh locations shown in Figure 2.

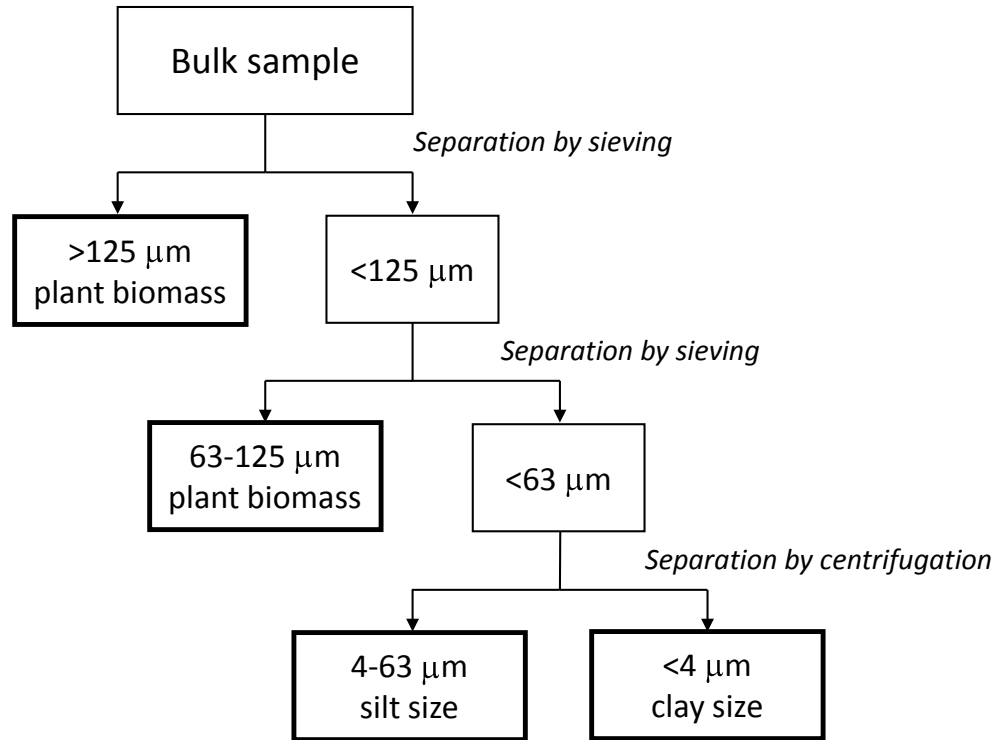


Figure 4: Soil fractionation scheme used for this study. The bold boxes denote the size fraction subjected to organic carbon analysis. See text for details.

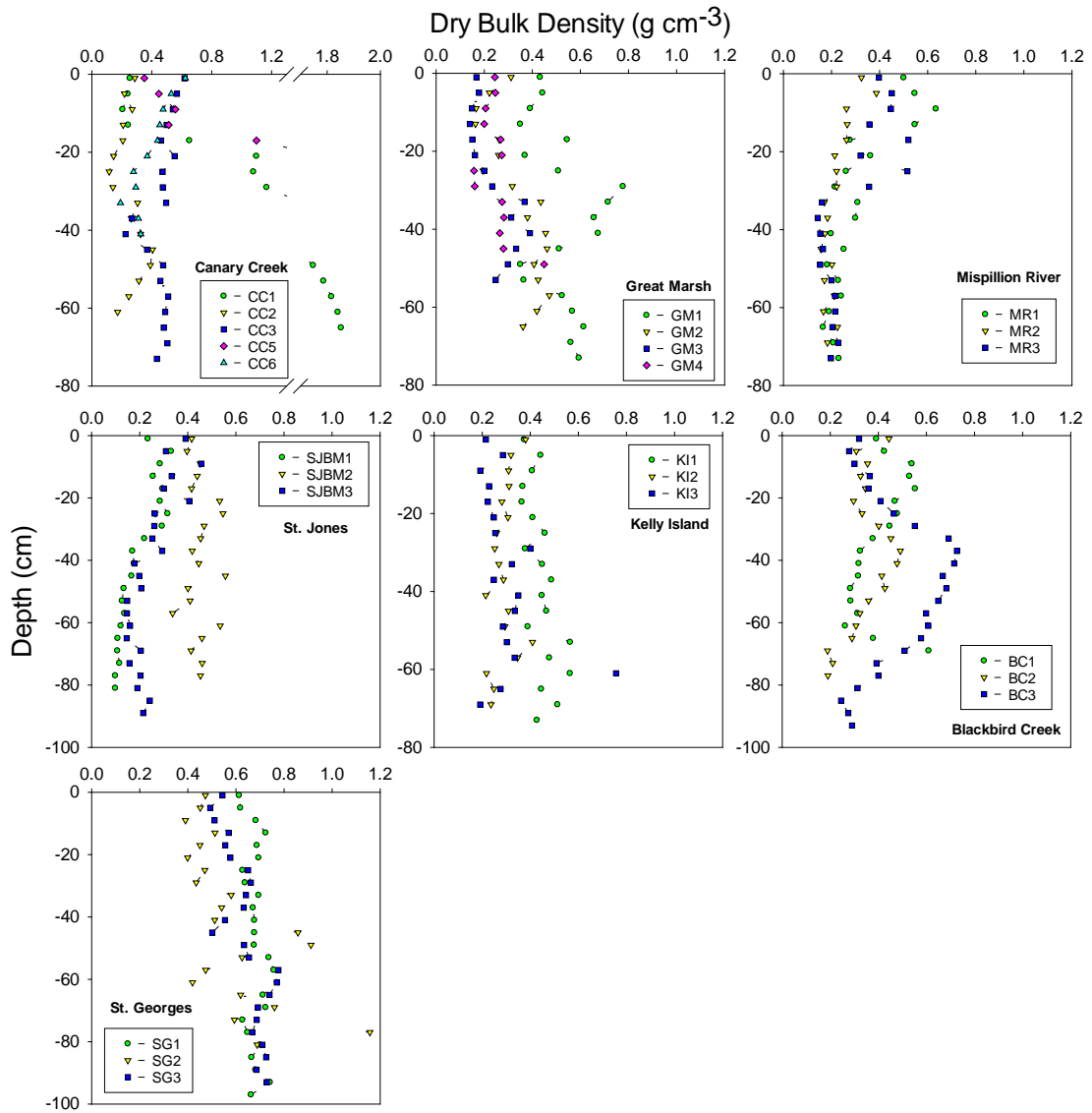


Figure 5: Depth profiles of dry bulk density for the short cores examined in this study.

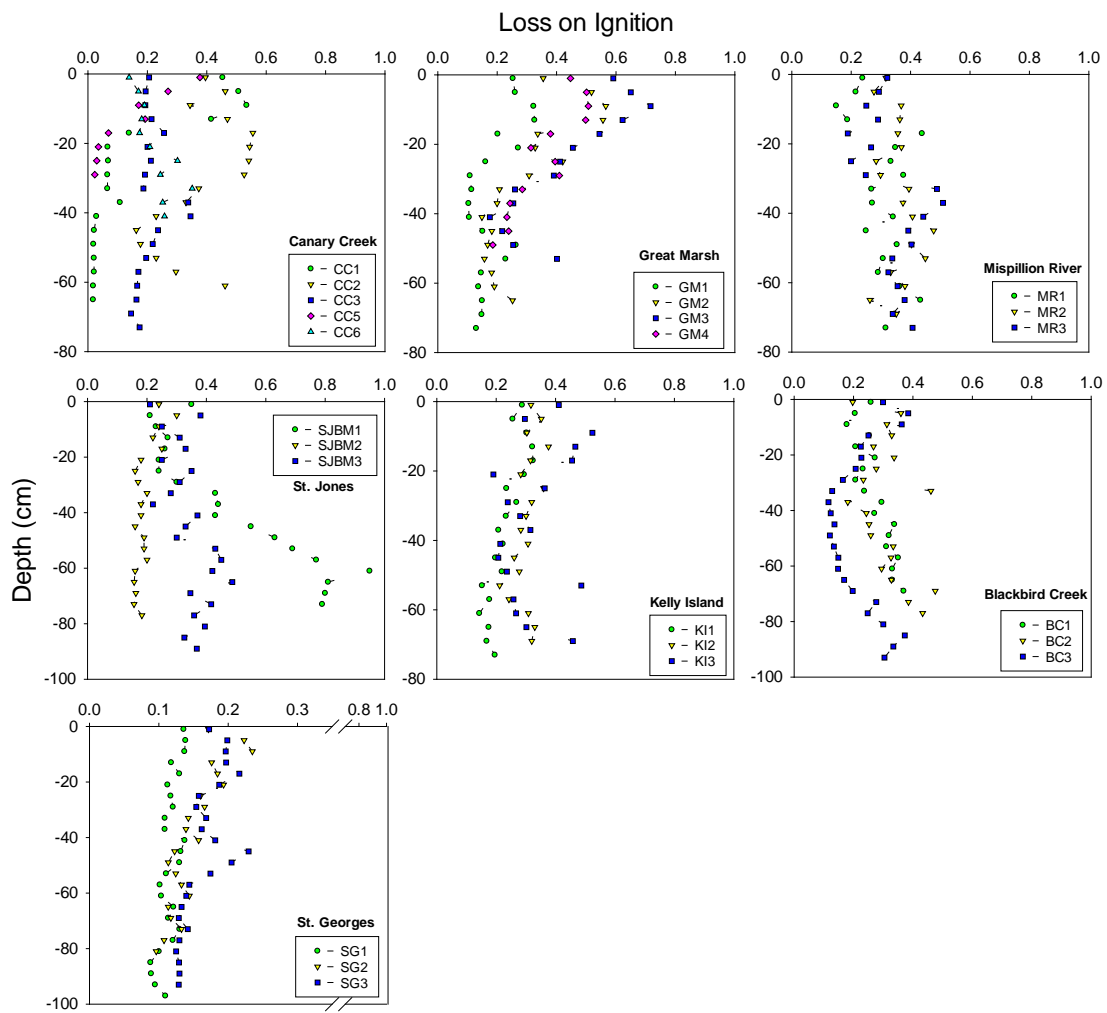


Figure 6: Depth profiles of loss on ignition for the short cores examined in this study.

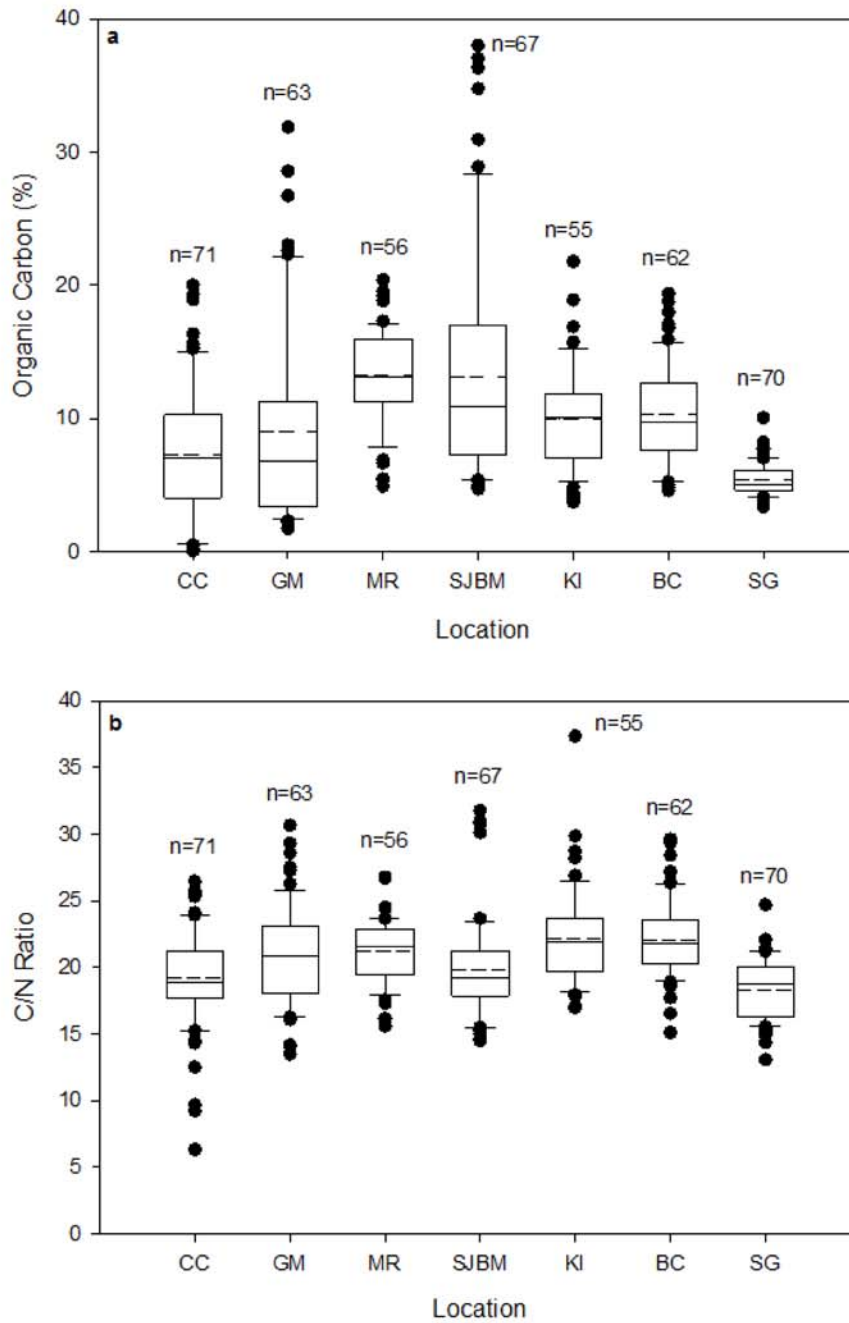


Figure 7: a) Total organic carbon (TOC) concentrations and b) C/N ratios for the short cores examined in this study. Solid and dashed lines are the median and mean of all samples, respectively. Black circles indicate outliers. The total number (n) of subsamples analyzed per core is noted.

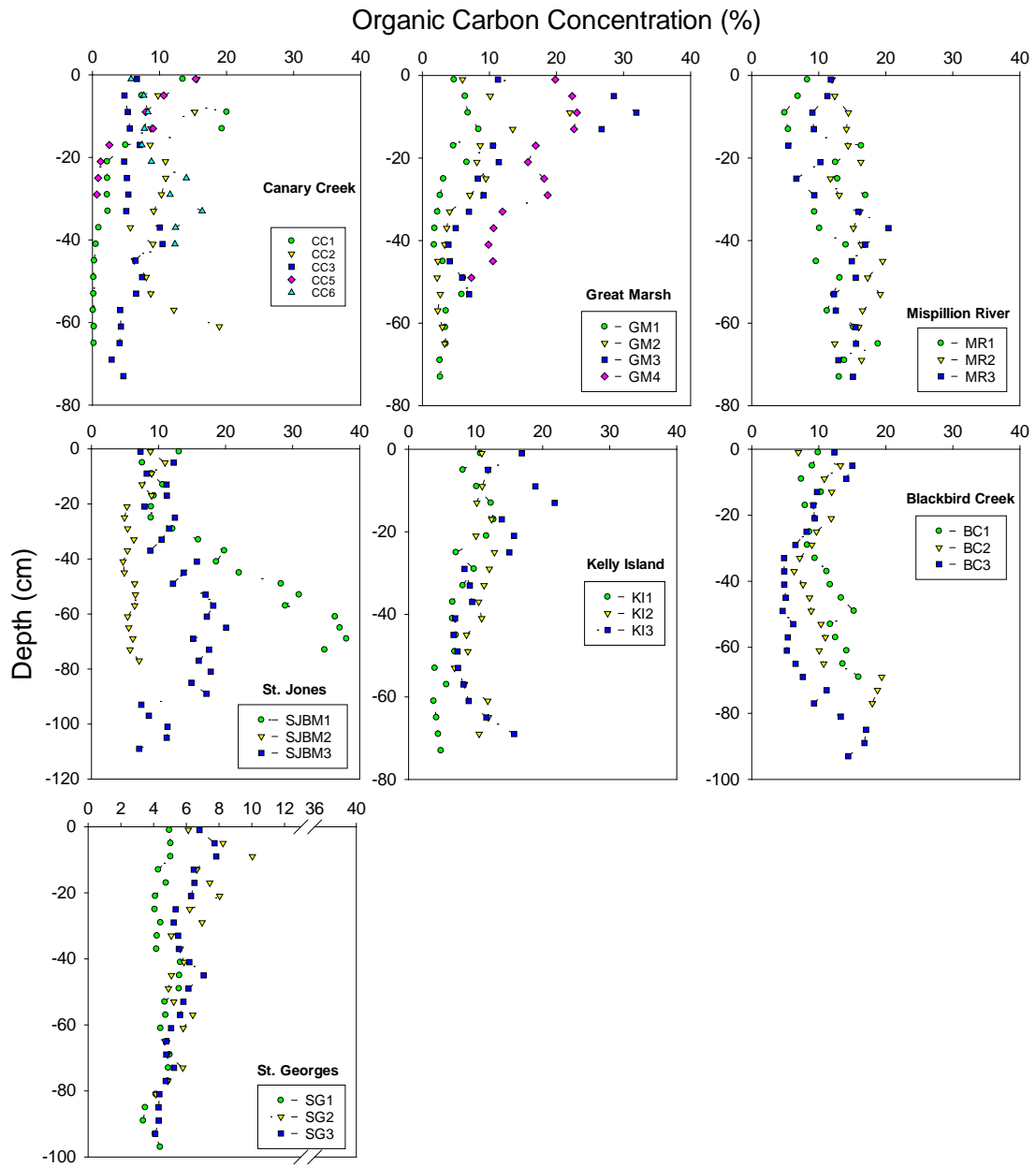


Figure 8: Depth profiles of total organic carbon (TOC) concentration for the short cores examined in this study.

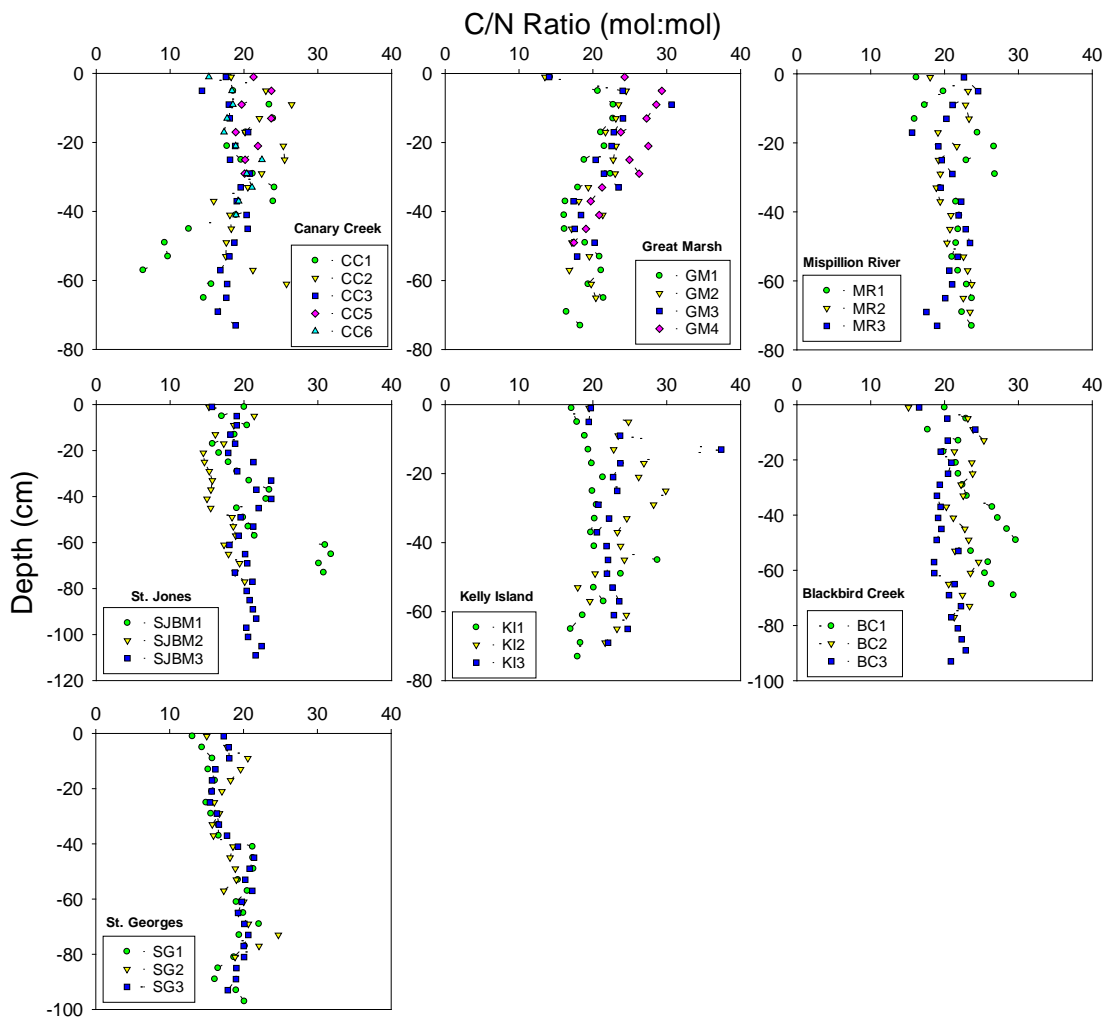


Figure 9: Depth variations in C/N ratio for the short cores examined in this study.

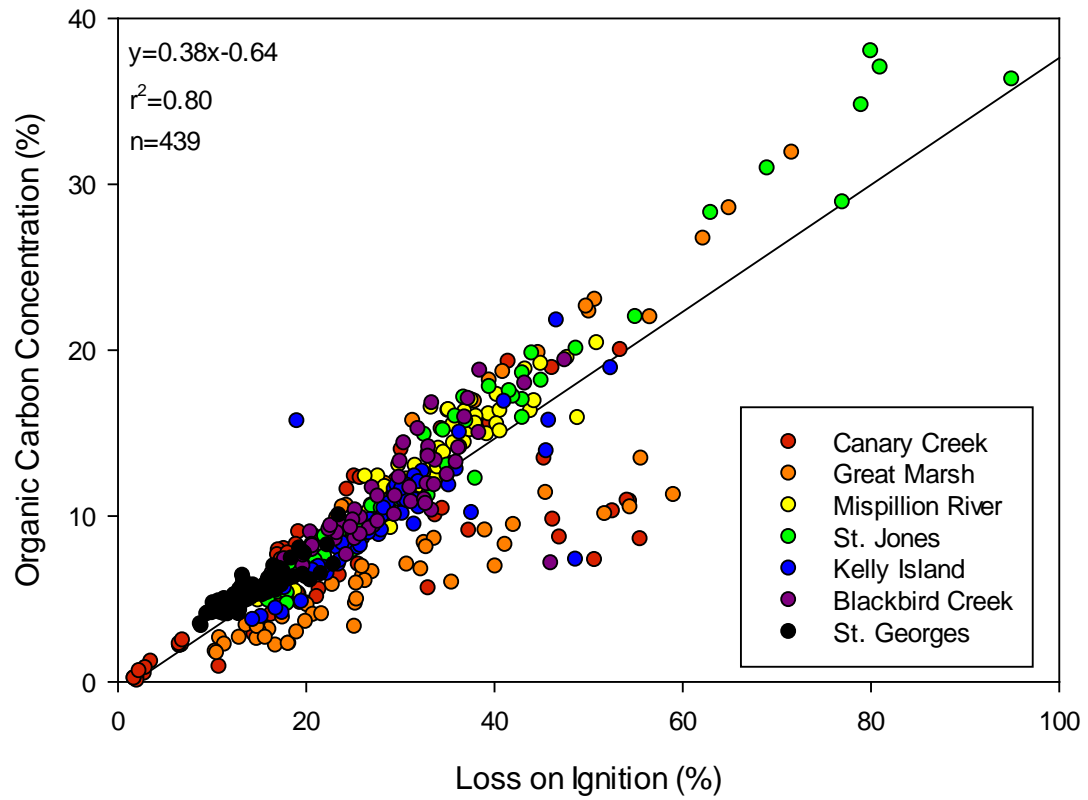


Figure 10: Regression analysis of total organic carbon (TOC) concentration versus loss on ignition (LOI) for the short cores examined in this study.

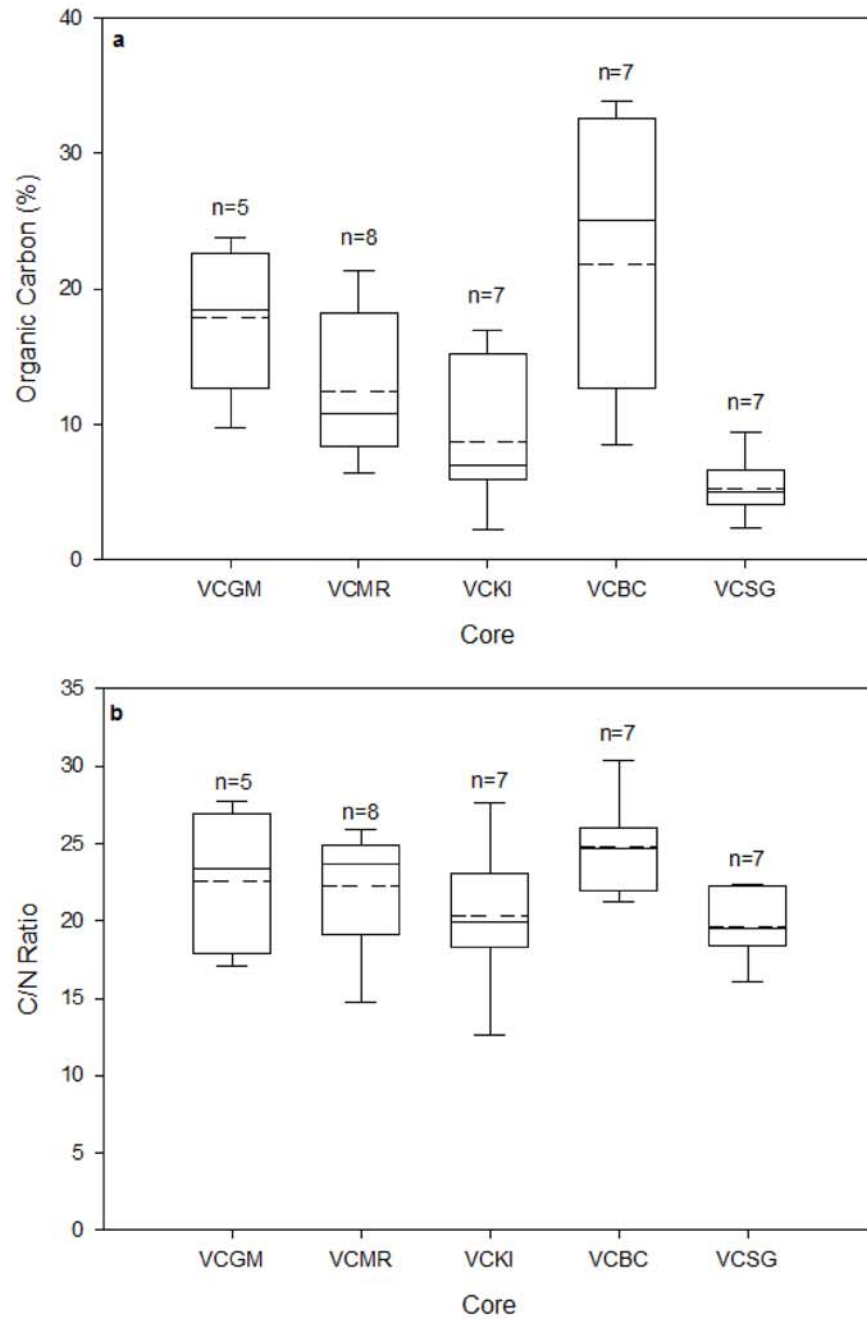


Figure 11: a) Total organic carbon (TOC) concentration and b) C/N ratio data for the long cores examined in this study. Solid and dashed lines are the median and mean of all samples, respectively. The total number of samples (n) analyzed for each core is shown.

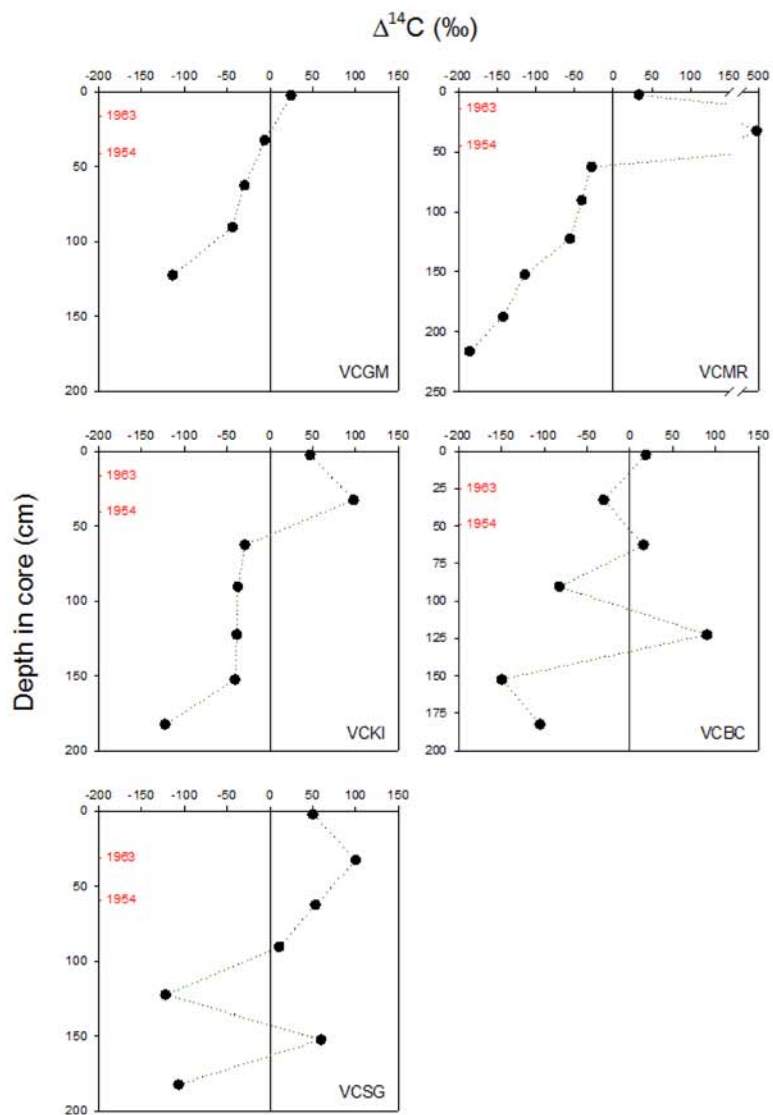


Figure 12: Depth profiles of $\Delta^{14}\text{C}$ for the long cores examined in this study. Depths corresponding to the years 1954 and 1963 are noted.

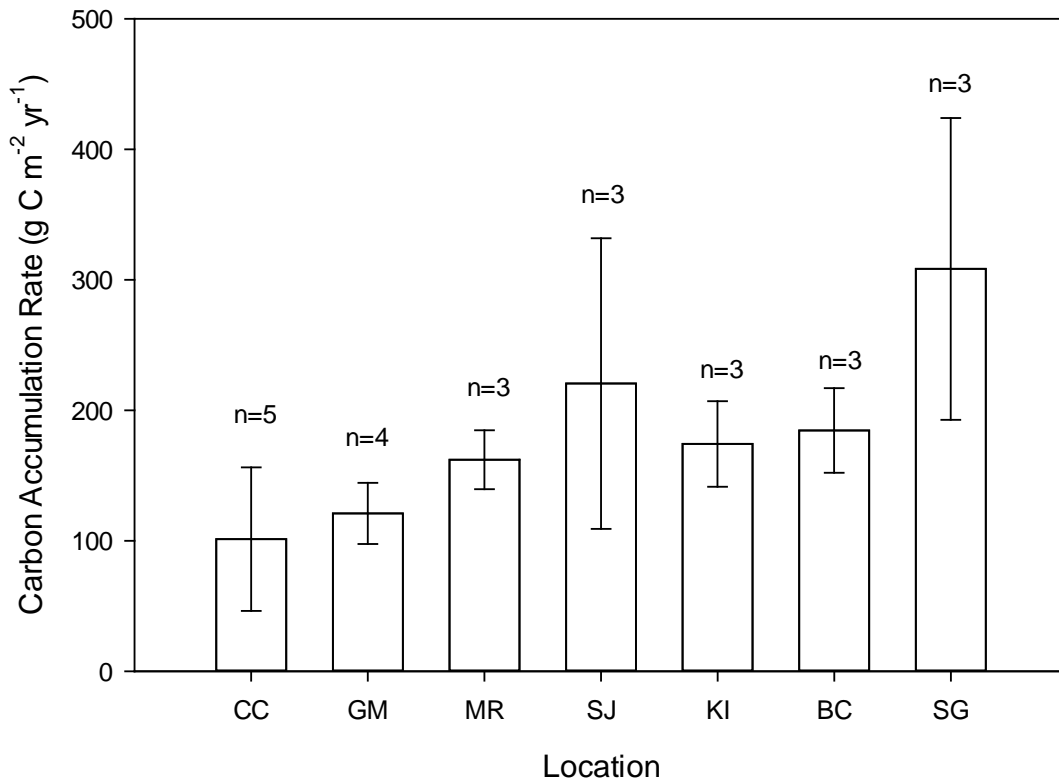


Figure 13: Organic carbon accumulation rates for the marsh sites based on ¹³⁷Cs or ²¹⁰Pb chronology. The mean and range of accumulation rates averaged for n coring sites are shown by the vertical bars and error bars, respectively.

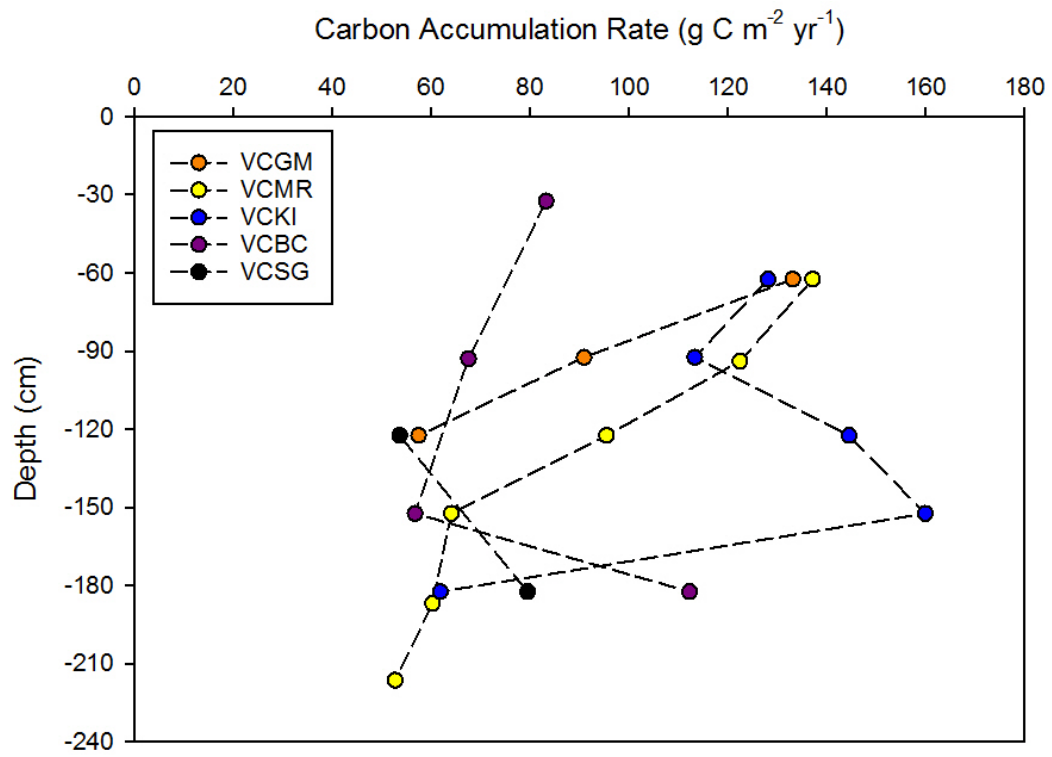


Figure 14: Depth profiles of organic carbon accumulation rate for the long cores examined in this study.

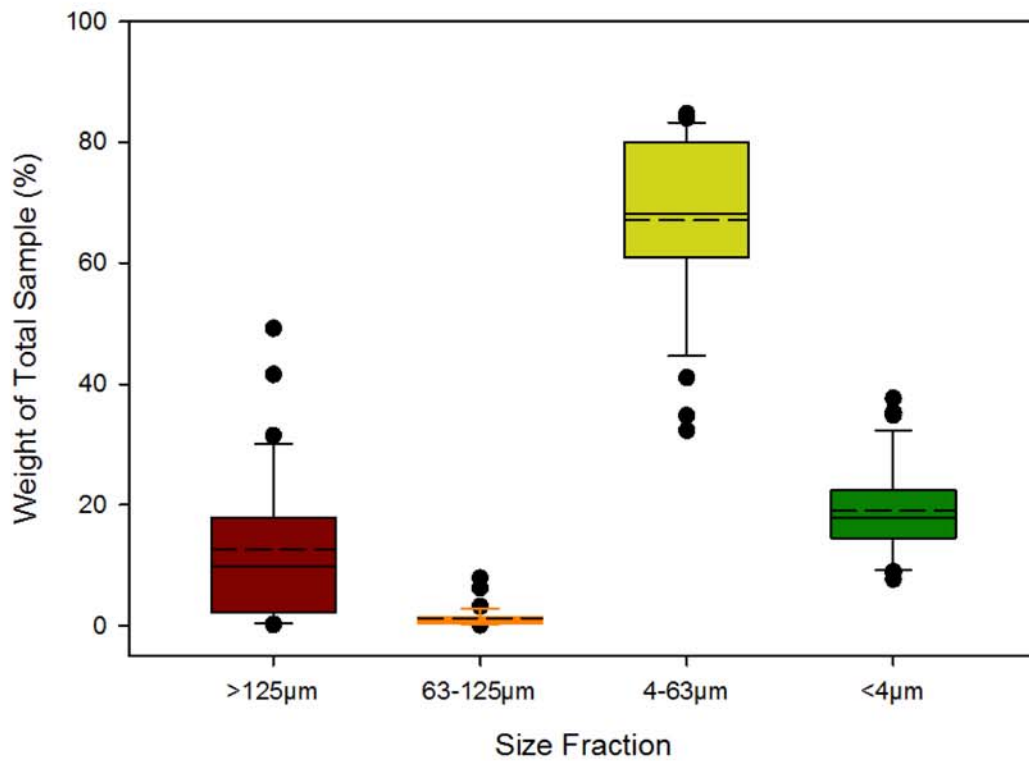


Figure 15: Box plots showing the weight percentages for the soil-size fractions examined for long cores (n=34 for all fractions). Solid and dashed lines within the boxes are the median and means of n samples, respectively, and the closed circles are individual outliers.

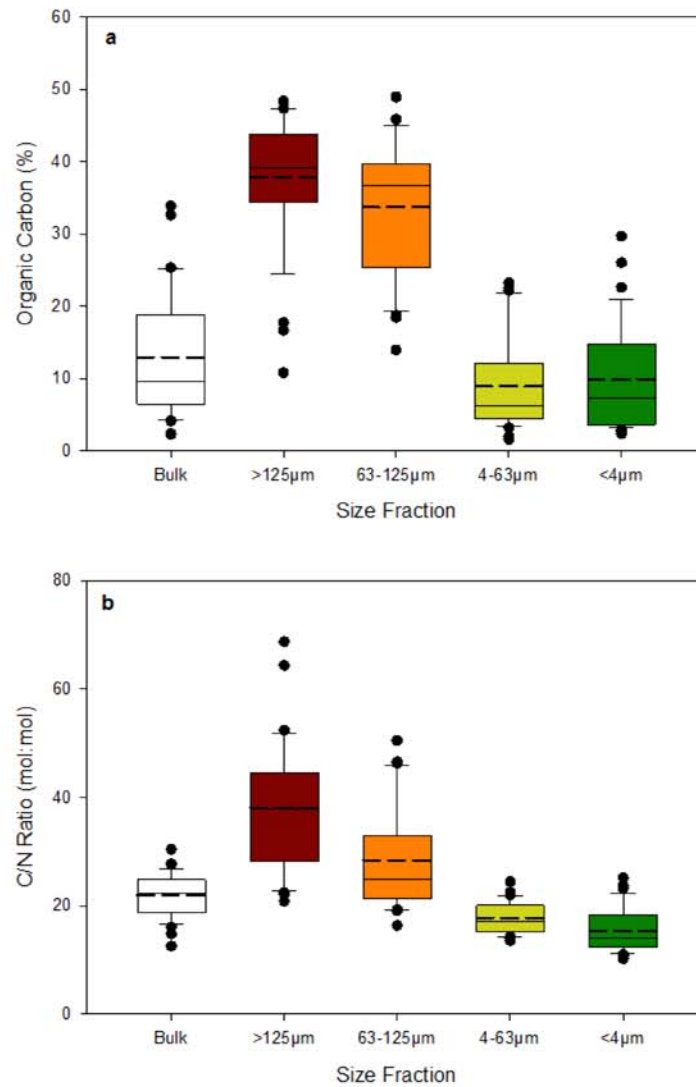


Figure 16: Box plots showing a) total organic carbon (TOC) concentrations and b) C/N ratios for bulk and size-fractionated soils from long cores examined in this study. Solid and dashed lines within the boxes are the median and means of n samples, respectively, and the closed circles are individual outliers.

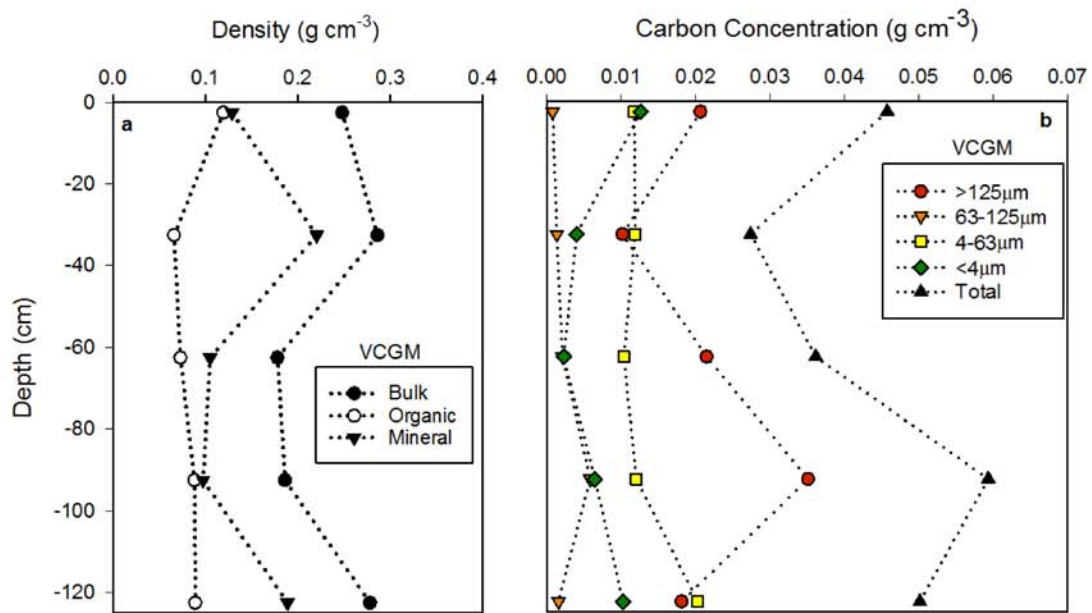


Figure 17: Down-core profiles for the Great Marsh vibracore showing a) variations in dry bulk density, organic matter density, and mineral matter density; and b) variations in total carbon concentration and the carbon concentration of individual size fractions.

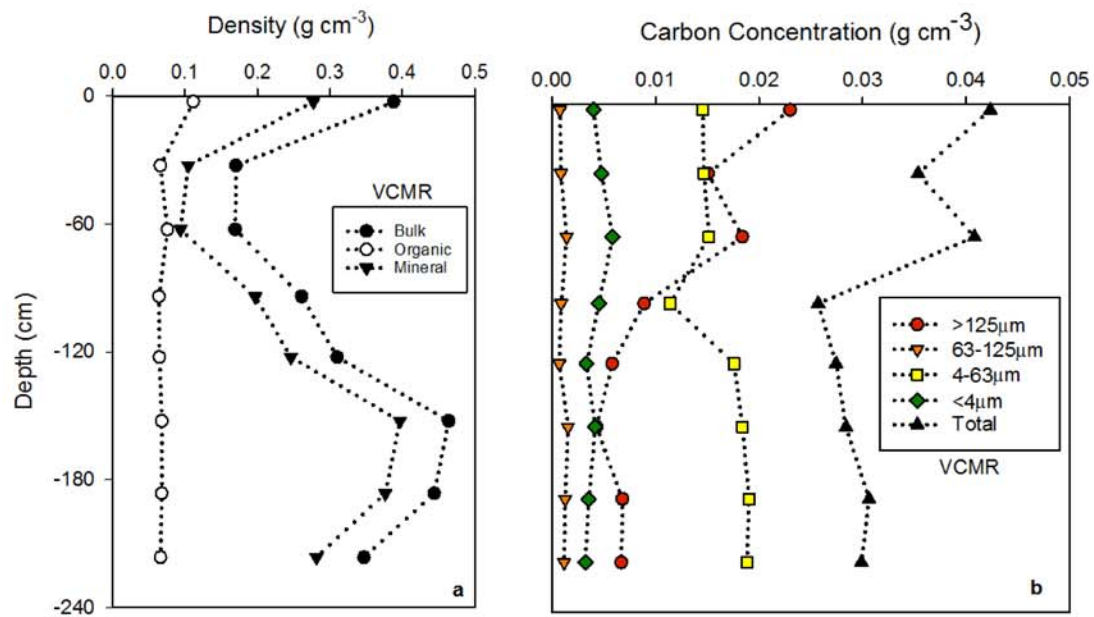


Figure 18: Down-core profiles for the Mispillion River vibracore showing a) variations in dry bulk density, organic matter density, and mineral matter density; and b) variations in total carbon concentration and the carbon concentration of individual size fractions.

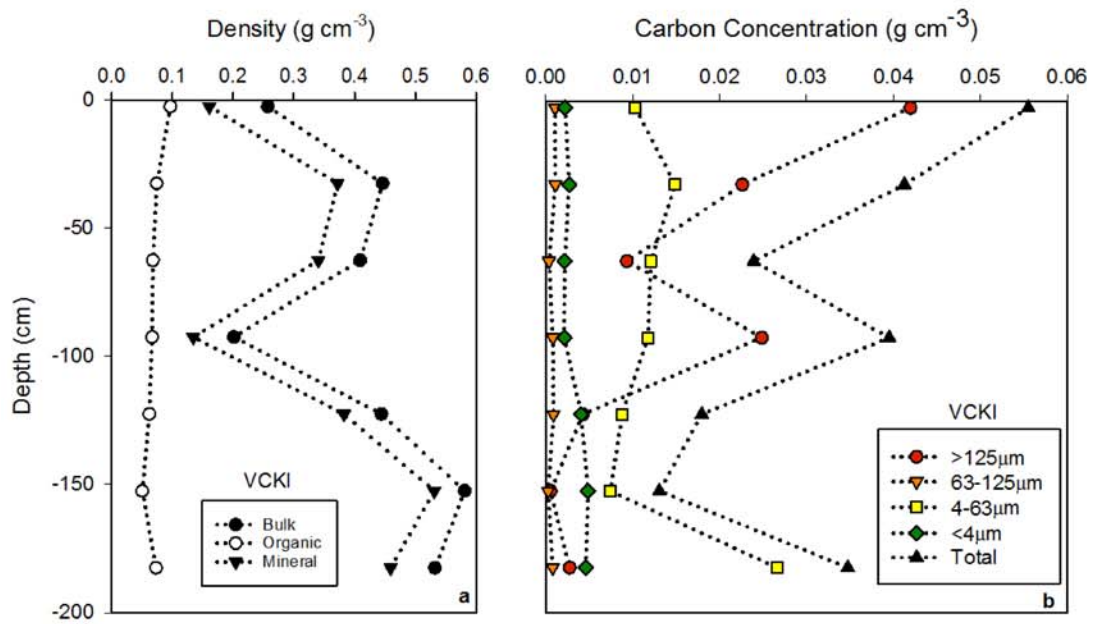


Figure 19: Down-core profiles for the Kelly Island vibracore showing a) variations in dry bulk density, organic matter density, and mineral matter density; and b) variations in total carbon concentration and the carbon concentration of individual size fractions.

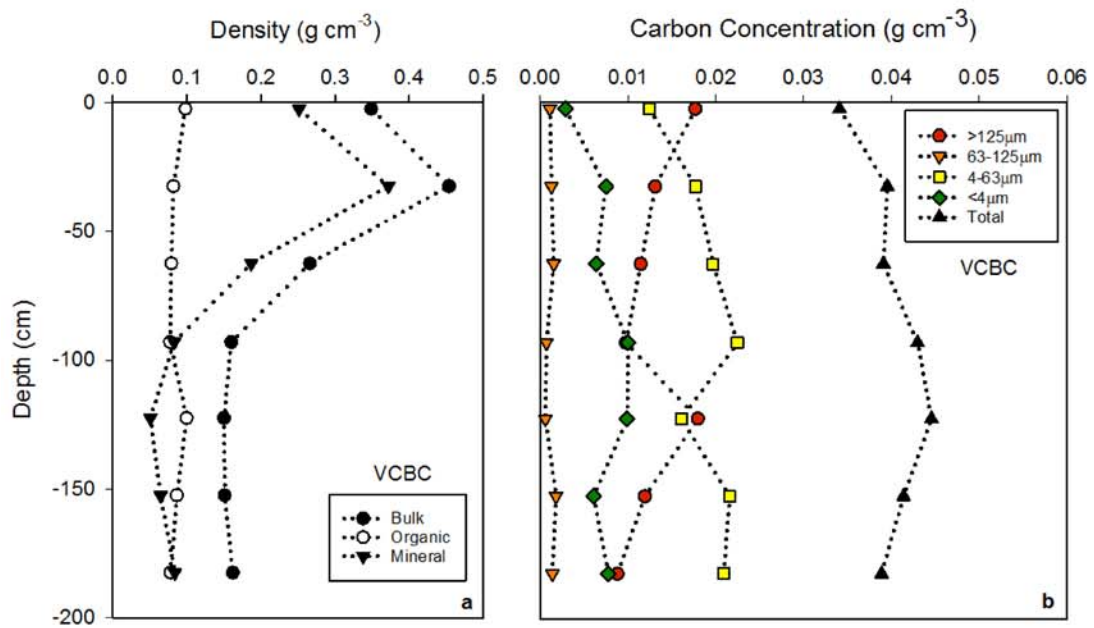


Figure 20: Down-core profiles for the Blackbird Creek vibracore showing a) variations in dry bulk density, organic matter density, and mineral matter density; and b) variations in total carbon concentration and the carbon concentration of individual size fractions.

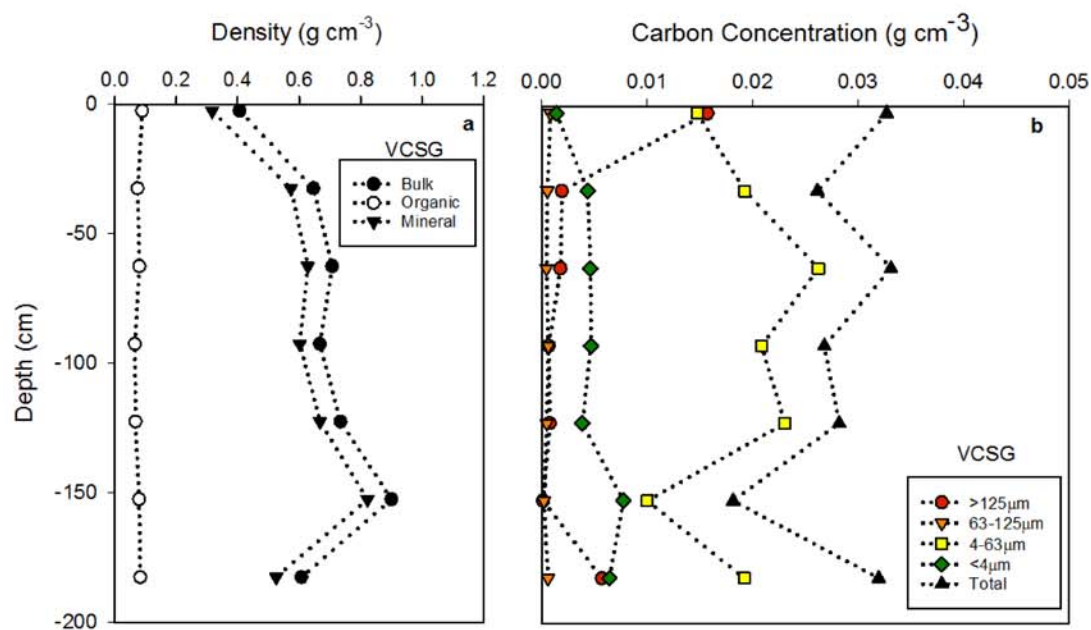


Figure 21: Down-core profiles for the St. Georges vibracore showing a) variations in dry bulk density, organic matter density, and mineral matter density; and b) variations in total carbon concentration and the carbon concentration of individual size fractions.

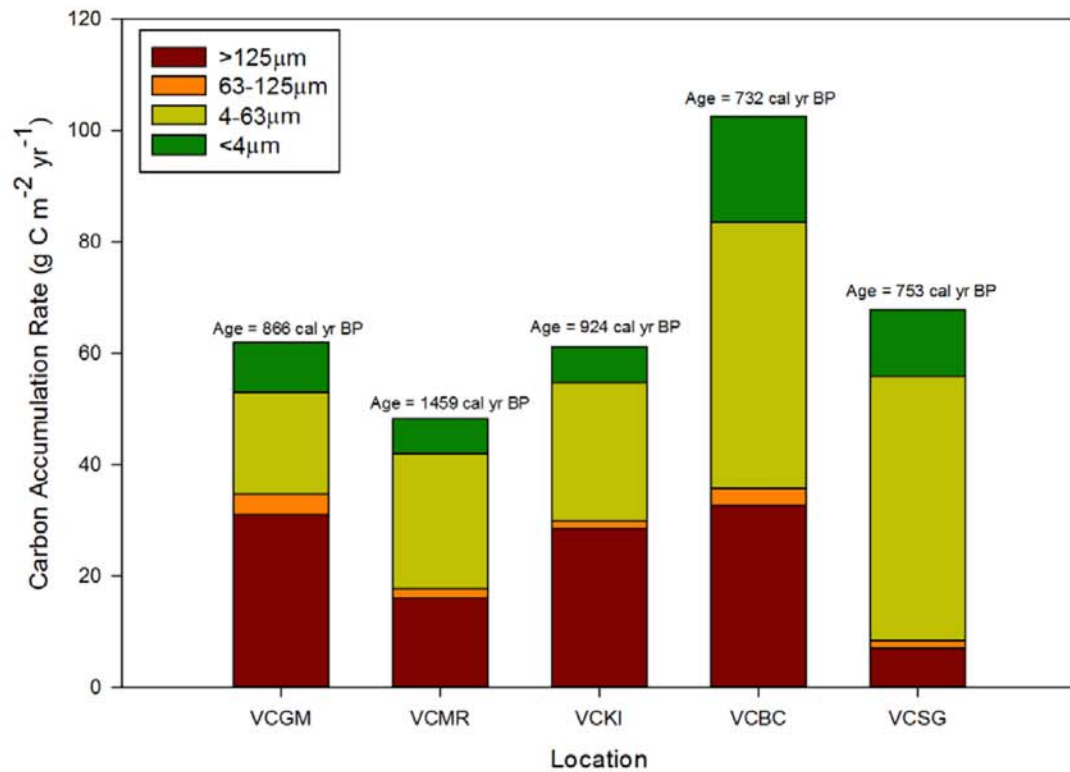


Figure 22: Stacked bar chart showing the relative contributions of the four soil size fractions to the long-term carbon accumulation rate determined for the five long cores. The age range over which these rates were averaged is noted in calibrated yr B.P. Note the significant contribution of the silt- and clay-sized carbon fractions of the total rate.

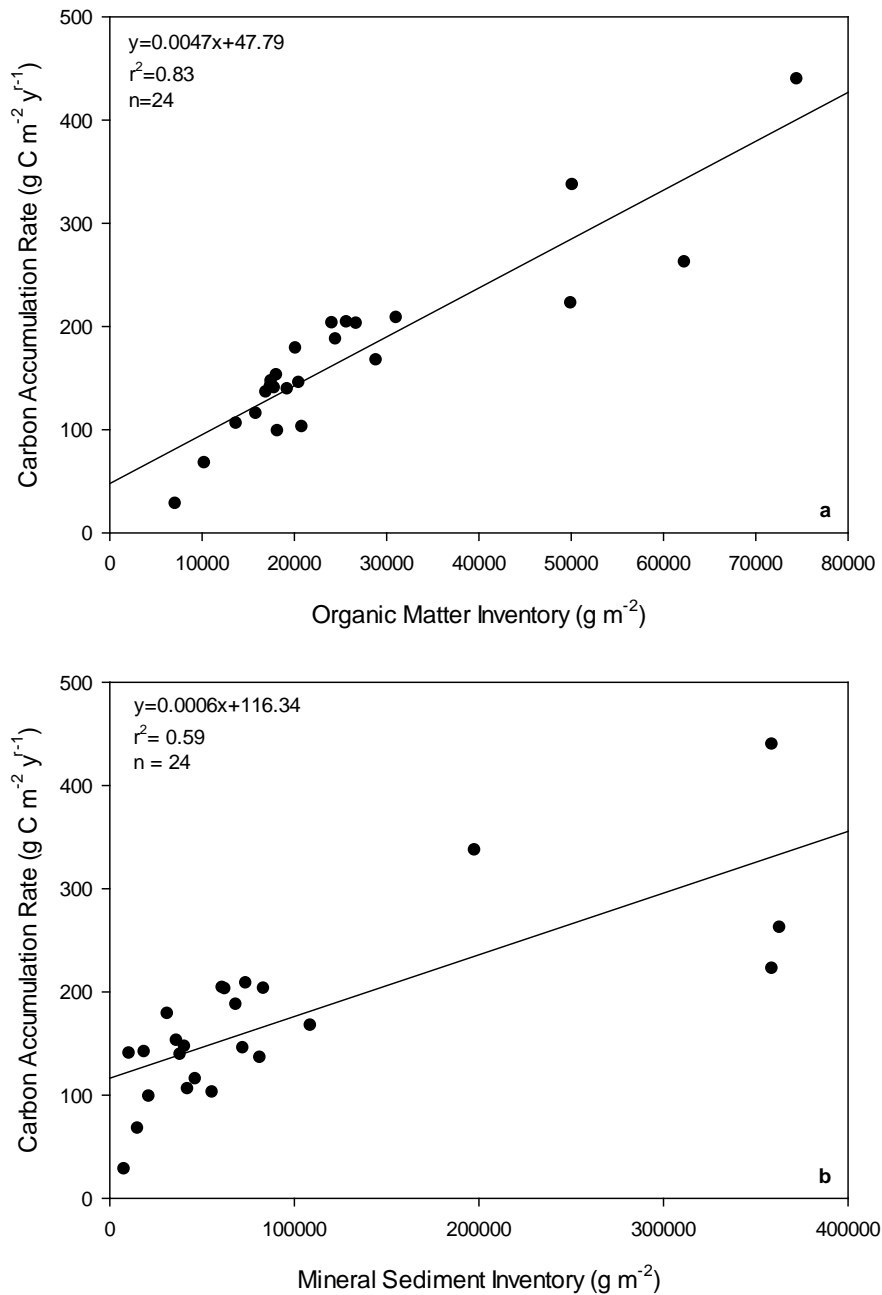


Figure 23: Correlation between a) carbon accumulation rate and mineral accumulation rate, and b) carbon accumulation rate and organic accumulation rate for the short cores examined in this study. Rates and inventories are calculated relative to 1963. See text for further discussion.

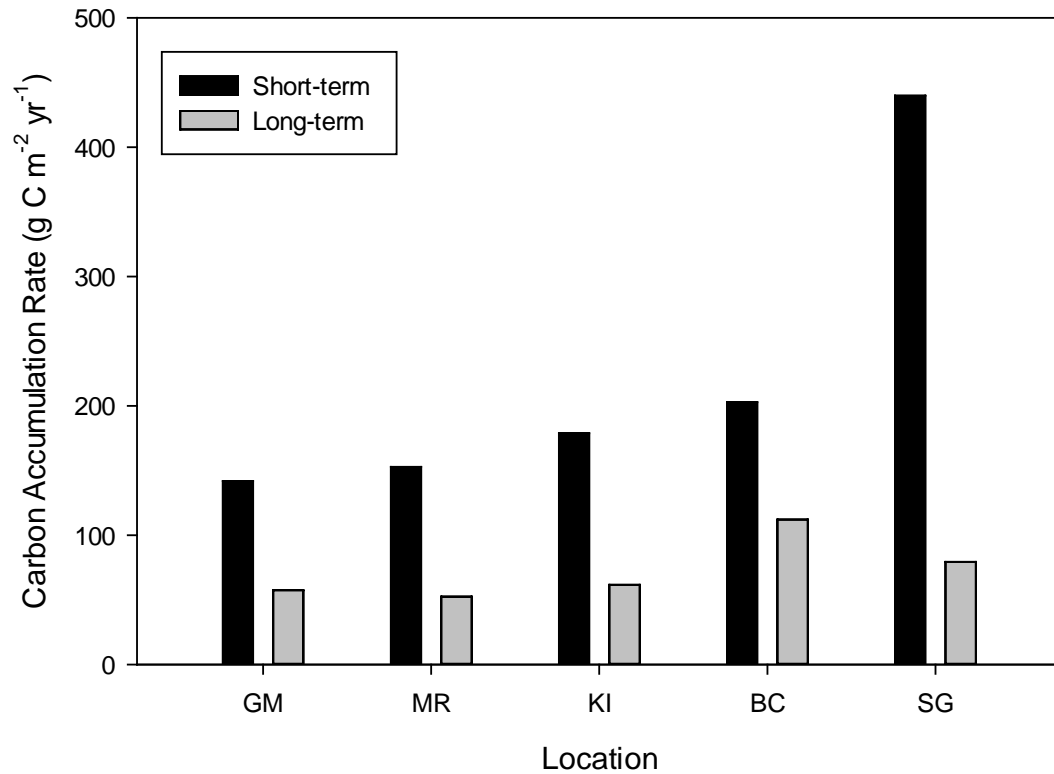


Figure 24: Comparison of short-term and long-term carbon accumulation rates. Black bars represent rates determined from ¹³⁷Cs or ²¹⁰Pb dating of the short cores; gray bars represent rates based on ¹⁴C dating of the long cores.

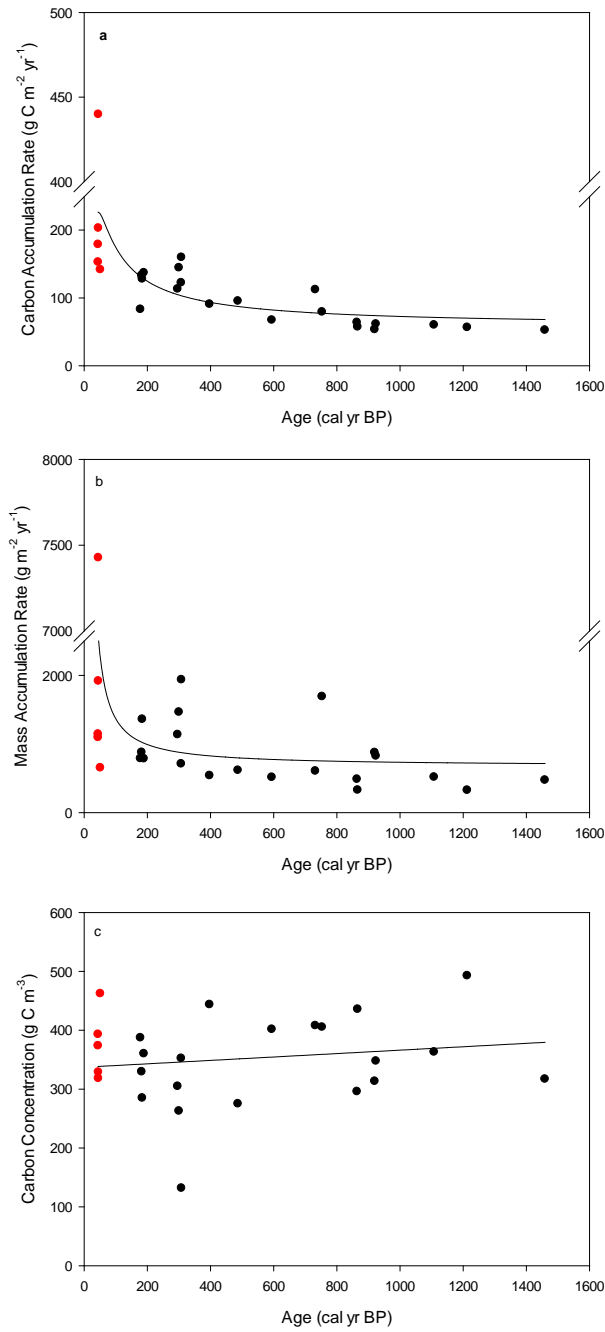


Figure 25: Scatter plots showing the dependence of a) carbon accumulation rate, b) mass accumulation rate (organic matter plus mineral sediment), and c) carbon concentration on soil age (cal yr B.P.). Red and black circles denote rates for short cores and long cores collected at the same locations.

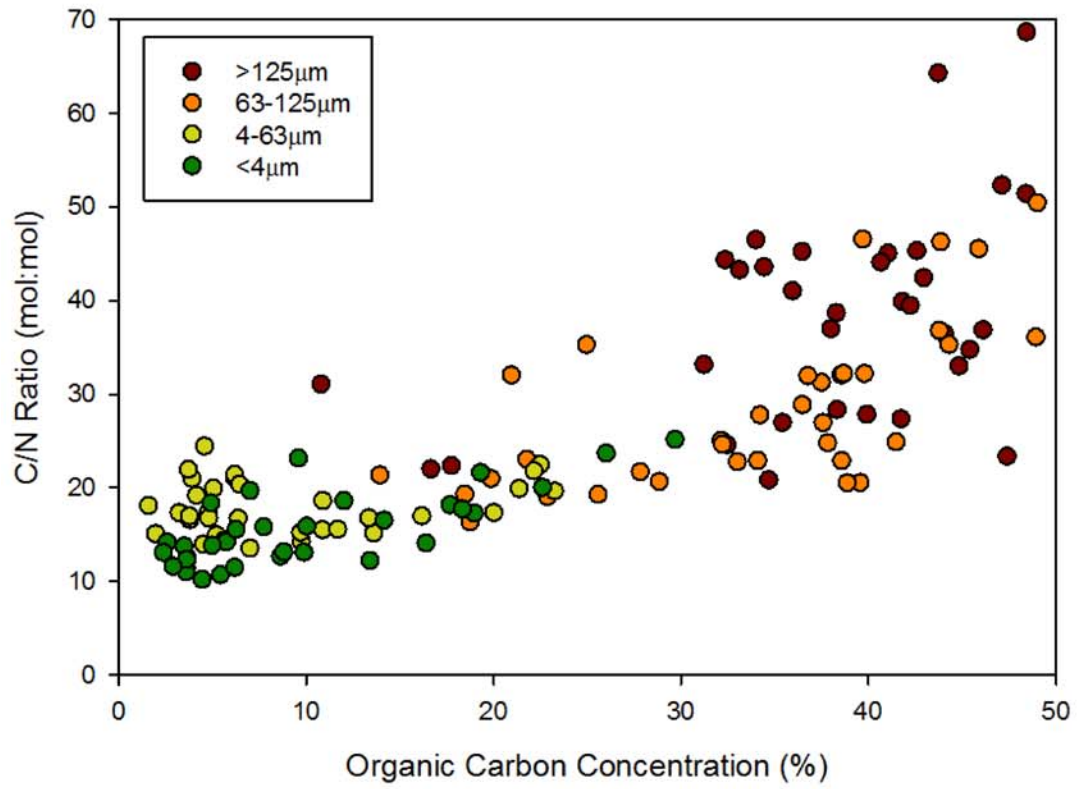


Figure 26: Relationship between C/N ratio and total organic carbon (TOC) concentration for the four size fractions of soil samples from the long cores examined in this study.

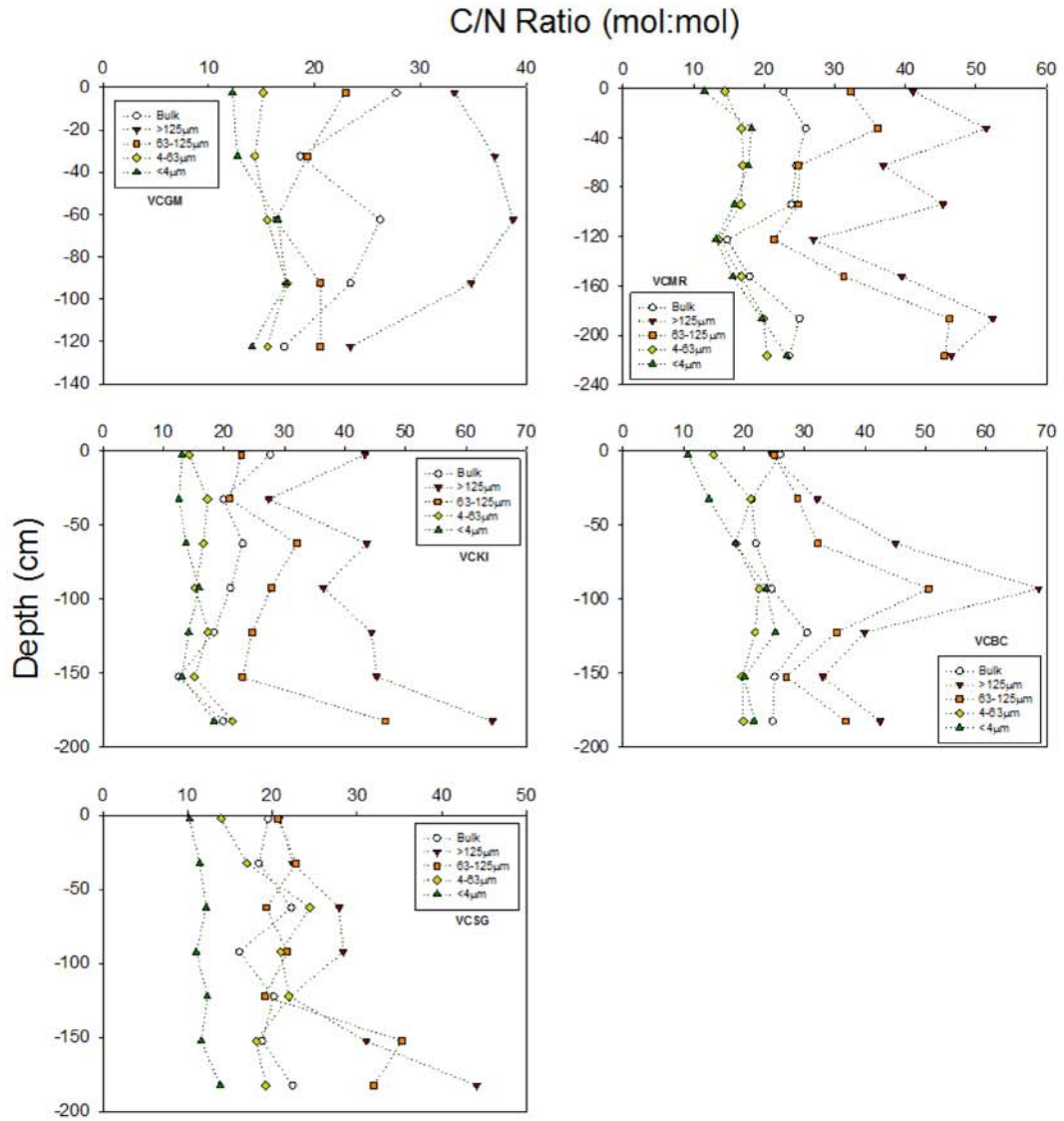


Figure 27: Depth variations in C/N ratio for bulk material and size fractions examined in long cores.

REFERENCES

- Anderson, D.W., 1979. Process of humus formation and transformation in soils of the Canadian Great Plains. *Journal of Soil Science*, 30: 77-84.
- Anderson, D.W., Saggar, S., Bettany, J.R., and Stewart, J.W.B., 1981. Particle size fractions and their use in studies of soil organic matter: I. The nature and distribution of forms of carbon, nitrogen, and sulfur. *Soil Science Society of America Journal*, 45: 767-772.
- Baldock, J.A., and Skjemstad, J.O., 2000. Role of the soil matrix and minerals in protecting natural organic materials against biological attack. *Organic Geochemistry*, 31: 697-710.
- Benner, R., Fogel, M.L., and Sprague, E.K., 1991. Diagenesis of belowground biomass of *Spartina alterniflora* in salt-marsh sediments. *Limnology and Oceanography*, 36(7): 1358-1374.
- Brenner, M., and Kenney, W.F., 2013. Dating wetland sediment cores. In: (DeLaune, R.D., Reedy, K.R., Richardson, C.J., and Megonigal, J.P., eds.) *Methods in Biogeochemistry of Wetlands*. Soil Science Society of America Book Series no. 10, pp. 879-900.
- Brevik, E.C., and Homburg, J.A., 2004. A 5000 year record of carbon sequestration from a coastal lagoon and wetland complex, Southern California, USA. *Catena*, 57: 221-232.
- Bridgham, S.D., Megonigal, J.P., Keller, J.K., Bliss, N.B., and Trettin, C., 2006. The carbon balance of North American wetlands. *Wetlands*, 26(4): 889-916.
- Callaway, J.C., Borgnis, E.L., Turner, R.E., and Milan, C.S., 2012. Carbon sequestration and sediment accretion in San Francisco Bay tidal wetlands. *Estuaries and Coasts*, 35: 1163-1181.
- Cambardella, C.A., and Elliott, E.T., 1993. Methods for physical separation and characterization of soil organic matter fractions. *Geoderma*, 56: 449-457.
- Chmura, G.L., Anisfeld, S.C., Cahoon, D.R., and Lynch, J.C., 2003. Global carbon sequestration in tidal, saline wetland soils. *Global Biogeochemical Cycles*, 17:doi:10.1029/2002GB001917.

- Chmura, G.L., and Hung, G.A., 2004. Controls on salt marsh accretion: a test in salt marshes of eastern Canada. *Estuaries*, 27(1): 70-81.
- Choi, Y., and Wang, Y., 2004. Dynamics of carbon sequestration in a coastal wetland using radiocarbon measurements. *Global Biogeochemical Cycles*, 18: GB4016.
- Christensen, B.T., 2001. Physical fractionation of soil and structural and functional complexity in organic matter turnover. *European Journal of Soil Science*, 52: 345-353.
- Connor, R.F., Chmura, G.L., and Beecher, C.B., 2001. Carbon accumulation in Bay of Fundy salt marshes: Implications for restoration of reclaimed marshes. *Global Biogeochemical Cycles*, 0(0): 1-12.
- Cook, T.L., Sommerfield, C.K., and Wong, K.C., 2007. Observations of tidal and springtime sediment transport in the upper Delaware Estuary. *Estuarine Coastal and Shelf Science*, 72(1-2): 235-246.
- Craft, C.B., 2007. Freshwater input structures soil properties, vertical accretion, and nutrient accumulation of Georgia and U.S. tidal marshes. *Limnology and Oceanography*, 52(3): 1220-1230.
- DeLaune, R.D., and White, J.R., 2012. Will coastal wetlands continue to sequester carbon in response to an increase in global sea level?: a case study of the rapidly subsiding Mississippi river deltaic plain. *Climatic Change*, 110: 297-314.
- Drexler, J.Z., 2011. Peat formation processes through the millennia in tidal marshes of the Sacramento-San Joaquin Delta, California, USA. *Estuaries and Coasts*, 34: 900-911.
- Dungait, J.A.J., Hopkins, D.W., Gregory, A.S., and Whitmore, A.P., 2012. Soil organic matter turnover is governed by accessibility not recalcitrance. *Global Change Biology*, 18(6): 1781-1796.
- Elliott, E.T., and Cambardella, C.A., 1991. Physical separation of soil organic matter. *Agriculture, Ecosystems and Environment*, 34: 407-419.
- Elsley-Quirk, T.E., Seliskar, D.M., Sommerfield, C.K., and Gallager, J.L., 2011. Salt marsh carbon pool distribution in a Mid-Atlantic lagoon, USA: sea level rise implications. *Wetlands*, 31: 87-99.

- Ember, L.M., Williams, D.F., and Morris, J.T., 1987. Processes that influence carbon isotope variations in salt marsh sediments. *Marine Ecology*, 36: 33-42.
- Fletcher, C.H., Knebel, H.J., and Kraft, J.C., 1990. Holocene evolution of an estuarine coast and tidal wetlands. *Geological Society of America Bulletin*, 102: 283-297.
- Fletcher, C.H., Knebel, H.J., and Kraft, J.C., 1992. Holocene depocenter migration and sediment accumulation in Delaware Bay: a submerging marginal marine sedimentary basin. *Marine Geology*, 103:165-183.
- French, J., 2006. Tidal marsh sedimentation and resilience to environmental change: Exploratory modeling of tidal, sea-level and sediment supply forcing in predominantly allochthonous systems. *Marine Geology*, 235(1-4): 119-136.
- Genrich, D.A., and Bremner, J.M., 1974. Isolation of soil particle-size fractions. *Soil Science Society of America Proceedings*, 38: 222-225.
- Haines, E.B., 1976. Stable carbon isotope ratios in the biota, soils and tidal water of a Georgia salt marsh. *Estuarine and Coastal Marine Science*, 4: 609-616.
- Harris, D., Horwáth, W.R., and van Kessel, C., 2001. Acid fumigation of soils to remove carbonates prior to total organic carbon or carbon-13 isotopic analysis. *Soil Science Society of America Journal*, 65: 1853-1856.
- Heiri, O., Lotter, A.F., and Lemcke, G., 2001. Loss on ignition as a method for estimating organic and carbonate content in sediments: reproducibility and comparability of results. *Journal of Paleolimnology*, 25: 101-110.
- Hopkinson, C.S., Gosselink, J.G., and Parrando, R.T., 1978. Aboveground production of seven marsh plant species in coastal Louisiana. *Ecology*, 59(4): 760-769.
- Hopkinson, C.S., Cai, W., and Hu, X., 2012. Carbon sequestration in wetland dominated coastal systems – a global sink of rapidly diminishing magnitude. *Current Opinion in Environmental Sustainability*, 4: 186-194.
- King, G.M., Klug, M.J., Wiegert, R.G., and Chalmers, A.G., 1982. Relation of soil water movement and sulfide concentration to *Spartina alterniflora* production in a Georgia salt marsh. *Science*, 218(4567): 61-63.
- Kirwan, M.L., Guntenspergen, G.R., and Langley, J.A., 2014. Temperature sensitivity of organic-matter decay in tidal marshes. *Biogeosciences*, 11: 4801-4808.

- Kirwan, M.L., Guntenspergen, G.R., and Morris, J.T., 2009. Latitudinal trends in *Spartina alterniflora* productivity and the response of coastal marshes to global change. *Global Change Biology*, 15:1982-1989.
- Komada, T., Anderson, M.R., and Dorfmeier, C.L., 2008. Carbonate removal from coastal sediments for the determination of organic carbon and its isotopic signatures, $\delta^{13}\text{C}$ and $\Delta^{14}\text{C}$: comparison of fumigation and direct acidification by hydrochloric acid. *Limnology and Oceanography: Methods*, 6: 254-262.
- Kraft, J.C., Yi, H., and Khalequzzaman, M., 1992. Geologic and human factors in the decline of the tidal salt marsh lithosome: the Delaware estuary and Atlantic coastal zone. *Sedimentary Geology*, 80: 233-246.
- Loomis, M.J., and Craft, C.B., 2010. Carbon sequestration and nutrient (nitrogen, phosphorus) accumulation in river-dominated tidal marshes, Georgia, USA. *Soil Science Society of America Journal*, 74(3): 1028-1036.
- Mayer, L.M., 1994. Relationships between mineral surfaces and organic carbon concentrations in soils and sediments. *Chemical Geology*, 114: 347-363.
- McKee, B.A., Nittrouer, C.A., and DeMaster, D.J., 1983. Concepts of sediment deposition and accumulation applied to the continental shelf near the mouth of the Yangtze River. *Geology*, 11: 631-633.
- McLeod, E., Chmura, G.L., Bouillon, S., Salm, R., Bjork, M., Duarte, C.M., Lovelock, C.E., Schlesinger, W.H., and Silliman, B.R., 2011. A blueprint for blue carbon: toward an improved understanding of the role of vegetated coastal habitats in sequestering CO_2 . *Frontiers in Ecology and the Environment*, 9(10): 552-560.
- Megonigal, J.P., and Neubauer, S.C., 2009. Biogeochemistry of tidal freshwater wetlands. In: (Perillo, G.M.E., Wolanski, E., Cahoon, D.R., Brinson, M.M., eds.) *Coastal wetlands: an integrated ecosystem approach*. Elsevier, Oxford, U.K., pp. 535-562.
- Meyers, P.A., 1994. Preservation of elemental and isotopic source identification of sedimentary organic matter. *Chemical Geology*, 114: 289-302.
- Middelburg, J.J., Nieuwenhuize, J., Lubberts, R.K., and van de Plassche, O., 1997. Organic carbon isotope systematics of coastal marshes. *Estuarine, Coastal, and Shelf Science*, 45: 681-687.

- Morris, J.T., and Bradley, P.M., 1999. Effects of nutrient loading on the carbon balance of coastal wetland sediments. *Limnology and Oceanography*, 44(3): 6999-702.
- Morris, J.T., Sundareshwar, P.V., Nietch, C.T., Kjerfve, B., and Cahoon, D.R., 2002. Responses of coastal wetlands to rising sea level. *Ecology*, 83(10): 2869-2877.
- Mudd, S.M., Howell, S.M., and Morris, J.T., 2009. Impact of dynamic feedbacks between sedimentation, sea-level rise, and biomass production on near-surface marsh stratigraphy and carbon accumulation. *Estuarine, Coastal, and Shelf Science*, 82: 377-389.
- Nellemann, C., Corcoran, E., Duarte, C., Valdés, L., Young, C.D., Fonseca, L., and Grimsditch, G., (eds.) 2009. Blue carbon – the role of healthy oceans in binding carbon. United Nations Environment Programme, GRID-Arendal.
- Neubauer, S.C., 2008. Contributions of mineral and organic components to tidal freshwater marsh accretion. *Estuarine, Coastal and Shelf Science*, 78: 78-88.
- Neubauer, S.C., Anderson, I.C., Constantine, J.A., and Kuehl, S.A., 2002. Sediment deposition and accretion in a Mid-Atlantic (U.S.A.) tidal freshwater marsh. *Estuarine, Coastal and Shelf Science*, 54: 713-727.
- Nilsson, M., Klarqvist, M., Bohlin, E., and Possnert, G., 2001. Variation in ¹⁴C age of macrofossils and different fractions of minute peat samples dated by AMS. *The Holocene*, 11(5): 579-586.
- Nyman, J.A., Walters, R.J., Delaune, R.D., and Patrick, W.H., 2006. Marsh vertical accretion via vegetative growth. *Estuarine, Coastal, and Shelf Science*, 69:370-380.
- Odum, W.E., and Heywood, M.A., 1978. Decomposition of intertidal freshwater plants. In: (Good, R.E., Whigham, F., and Simpson, R.L., eds.) *Freshwater wetlands, ecological processes and management potential*. Academic Press, New York, pp. 89-97.
- Odum, W.E., and Hoover, J.K., 1987. A comparison of vascular plant communities in tidal freshwater and saltwater marshes. In: (Hook, D.D., McKee, W.H., Smith, H.K., Gregory, J., Burrell, V.G., Jr., DeVoe, M.R., Sojka, R.E., Gilbert, S., Banks, R., Stolzy, L.H., Brooks, C., Matthews, T.D., and Shear, T.H., eds.) *The ecology and management of wetlands. v1: ecology of wetlands*. Timber Press, Portland, Oregon, pp. 526-534.

- Ouyang, X., and Lee, S.Y., 2014. Updated estimates of carbon accumulation rates in coastal marsh sediments. *Biogeosciences*, 11: 5057-5071.
- Pizzuto, J.E., and Rogers, E.W., 1992. The Holocene history and stratigraphy of palustrine and estuarine wetland deposits of central Delaware. *Journal of Coastal Research*, 8(4): 854-867.
- Post, W.M., Emanuel, W.R., Zinke, P.J., and Stangenberger, A.G., 1982. Soil carbon pools and world life zones. *Nature*, 298: 156-159.
- Reimer, P.J., Bard, E., Bayliss, A., Beck, J.W., Blackwell, P.G., Ramsey, C.B., Buck, C.E., Cheng, H., Edwards, R.L., Friedrich, M., Grootes, P.M., Guilderson, T.P., Haflidason, H., Hajdas, I., Hatte, C., Heaton, T.J., Hoffmann, D.L., Hogg, A.G., Hughen, K.A., Kaiser, K.F., Kromer, B., Manning, S.W., Niu, M., Reimer, R.W., Richards, D.A., Scott, E.M., Southon, J.R., Staff, R.A., Turney, C.S.M., and van der Plicht, J., 2013. INTCAL13 and MARINE13 radiocarbon age calibration curves 0-50,000 years cal BP. *Radiocarbon*, 55(4): 1869-1887.
- Ritchie, J.C., and McHenry, J.R., 1990. Application of radioactive fallout cesium-137 for measuring soil erosion and sediment accumulation rates and patterns: a review. *Journal of Environmental Quality*, 19: 215-233.
- Rooth, J.E., Stevenson, J.C., and Cornwell, J.C., 2003. Increased sediment accretion rates following invasion by *Phragmites australis*: The role of litter. *Estuaries*, 26(2): 475-483.
- Schubauer, J.P., and Hopkinson, C.S., 1984. Above- and belowground emergent macrophyte production and turnover in a coastal marsh ecosystem, Georgia. *Limnology and Oceanography*, 29(5) 1052-1065.
- Sommerfield, C.K., 2006. On sediment accumulation rates and stratigraphic completeness: Lessons from Holocene ocean margins. *Continental Shelf Research*, 26: 2225-2240.
- Sommerfield, C.K. and Velinsky, D., 2010. Controls on sediment accumulation and accretion rates in tidal marshes of a coastal plain estuary. *Eos Transactions, American Geophysical Union*, 91(26), Meet. Am. Supplement.
- Sommerfield, C.K. and Wong, K.C., 2011. Mechanisms of sediment flux and turbidity maintenance in the Delaware Estuary. *Journal of Geophysical Research*, 116, C01005, doi:10.1029/2010JC006462.

- Stuiver, M., and Polach, H.A., 1977. Discussion: Reporting of ^{14}C data. *Radiocarbon*, 19(3): 355-363.
- Stuiver, M., Reimer, P.J., and Reimer, R., 2015. Radiocarbon calibration program revision 7.1. Copyright 1986-2015.
- Tiner, R.W., Biddle, M.A., Jacobs, A.D., Rogerson, A.B., and McGuckin, K.G., 2011. Delaware wetlands: status and changes from 1992 to 2007. Cooperative National Wetlands Inventory Publication. U.S. Fish and Wildlife Service, Northeast Region, Hadley, MA and the Delaware Department of Natural Resources and Environmental Control, Dover, DE. 35 pp.
- Tobias, C., and Neubauer, S.C., 2009. Salt marsh biogeochemistry- an overview. In: (Perillo, G.M.E., Wolanski, E., Cahoon, D.R., Brinson, M.M., eds.) *Coastal wetlands: an integrated ecosystem approach*. Elsevier, Oxford, U.K., pp. 445-492.
- Torn, M.S., Trumbore, S.E., Chadwick, O.A., Vitousek, P.M., and Hendricks, D.M., 1997. Mineral control of soil organic carbon storage and turnover. *Nature*, 389: 170-173.
- Törnqvist, T.E., de Jong, A., Oosterbaan, W.A., and van der Borg, K., 1992. Accurate dating of organic deposits by AMS ^{14}C measurement of macrofossils. *Radiocarbon*, 34(3): 566-577.
- Trumbore, S., 2009. Radiocarbon and soil carbon dynamics. *Annual Review of Earth and Planetary Sciences*, 37: 47-66.
- Trumbore, S.E., and Zheng, S., 1996. Comparison of fractionation methods for soil organic matter ^{14}C analysis. *Radiocarbon*, 38(2) 219-229.
- Turetsky, M.R., Manning, S.W., and Wieder, R.K., 2004. Dating recent peat deposits. *Wetlands*, 24(2) 324-356.
- Turner, R.E., Swenson, E.M., and Milan, C.S., 2000. Organic and inorganic contributions to vertical accretion in salt marsh sediments. In: (Weinstein, M., and Kreeger, D.A., eds.), *Concepts and controversies in tidal marsh ecology*. Kluwer Academic Publish, Dordrecht, pp. 583-595.
- Valiela, I., Teal, J.M., Allen, S.D., van Etten, R.V., Goehring, D., and Volkmann, S., 1985. *Journal of Experimental Marine Biology and Ecology*, 89: 29-54.
- Waddington, J.M., and Roulet, N.T., 1997. Groundwater flow and dissolved carbon movement in a boreal peatland. *Journal of Hydrology*, 191: 122-138.

- Wakeham, S.G., Canuel, E.A., Lerber, E.J., Mason, P., Sampere, T.P., and Bianchi, T.S., 2009. Partitioning of organic matter in continental margin sediments among density fractions. *Marine Chemistry*, 115(3-4): 211-225.
- Wallbrink, P.J., Walling, D.E., and He, Q., 2002. Radionuclide measurement using HPGe gamma spectrometry. In: (Zapata, F., ed.) *Handbook for the assessment of soil erosion and sedimentation using environmental radionuclides*. Kluwer Academic Publisher, pp. 67-96.
- Wang, X.C., Chen, R.F., and Berry, A., 2003. Sources and preservation of organic matter in Plum Island salt marsh sediments (MA, USA): long-chain *n*-alkanes and stable carbon isotope compositions. *Estuarine, Coastal and Shelf Science*, 58: 917-928.
- Weston, N.B., Dixon, R.E., and Joye, S.B., 2006. Ramifications of increased salinity in tidal freshwater sediments: Geochemistry and microbial pathways of organic matter mineralization. *Journal of Geophysical Research*, 111: G01009.
- Whiting, G.J., and Chanton, J.P., 2001. Greenhouse carbon balance of wetlands: methane emissions versus carbon sequestration. *Tellus B*, 53(5): 521-528.
- Windham, L., 2001. Comparison of biomass production and decomposition between *Phragmites australis* (common reed) and *Spartina patens* (salt hay grass) in brackish tidal marshes of New Jersey, USA. *Wetlands*, 21(2): 179-188.
- Zervas, C., 2009. Sea level variations of the United States 1854-2006. NOAA Tech. Rpt., NOS CO-OPS 053, NOAA National Ocean Service, Silver Spring, MD.
- Zhou, J., Wu, Y., Zhang, J., Kang, Q., and Liu, Z., 2006. Carbon and nitrogen composition and stable isotope as potential indicators of source and fate of organic matter in the salt marsh of Changjiang Estuary, China. *Chemosphere*, 65: 310-317.
- Zhou, J., Wu, Y., Kang, Q., and Zhang, J., 2007. Spatial variations of carbon, nitrogen, phosphorous and sulfur in the salt marsh sediments of the Yangtze Estuary in China. *Estuarine, Coastal and Shelf Science*, 71: 47-59.

Appendix A

CARBON ACCUMULATION RATES AND RADIOCARBON DATA

This appendix includes physical property data, as well as carbon concentrations and densities for individual size fractions.

Table A1: Physical property data, C/N ratios, and total organic carbon concentrations for bulk material of long cores.

| Core ID | Depth (cm) | Dry Bulk Density (g cm ⁻³) | Gravimetric Porosity | Loss on Ignition | C/N Ratio (mol:mol) | TOC (%) |
|---------|------------|--|----------------------|------------------|---------------------|---------|
| VCGM | 2.5 | 0.248 | 0.873 | 0.481 | 27.69 | 21.49 |
| VCGM | 32.5 | 0.286 | 0.876 | 0.230 | 18.62 | 9.75 |
| VCGM | 62.5 | 0.178 | 0.913 | 0.409 | 26.17 | 18.52 |
| VCGM | 92.5 | 0.186 | 0.905 | 0.475 | 23.35 | 23.86 |
| VCGM | 122.5 | 0.278 | 0.873 | 0.320 | 17.12 | 15.68 |
| VCMR | 2.5 | 0.388 | 0.826 | 0.286 | 22.74 | 12.45 |
| VCMR | 32.5 | 0.170 | 0.919 | 0.386 | 25.85 | 19.89 |
| VCMR | 62.5 | 0.169 | 0.916 | 0.447 | 24.52 | 21.32 |
| VCMR | 94 | 0.261 | 0.886 | 0.245 | 23.85 | 13.50 |
| VCMR | 122.5 | 0.310 | 0.868 | 0.208 | 14.76 | 8.88 |
| VCMR | 152.5 | 0.464 | 0.810 | 0.146 | 17.94 | 6.38 |
| VCMR | 186.5 | 0.444 | 0.817 | 0.152 | 24.99 | 8.18 |
| VCMR | 216.5 | 0.347 | 0.854 | 0.190 | 23.49 | 9.14 |
| VCKI | 2.5 | 0.257 | 0.878 | 0.376 | 27.63 | 16.96 |
| VCKI | 32.5 | 0.446 | 0.815 | 0.166 | 19.93 | 7.35 |
| VCKI | 62.5 | 0.409 | 0.830 | 0.167 | 23.10 | 6.97 |
| VCKI | 92.5 | 0.201 | 0.907 | 0.331 | 21.06 | 15.17 |
| VCKI | 122.5 | 0.444 | 0.818 | 0.140 | 18.32 | 5.92 |
| VCKI | 152.5 | 0.581 | 0.770 | 0.087 | 12.57 | 2.27 |
| VCKI | 182.5 | 0.532 | 0.783 | 0.137 | 19.86 | 6.54 |
| VCBC | 2.5 | 0.349 | 0.844 | 0.280 | 25.97 | 12.72 |
| VCBC | 32.5 | 0.454 | 0.810 | 0.180 | 21.23 | 8.53 |
| VCBC | 62.5 | 0.266 | 0.880 | 0.298 | 21.93 | 14.77 |
| VCBC | 93 | 0.160 | 0.918 | 0.483 | 24.57 | 25.11 |
| VCBC | 122.5 | 0.150 | 0.911 | 0.663 | 30.39 | 33.86 |
| VCBC | 152.5 | 0.151 | 0.917 | 0.573 | 25.03 | 32.63 |
| VCBC | 182.5 | 0.162 | 0.917 | 0.482 | 24.72 | 25.35 |
| VCSG | 2.5 | 0.406 | 0.826 | 0.220 | 19.51 | 9.41 |
| VCSG | 32.5 | 0.646 | 0.740 | 0.114 | 18.41 | 5.05 |
| VCSG | 62.5 | 0.707 | 0.716 | 0.113 | 22.24 | 4.99 |
| VCSG | 92.5 | 0.667 | 0.734 | 0.097 | 16.08 | 4.15 |
| VCSG | 122.5 | 0.734 | 0.708 | 0.091 | 20.15 | 4.27 |
| VCSG | 152.5 | 0.900 | 0.643 | 0.087 | 18.77 | 2.37 |
| VCSG | 182.5 | 0.607 | 0.752 | 0.136 | 22.38 | 6.68 |

Table A2: C/N ratios and total organic carbon concentrations for size fractions of the Great Marsh long core.

| Core | Interval | Depth (cm) | Size Fraction | C/N | TOC (%) |
|------|----------|------------|----------------|-------|---------|
| VCGM | 0-5 | 2.5 | >125 μ m | 33.17 | 31.22 |
| | | | 63–125 μ m | 22.90 | 34.09 |
| | | | 4–63 μ m | 15.14 | 13.61 |
| | | | <4 μ m | 12.23 | 13.41 |
| VCGM | 30-35 | 32.5 | >125 μ m | 36.99 | 37.99 |
| | | | 63–125 μ m | 19.30 | 18.46 |
| | | | 4–63 μ m | 14.34 | 5.78 |
| | | | <4 μ m | 12.70 | 8.64 |
| VCGM | 60-65 | 62.5 | >125 μ m | 38.70 | 38.29 |
| | | | 63–125 μ m | 16.35 | 18.75 |
| | | | 4–63 μ m | 15.51 | 10.89 |
| | | | <4 μ m | 16.53 | 14.16 |
| VCGM | 90-95 | 92.5 | >125 μ m | 34.78 | 45.40 |
| | | | 63–125 μ m | 20.54 | 39.55 |
| | | | 4–63 μ m | 17.35 | 20.01 |
| | | | <4 μ m | 17.28 | 18.98 |
| VCGM | 120-125 | 122.5 | >125 μ m | 23.36 | 47.39 |
| | | | 63–125 μ m | 20.52 | 38.86 |
| | | | 4–63 μ m | 15.55 | 11.69 |
| | | | <4 μ m | 14.08 | 16.39 |

Table A3: C/N ratios and total organic carbon concentrations for size fractions of the Mispillion River long core.

| Core | Interval | Depth (cm) | Size Fraction | C/N | TOC (%) |
|------|-----------|------------|----------------|-------|---------|
| VCMR | 0-5 | 2.5 | >125 μ m | 41.05 | 35.95 |
| | | | 63–125 μ m | 32.22 | 39.78 |
| | | | 4–63 μ m | 14.43 | 5.66 |
| | | | <4 μ m | 11.52 | 6.19 |
| VCMR | 30-35 | 32.5 | >125 μ m | 51.43 | 48.40 |
| | | | 63–125 μ m | 36.09 | 48.93 |
| | | | 4–63 μ m | 16.79 | 13.34 |
| | | | <4 μ m | 18.18 | 17.68 |
| VCMR | 60-65 | 62.5 | >125 μ m | 36.86 | 46.11 |
| | | | 63–125 μ m | 24.89 | 41.46 |
| | | | 4–63 μ m | 16.98 | 16.17 |
| | | | <4 μ m | 17.73 | 18.33 |
| VCMR | 91.5-96.5 | 94 | >125 μ m | 45.31 | 42.58 |
| | | | 63–125 μ m | 24.81 | 37.82 |
| | | | 4–63 μ m | 16.72 | 6.37 |
| | | | <4 μ m | 15.80 | 7.74 |
| VCMR | 120-125 | 122.5 | >125 μ m | 26.97 | 35.42 |
| | | | 63–125 μ m | 21.37 | 13.93 |
| | | | 4–63 μ m | 13.52 | 7.00 |
| | | | <4 μ m | 13.15 | 8.82 |
| VCMR | 150-155 | 152.5 | >125 μ m | 39.48 | 42.23 |
| | | | 63–125 μ m | 31.26 | 37.49 |
| | | | 4–63 μ m | 16.76 | 4.80 |
| | | | <4 μ m | 15.54 | 6.25 |
| VCMR | 184-189 | 186.5 | >125 μ m | 52.35 | 47.11 |
| | | | 63–125 μ m | 46.26 | 43.85 |
| | | | 4–63 μ m | 19.95 | 5.06 |
| | | | <4 μ m | 19.68 | 7.01 |
| VCMR | 214-219 | 216.5 | >125 μ m | 46.51 | 33.99 |
| | | | 63–125 μ m | 45.54 | 45.87 |
| | | | 4–63 μ m | 20.36 | 6.45 |
| | | | <4 μ m | 23.17 | 9.59 |

Table A4: C/N ratios and total organic carbon concentrations for size fractions of the Kelly Island long core.

| Core | Interval | Depth (cm) | Size Fraction | C/N | TOC (%) |
|------|----------|------------|----------------|-------|---------|
| VCKI | 0-5 | 2.5 | >125 μ m | 43.29 | 33.12 |
| | | | 63–125 μ m | 22.89 | 38.57 |
| | | | 4–63 μ m | 14.26 | 9.75 |
| | | | <4 μ m | 13.10 | 9.89 |
| VCKI | 30-35 | 32.5 | >125 μ m | 27.37 | 41.73 |
| | | | 63–125 μ m | 20.97 | 19.86 |
| | | | 4–63 μ m | 17.30 | 4.78 |
| | | | <4 μ m | 12.54 | 3.65 |
| VCKI | 60-65 | 62.5 | >125 μ m | 43.59 | 34.42 |
| | | | 63–125 μ m | 32.05 | 20.94 |
| | | | 4–63 μ m | 16.59 | 3.80 |
| | | | <4 μ m | 13.76 | 3.49 |
| VCKI | 90-95 | 92.5 | >125 μ m | 36.43 | 44.07 |
| | | | 63–125 μ m | 27.78 | 34.21 |
| | | | 4–63 μ m | 15.22 | 9.70 |
| | | | <4 μ m | 15.89 | 10.03 |
| VCKI | 120-125 | 122.5 | >125 μ m | 44.96 | 30.97 |
| | | | 63–125 μ m | 24.64 | 32.21 |
| | | | 4–63 μ m | 17.34 | 3.22 |
| | | | <4 μ m | 14.16 | 2.59 |
| VCKI | 150-155 | 152.5 | >125 μ m | 45.24 | 36.45 |
| | | | 63–125 μ m | 23.04 | 21.77 |
| | | | 4–63 μ m | 15.09 | 1.97 |
| | | | <4 μ m | 13.09 | 2.39 |
| VCKI | 180-185 | 182.5 | >125 μ m | 64.32 | 43.71 |
| | | | 63–125 μ m | 46.57 | 39.69 |
| | | | 4–63 μ m | 21.41 | 6.19 |
| | | | <4 μ m | 18.38 | 4.92 |

Table A5: C/N ratios and total organic carbon concentrations for size fractions of the Blackbird Creek long core.

| Core | Interval | Depth (cm) | Size Fraction | C/N | TOC (%) |
|------|-----------|------------|----------------|-------|---------|
| VCBC | 0-5 | 2.5 | >125 μ m | 24.59 | 32.46 |
| | | | 63–125 μ m | 25.03 | 32.14 |
| | | | 4–63 μ m | 14.97 | 5.22 |
| | | | <4 μ m | 10.70 | 5.43 |
| VCBC | 30-35 | 32.5 | >125 μ m | 32.07 | 38.54 |
| | | | 63–125 μ m | 28.88 | 36.48 |
| | | | 4–63 μ m | 21.07 | 6.18 |
| | | | <4 μ m | 14.22 | 5.75 |
| VCBC | 60-65 | 62.5 | >125 μ m | 45.05 | 41.04 |
| | | | 63–125 μ m | 32.21 | 38.66 |
| | | | 4–63 μ m | 18.63 | 10.89 |
| | | | <4 μ m | 18.60 | 12.02 |
| VCBC | 90.5-95.5 | 93 | >125 μ m | 68.68 | 48.43 |
| | | | 63–125 μ m | 50.45 | 49.00 |
| | | | 4–63 μ m | 22.46 | 22.48 |
| | | | <4 μ m | 23.69 | 26.01 |
| VCBC | 120-125 | 122.5 | >125 μ m | 39.88 | 41.81 |
| | | | 63–125 μ m | 35.31 | 44.30 |
| | | | 4–63 μ m | 21.81 | 22.15 |
| | | | <4 μ m | 25.16 | 29.68 |
| VCBC | 150-155 | 152.5 | >125 μ m | 33.01 | 44.83 |
| | | | 63–125 μ m | 26.98 | 37.57 |
| | | | 4–63 μ m | 19.65 | 23.26 |
| | | | <4 μ m | 20.05 | 22.61 |
| VCBC | 180-185 | 182.5 | >125 μ m | 42.45 | 42.94 |
| | | | 63–125 μ m | 36.80 | 43.78 |
| | | | 4–63 μ m | 19.91 | 21.37 |
| | | | <4 μ m | 21.63 | 19.31 |

Table A6: C/N ratios and total organic carbon concentrations for size fractions of the St. Georges long core.

| Core | Interval | Depth (cm) | Size Fraction | C/N | TOC (%) |
|------|----------|------------|----------------|-------|---------|
| VCSG | 0-5 | 2.5 | >125 μ m | 20.84 | 34.68 |
| | | | 63–125 μ m | 20.67 | 28.84 |
| | | | 4–63 μ m | 13.98 | 4.53 |
| | | | <4 μ m | 10.21 | 4.46 |
| VCSG | 30-35 | 32.5 | >125 μ m | 22.37 | 17.75 |
| | | | 63–125 μ m | 22.79 | 33.01 |
| | | | 4–63 μ m | 16.96 | 3.77 |
| | | | <4 μ m | 11.41 | 3.61 |
| VCSG | 60-65 | 62.5 | >125 μ m | 27.85 | 39.91 |
| | | | 63–125 μ m | 19.29 | 25.58 |
| | | | 4–63 μ m | 24.44 | 4.58 |
| | | | <4 μ m | 12.20 | 3.63 |
| VCSG | 90-95 | 92.5 | >125 μ m | 28.35 | 38.32 |
| | | | 63–125 μ m | 21.71 | 27.81 |
| | | | 4–63 μ m | 20.98 | 3.91 |
| | | | <4 μ m | 11.01 | 3.60 |
| VCSG | 120-125 | 122.5 | >125 μ m | 22.03 | 16.65 |
| | | | 63–125 μ m | 19.08 | 22.87 |
| | | | 4–63 μ m | 21.94 | 3.98 |
| | | | <4 μ m | 12.33 | 3.62 |
| VCSG | 150-155 | 152.5 | >125 μ m | 31.07 | 10.79 |
| | | | 63–125 μ m | 35.29 | 24.95 |
| | | | 4–63 μ m | 18.11 | 1.59 |
| | | | <4 μ m | 11.61 | 2.90 |
| VCSG | 180-185 | 182.5 | >125 μ m | 44.10 | 40.65 |
| | | | 63–125 μ m | 31.97 | 36.77 |
| | | | 4–63 μ m | 19.21 | 4.15 |
| | | | <4 μ m | 13.84 | 5.00 |

Table A7: Total carbon concentration and carbon concentrations of soil size fractions for long cores.

| Core | Interval (cm) | >125 μm (g C cm ⁻³) | 63–125 μm (g C cm ⁻³) | 4–63 μm (g C cm ⁻³) | <4 μm (g C cm ⁻³) | Total (g C cm ⁻³) |
|------|---------------|---|---|---|---|----------------------------------|
| VCGM | 0-5 | 0.0207 | 0.0008 | 0.0117 | 0.0126 | 0.0458 |
| VCGM | 30-35 | 0.0102 | 0.0013 | 0.0119 | 0.0040 | 0.0274 |
| VCGM | 60-65 | 0.0215 | 0.0021 | 0.0103 | 0.0023 | 0.0361 |
| VCGM | 90-95 | 0.0351 | 0.0058 | 0.0120 | 0.0064 | 0.0594 |
| VCGM | 120-125 | 0.0181 | 0.0016 | 0.0203 | 0.0102 | 0.0502 |
| VCMR | 0-5 | 0.0230 | 0.0008 | 0.0146 | 0.0040 | 0.0423 |
| VCMR | 30-35 | 0.0151 | 0.0009 | 0.0147 | 0.0048 | 0.0354 |
| VCMR | 60-65 | 0.0184 | 0.0014 | 0.0152 | 0.0059 | 0.0408 |
| VCMR | 91.5-96.5 | 0.0089 | 0.0009 | 0.0114 | 0.0045 | 0.0257 |
| VCMR | 120-125 | 0.0058 | 0.0007 | 0.0176 | 0.0033 | 0.0274 |
| VCMR | 150-155 | 0.0043 | 0.0015 | 0.0184 | 0.0042 | 0.0284 |
| VCMR | 184-189 | 0.0068 | 0.0013 | 0.0190 | 0.0035 | 0.0306 |
| VCMR | 214-219 | 0.0067 | 0.0012 | 0.0188 | 0.0032 | 0.0299 |
| VCKI | 0-5 | 0.0419 | 0.0011 | 0.0103 | 0.0022 | 0.0555 |
| VCKI | 30-35 | 0.0226 | 0.0011 | 0.0149 | 0.0027 | 0.0412 |
| VCKI | 60-65 | 0.0093 | 0.0004 | 0.0121 | 0.0022 | 0.0239 |
| VCKI | 90-95 | 0.0249 | 0.0008 | 0.0118 | 0.0021 | 0.0395 |
| VCKI | 120-125 | 0.0042 | 0.0009 | 0.0087 | 0.0041 | 0.0179 |
| VCKI | 150-155 | 0.0005 | 0.0003 | 0.0074 | 0.0048 | 0.0130 |
| VCKI | 180-185 | 0.0027 | 0.0008 | 0.0266 | 0.0046 | 0.0347 |
| VCBC | 0-5 | 0.0177 | 0.0011 | 0.0125 | 0.0029 | 0.0341 |
| VCBC | 30-35 | 0.0131 | 0.0013 | 0.0177 | 0.0075 | 0.0395 |
| VCBC | 60-65 | 0.0115 | 0.0015 | 0.0197 | 0.0064 | 0.0391 |
| VCBC | 90.5-95.5 | 0.0098 | 0.0007 | 0.0225 | 0.0100 | 0.0430 |
| VCBC | 120-125 | 0.0180 | 0.0006 | 0.0161 | 0.0099 | 0.0446 |
| VCBC | 150-155 | 0.0119 | 0.0018 | 0.0216 | 0.0061 | 0.0414 |
| VCBC | 180-185 | 0.0088 | 0.0014 | 0.0209 | 0.0078 | 0.0389 |
| VCSG | 0-5 | 0.0157 | 0.0008 | 0.0148 | 0.0014 | 0.0327 |
| VCSG | 30-35 | 0.0019 | 0.0006 | 0.0193 | 0.0044 | 0.0262 |
| VCSG | 60-65 | 0.0018 | 0.0005 | 0.0263 | 0.0046 | 0.0331 |
| VCSG | 90-95 | 0.0007 | 0.0006 | 0.0208 | 0.0047 | 0.0268 |
| VCSG | 120-125 | 0.0008 | 0.0005 | 0.0231 | 0.0039 | 0.0282 |
| VCSG | 150-155 | 0.0002 | 0.0002 | 0.0100 | 0.0078 | 0.0182 |
| VCSG | 180-185 | 0.0057 | 0.0006 | 0.0192 | 0.0064 | 0.0320 |

Appendix B
NITROGEN DATA

This appendix includes nitrogen data from short and long cores.

Table B1: Nitrogen accumulation rates for short cores.

| Location (Abbreviation) | Core Id | Nitrogen Accumulation Rate (g N m ⁻² yr ⁻¹) |
|-------------------------------|---------|--|
| | CC-1 | 1.8 |
| Canary Creek, DE (CC) | CC-2 | 3.6 |
| | CC-3 | 11.0 |
| | CC-5 | 5.7 |
| | CC-6 | 9.0 |
| | GM-1 | 15.1 |
| Great Marsh, DE (GM) | GM-2 | 8.0 |
| | GM-3 | 4.7 |
| | GM-4 | 3.2 |
| | KI-1 | 12.5 |
| Kelly Island, DE (KI) | KI-2 | 7.0 |
| | KI-3 | 8.6 |
| | MR-1 | 9.1 |
| Mispillion River, DE (MR) | MR-2 | 8.3 |
| | MR-3 | 10.6 |
| | BC-1 | 11.6 |
| Blackbird Creek, DE (BC) | BC-2 | 10.6 |
| | BC-3 | 8.5 |
| | SG-1 | 15.2 |
| St. Georges Marsh, DE (SG) | SG-2 | 16.7 |
| | SG-3 | 28.3 |
| | SJBM-1 | 7.5 |
| St. Jones Reserve, DE (SJ) | SJBM-2 | 23.7 |
| | SJBM-3 | 13.0 |

Table B2: Total nitrogen concentrations for bulk material of long cores.

| Core | Depth (cm) | Nitrogen (%) |
|-------|---------------|-----------------|
| VCGM | 2.5 | 0.91 |
| | 32.5 | 0.61 |
| | 62.5 | 0.83 |
| | 92.5 | 1.19 |
| | 122.5 | 1.07 |
| VCMR | 2.5 | 0.64 |
| | 32.5 | 0.90 |
| | 62.5 | 1.01 |
| | 94 | 0.66 |
| | 122.5 | 0.70 |
| | 152.5 | 0.42 |
| | 186.5 | 0.38 |
| 216.5 | 0.45 | |
| VCKI | 2.5 | 0.72 |
| | 32.5 | 0.43 |
| | 62.5 | 0.35 |
| | 92.5 | 0.84 |
| | 122.5 | 0.38 |
| | 152.5 | 0.21 |
| | 182.5 | 0.38 |
| VCBC | 2.5 | 0.57 |
| | 32.5 | 0.47 |
| | 62.5 | 0.79 |
| | 93 | 1.19 |
| | 122.5 | 1.30 |
| | 152.5 | 1.52 |
| | 182.5 | 1.20 |
| VCSG | 2.5 | 0.56 |
| | 32.5 | 0.32 |
| | 62.5 | 0.26 |
| | 92.5 | 0.30 |
| | 122.5 | 0.25 |
| | 152.5 | 0.15 |
| | 182.5 | 0.35 |

Table B3: Long-term nitrogen accumulation rates. Rates were calculated based on ages shown.

| Core Id | Depth (cm) | 2-sigma Calibrated Age (Cal yr BP) | Nitrogen Accumulation Rate (g N m ⁻² yr ⁻¹) |
|---------|------------|------------------------------------|--|
| VCGM | 62.5 | 182 | 6.6 |
| VCGM | 92.5 | 397 | 4.4 |
| VCGM | 122.5 | 866 | 3.0 |
| VCMR | 62.5 | 189 | 6.5 |
| VCMR | 94 | 307 | 5.8 |
| VCMR | 122.5 | 487 | 4.8 |
| VCMR | 152.5 | 864 | 3.5 |
| VCMR | 186.5 | 1108 | 3.3 |
| VCMR | 216.5 | 1459 | 2.8 |
| VCKI | 62.5 | 184 | 6.4 |
| VCKI | 92.5 | 296 | 5.8 |
| VCKI | 122.5 | 300 | 7.7 |
| VCKI | 152.5 | 308 | 8.9 |
| VCKI | 182.5 | 924 | 3.5 |
| VCBC | 32.5 | 178 | 4.1 |
| VCBC | 93 | 594 | 3.4 |
| VCBC | 152.5 | 1213 | 2.7 |
| VCBC | 182.5 | 732 | 5.3 |
| VCSG | 122.5 | 920 | 2.8 |
| VCSG | 182.5 | 753 | 4.8 |

Table B4: Total nitrogen concentrations for size fractions of the Great Marsh long core.

| Core | Interval | Depth (cm) | Size Fraction | Nitrogen (%) |
|------|----------|------------|----------------|--------------|
| VCGM | 0-5 | 2.5 | >125 μ m | 1.10 |
| | | | 63-125 μ m | 1.74 |
| | | | 4-63 μ m | 1.05 |
| | | | <4 μ m | 1.28 |
| VCGM | 30-35 | 32.5 | >125 μ m | 1.20 |
| | | | 63-125 μ m | 1.12 |
| | | | 4-63 μ m | 0.47 |
| | | | <4 μ m | 0.79 |
| VCGM | 60-65 | 62.5 | >125 μ m | 1.15 |
| | | | 63-125 μ m | 1.34 |
| | | | 4-63 μ m | 0.82 |
| | | | <4 μ m | 1.00 |
| VCGM | 90-95 | 92.5 | >125 μ m | 1.52 |
| | | | 63-125 μ m | 2.25 |
| | | | 4-63 μ m | 1.34 |
| | | | <4 μ m | 1.28 |
| VCGM | 120-125 | 122.5 | >125 μ m | 2.37 |
| | | | 63-125 μ m | 2.21 |
| | | | 4-63 μ m | 0.88 |
| | | | <4 μ m | 1.36 |

Table B5: Total nitrogen concentrations for size fractions of the Mispillion River long core.

| Core | Interval | Depth (cm) | Size Fraction | Nitrogen (%) |
|------|-----------|------------|----------------|--------------|
| VCMR | 0-5 | 2.5 | >125 μ m | 1.02 |
| | | | 63-125 μ m | 1.44 |
| | | | 4-63 μ m | 0.46 |
| | | | <4 μ m | 0.63 |
| VCMR | 30-35 | 32.5 | >125 μ m | 1.10 |
| | | | 63-125 μ m | 1.58 |
| | | | 4-63 μ m | 0.93 |
| | | | <4 μ m | 1.13 |
| VCMR | 60-65 | 62.5 | >125 μ m | 1.46 |
| | | | 63-125 μ m | 1.94 |
| | | | 4-63 μ m | 1.11 |
| | | | <4 μ m | 1.21 |
| VCMR | 91.5-96.5 | 94 | >125 μ m | 1.10 |
| | | | 63-125 μ m | 1.78 |
| | | | 4-63 μ m | 0.44 |
| | | | <4 μ m | 0.57 |
| VCMR | 120-125 | 122.5 | >125 μ m | 1.53 |
| | | | 63-125 μ m | 0.76 |
| | | | 4-63 μ m | 0.60 |
| | | | <4 μ m | 0.78 |
| VCMR | 150-155 | 152.5 | >125 μ m | 1.25 |
| | | | 63-125 μ m | 1.40 |
| | | | 4-63 μ m | 0.33 |
| | | | <4 μ m | 0.47 |
| VCMR | 184-189 | 186.5 | >125 μ m | 1.05 |
| | | | 63-125 μ m | 1.11 |
| | | | 4-63 μ m | 0.30 |
| | | | <4 μ m | 0.42 |
| VCMR | 214-219 | 216.5 | >125 μ m | 0.85 |
| | | | 63-125 μ m | 1.17 |
| | | | 4-63 μ m | 0.37 |
| | | | <4 μ m | 0.48 |

Table B6: Total nitrogen concentrations for size fractions of the Kelly Island long core.

| Core | Interval | Depth (cm) | Size Fraction | Nitrogen (%) |
|------|----------|------------|----------------|--------------|
| VCKI | 0-5 | 2.5 | >125 μ m | 0.89 |
| | | | 63–125 μ m | 1.96 |
| | | | 4–63 μ m | 0.80 |
| | | | <4 μ m | 0.88 |
| VCKI | 30-35 | 32.5 | >125 μ m | 1.78 |
| | | | 63–125 μ m | 1.10 |
| | | | 4–63 μ m | 0.32 |
| | | | <4 μ m | 0.34 |
| VCKI | 60-65 | 62.5 | >125 μ m | 0.92 |
| | | | 63–125 μ m | 0.76 |
| | | | 4–63 μ m | 0.27 |
| | | | <4 μ m | 0.30 |
| VCKI | 90-95 | 92.5 | >125 μ m | 1.41 |
| | | | 63–125 μ m | 1.44 |
| | | | 4–63 μ m | 0.74 |
| | | | <4 μ m | 0.74 |
| VCKI | 120-125 | 122.5 | >125 μ m | 0.80 |
| | | | 63–125 μ m | 1.52 |
| | | | 4–63 μ m | 0.22 |
| | | | <4 μ m | 0.21 |
| VCKI | 150-155 | 152.5 | >125 μ m | 0.94 |
| | | | 63–125 μ m | 1.10 |
| | | | 4–63 μ m | 0.15 |
| | | | <4 μ m | 0.21 |
| VCKI | 180-185 | 182.5 | >125 μ m | 0.79 |
| | | | 63–125 μ m | 1.00 |
| | | | 4–63 μ m | 0.34 |
| | | | <4 μ m | 0.31 |

Table B7: Total nitrogen concentrations for size fractions of the Blackbird Creek long core.

| Core | Interval | Depth (cm) | Size Fraction | Nitrogen (%) |
|------|-----------|------------|----------------|--------------|
| VCBC | 0-5 | 2.5 | >125 μ m | 1.54 |
| | | | 63–125 μ m | 1.50 |
| | | | 4–63 μ m | 0.41 |
| | | | <4 μ m | 0.59 |
| VCBC | 30-35 | 32.5 | >125 μ m | 1.40 |
| | | | 63–125 μ m | 1.47 |
| | | | 4–63 μ m | 0.34 |
| | | | <4 μ m | 0.47 |
| VCBC | 60-65 | 62.5 | >125 μ m | 1.06 |
| | | | 63–125 μ m | 1.40 |
| | | | 4–63 μ m | 0.68 |
| | | | <4 μ m | 0.75 |
| VCBC | 90.5-95.5 | 93 | >125 μ m | 0.82 |
| | | | 63–125 μ m | 1.13 |
| | | | 4–63 μ m | 1.17 |
| | | | <4 μ m | 1.28 |
| VCBC | 120-125 | 122.5 | >125 μ m | 1.23 |
| | | | 63–125 μ m | 1.46 |
| | | | 4–63 μ m | 1.18 |
| | | | <4 μ m | 1.38 |
| VCBC | 150-155 | 152.5 | >125 μ m | 1.58 |
| | | | 63–125 μ m | 1.62 |
| | | | 4–63 μ m | 1.38 |
| | | | <4 μ m | 1.32 |
| VCBC | 180-185 | 182.5 | >125 μ m | 1.18 |
| | | | 63–125 μ m | 1.39 |
| | | | 4–63 μ m | 1.25 |
| | | | <4 μ m | 1.04 |

Table B8: Total nitrogen concentrations for size fractions of the St. Georges long core.

| Core | Interval | Depth (cm) | Size Fraction | Nitrogen (%) |
|------|----------|------------|----------------|--------------|
| VCSG | 0-5 | 2.5 | >125 μ m | 1.94 |
| | | | 63–125 μ m | 1.63 |
| | | | 4–63 μ m | 0.38 |
| | | | <4 μ m | 0.51 |
| VCSG | 30-35 | 32.5 | >125 μ m | 0.93 |
| | | | 63–125 μ m | 1.69 |
| | | | 4–63 μ m | 0.26 |
| | | | <4 μ m | 0.37 |
| VCSG | 60-65 | 62.5 | >125 μ m | 1.67 |
| | | | 63–125 μ m | 1.55 |
| | | | 4–63 μ m | 0.22 |
| | | | <4 μ m | 0.35 |
| VCSG | 90-95 | 92.5 | >125 μ m | 1.58 |
| | | | 63–125 μ m | 1.50 |
| | | | 4–63 μ m | 0.22 |
| | | | <4 μ m | 0.38 |
| VCSG | 120-125 | 122.5 | >125 μ m | 0.88 |
| | | | 63–125 μ m | 1.40 |
| | | | 4–63 μ m | 0.21 |
| | | | <4 μ m | 0.34 |
| VCSG | 150-155 | 152.5 | >125 μ m | 0.41 |
| | | | 63–125 μ m | 0.82 |
| | | | 4–63 μ m | 0.10 |
| | | | <4 μ m | 0.29 |
| VCSG | 180-185 | 182.5 | >125 μ m | 1.07 |
| | | | 63–125 μ m | 1.34 |
| | | | 4–63 μ m | 0.25 |
| | | | <4 μ m | 0.42 |

Table B9: Total nitrogen concentrations and nitrogen concentrations of soil size fractions for long cores.

| Core | Interval (cm) | >125 μm (g N cm ⁻³) | 63–125 μm (g N cm ⁻³) | 4–63 μm (g N cm ⁻³) | <4 μm (g N cm ⁻³) | Total (g N cm ⁻³) |
|------|---------------|---|---|---|---|----------------------------------|
| VCGM | 0-5 | 7.3E-04 | 4.0E-05 | 9.1E-04 | 1.2E-03 | 0.0029 |
| VCGM | 30-35 | 3.2E-04 | 8.1E-05 | 9.7E-04 | 3.7E-04 | 0.0017 |
| VCGM | 60-65 | 6.4E-04 | 1.5E-04 | 7.8E-04 | 1.6E-04 | 0.0017 |
| VCGM | 90-95 | 1.2E-03 | 3.3E-04 | 8.1E-04 | 4.3E-04 | 0.0027 |
| VCGM | 120-125 | 9.1E-04 | 8.9E-05 | 1.5E-03 | 8.5E-04 | 0.0034 |
| VCMR | 0-5 | 6.5E-04 | 2.7E-05 | 1.2E-03 | 4.1E-04 | 0.0023 |
| VCMR | 30-35 | 3.4E-04 | 2.7E-05 | 1.0E-03 | 3.0E-04 | 0.0017 |
| VCMR | 60-65 | 5.8E-04 | 6.6E-05 | 1.0E-03 | 3.9E-04 | 0.0021 |
| VCMR | 91.5-96.5 | 2.7E-04 | 4.1E-05 | 7.9E-04 | 3.3E-04 | 0.0014 |
| VCMR | 120-125 | 2.5E-04 | 3.8E-05 | 1.5E-03 | 3.0E-04 | 0.0021 |
| VCMR | 150-155 | 1.3E-04 | 5.7E-05 | 1.3E-03 | 3.1E-04 | 0.0018 |
| VCMR | 184-189 | 1.5E-04 | 3.2E-05 | 1.1E-03 | 2.1E-04 | 0.0015 |
| VCMR | 214-219 | 1.7E-04 | 3.0E-05 | 1.1E-03 | 1.6E-04 | 0.0014 |
| VCKI | 0-5 | 1.1E-03 | 5.4E-05 | 8.5E-04 | 2.0E-04 | 0.0022 |
| VCKI | 30-35 | 9.6E-04 | 6.0E-05 | 1.0E-03 | 2.5E-04 | 0.0023 |
| VCKI | 60-65 | 2.5E-04 | 1.3E-05 | 8.6E-04 | 1.9E-04 | 0.0013 |
| VCKI | 90-95 | 8.0E-04 | 3.3E-05 | 9.0E-04 | 1.5E-04 | 0.0019 |
| VCKI | 120-125 | 1.1E-04 | 4.1E-05 | 6.0E-04 | 3.3E-04 | 0.0011 |
| VCKI | 150-155 | 1.4E-05 | 1.3E-05 | 5.6E-04 | 4.3E-04 | 0.0010 |
| VCKI | 180-185 | 4.9E-05 | 1.9E-05 | 1.5E-03 | 2.9E-04 | 0.0018 |
| VCBC | 0-5 | 8.4E-04 | 5.2E-05 | 9.7E-04 | 3.1E-04 | 0.0022 |
| VCBC | 30-35 | 4.8E-04 | 5.1E-05 | 9.7E-04 | 6.1E-04 | 0.0021 |
| VCBC | 60-65 | 3.0E-04 | 5.6E-05 | 1.2E-03 | 4.0E-04 | 0.0020 |
| VCBC | 90.5-95.5 | 1.7E-04 | 1.6E-05 | 1.2E-03 | 4.9E-04 | 0.0018 |
| VCBC | 120-125 | 5.3E-04 | 2.0E-05 | 8.6E-04 | 4.6E-04 | 0.0019 |
| VCBC | 150-155 | 4.2E-04 | 7.8E-05 | 1.3E-03 | 3.6E-04 | 0.0021 |
| VCBC | 180-185 | 2.4E-04 | 4.5E-05 | 1.2E-03 | 4.2E-04 | 0.0019 |
| VCSG | 0-5 | 8.8E-04 | 4.8E-05 | 1.2E-03 | 1.6E-04 | 0.0023 |
| VCSG | 30-35 | 1.0E-04 | 2.8E-05 | 1.3E-03 | 4.5E-04 | 0.0019 |
| VCSG | 60-65 | 7.5E-05 | 2.8E-05 | 1.3E-03 | 4.5E-04 | 0.0018 |
| VCSG | 90-95 | 2.8E-05 | 3.4E-05 | 1.2E-03 | 4.9E-04 | 0.0017 |
| VCSG | 120-125 | 4.1E-05 | 3.1E-05 | 1.3E-03 | 3.6E-04 | 0.0017 |
| VCSG | 150-155 | 5.7E-06 | 7.4E-06 | 6.3E-04 | 7.8E-04 | 0.0014 |
| VCSG | 180-185 | 1.5E-04 | 2.2E-05 | 1.2E-03 | 5.4E-04 | 0.0019 |

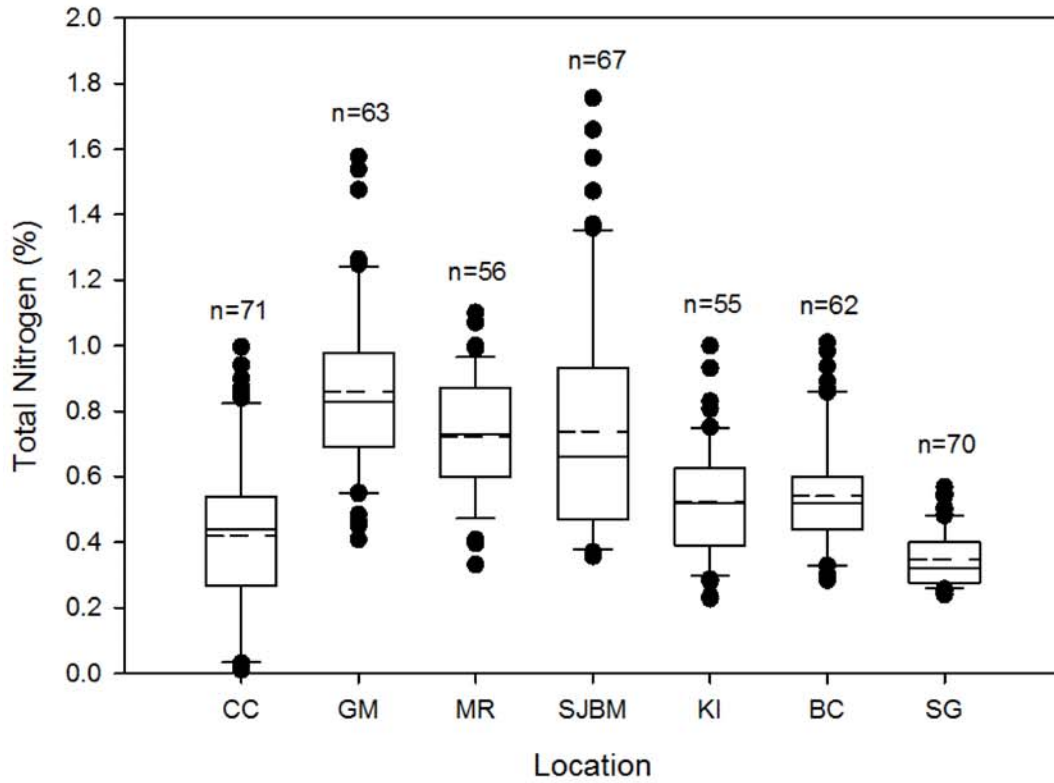


Figure B1: Total nitrogen concentrations for the short cores examined in this study. Solid and dashed lines are the median and mean of all samples, respectively. Black circles are outliers. The total number (n) of subsamples analyzed per core is noted.

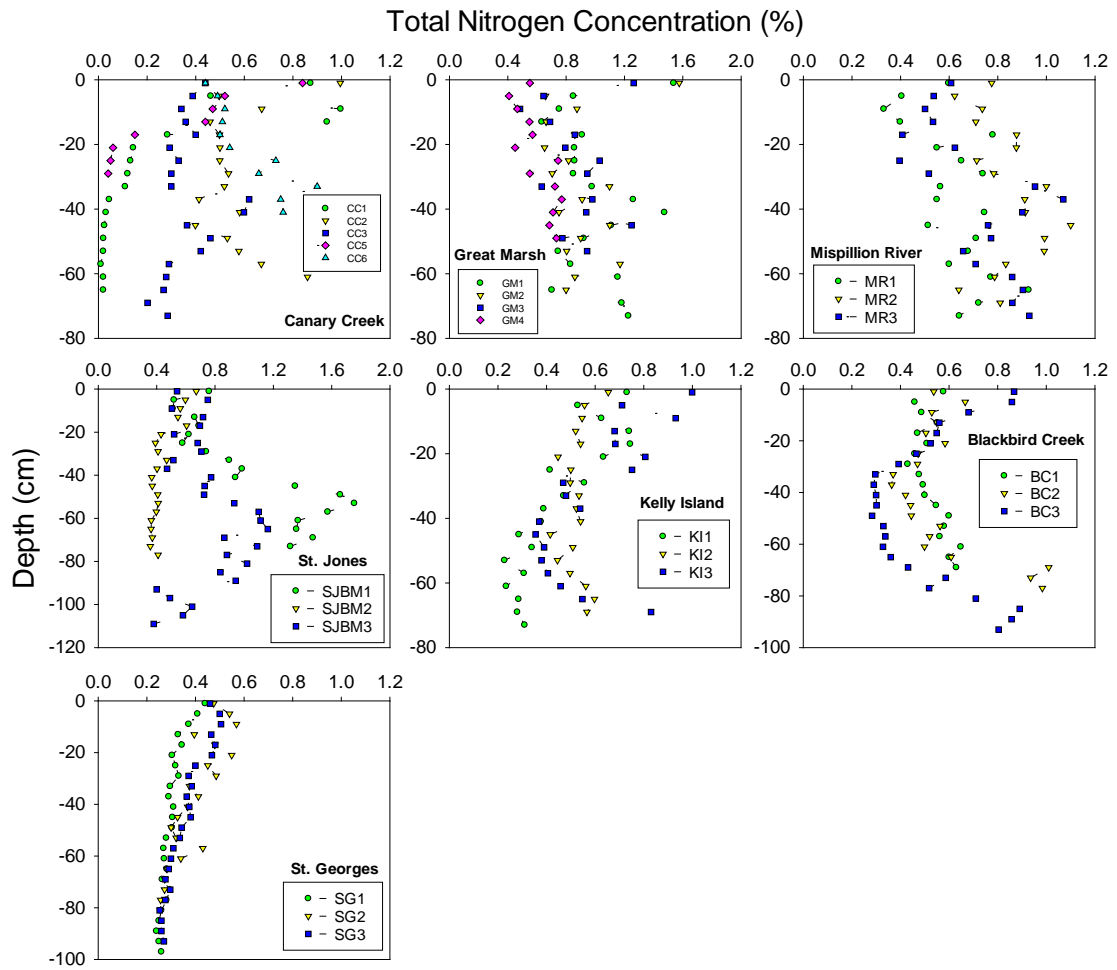


Figure B2: Depth profiles of total nitrogen concentration for the short cores examined in this study.

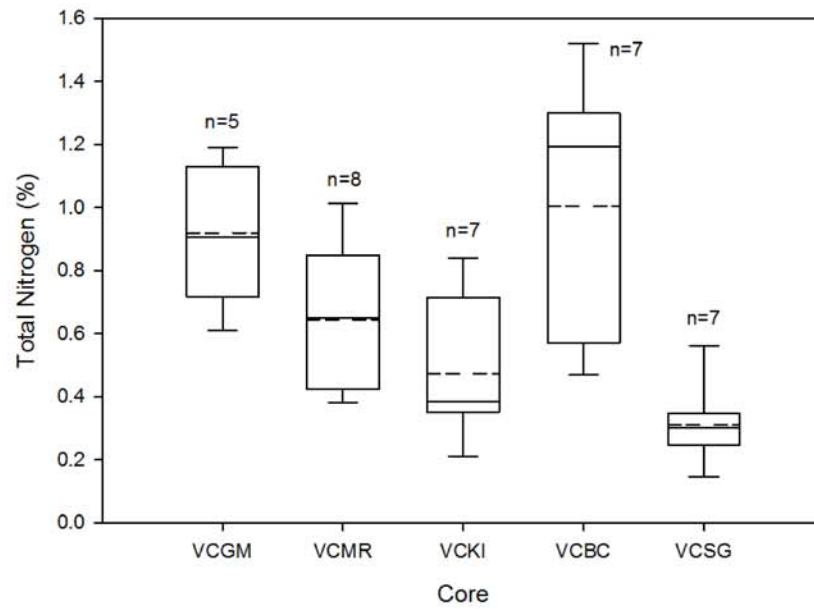


Figure B3: Total nitrogen concentrations for the long cores examined in this study. Solid and dashed lines are the median and mean of all samples, respectively. The total number (n) of subsamples analyzed per core is noted.

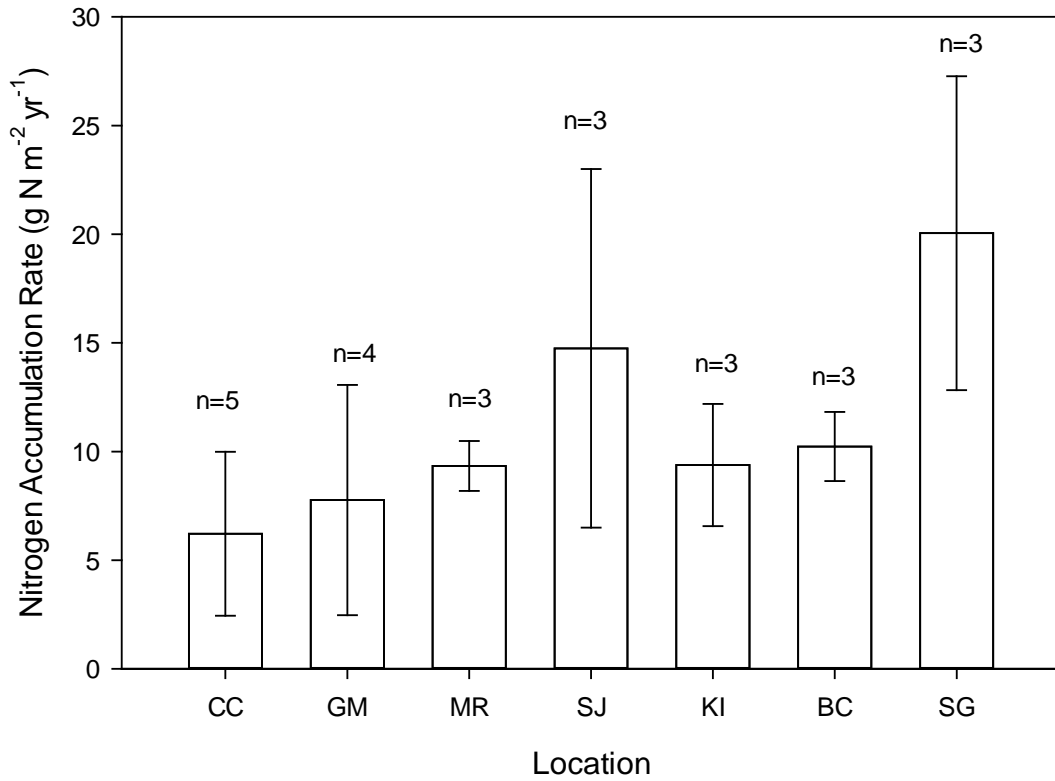


Figure B4: Nitrogen accumulation rates for the marsh sites based on ¹³⁷Cs and ²¹⁰Pb chronology. The mean and range of accumulation rates average for n coring sites are shown by the vertical bars and error bars, respectively.

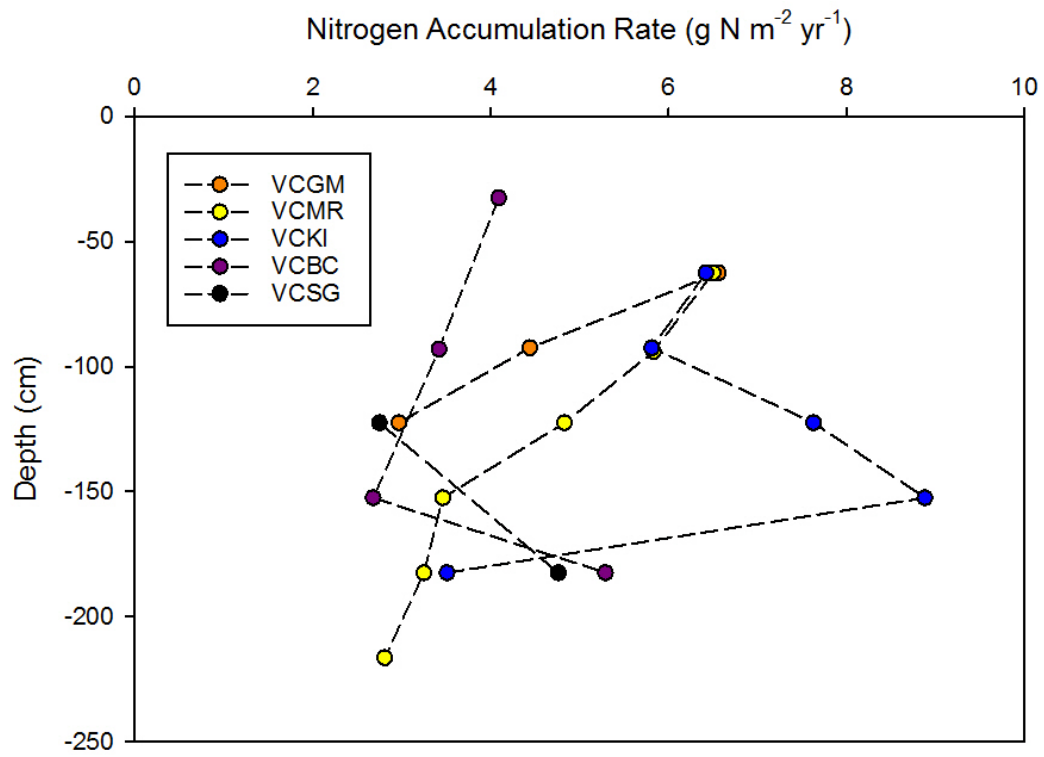


Figure B5: Depth profiles of nitrogen accumulation rates for the long cores examined in this study.

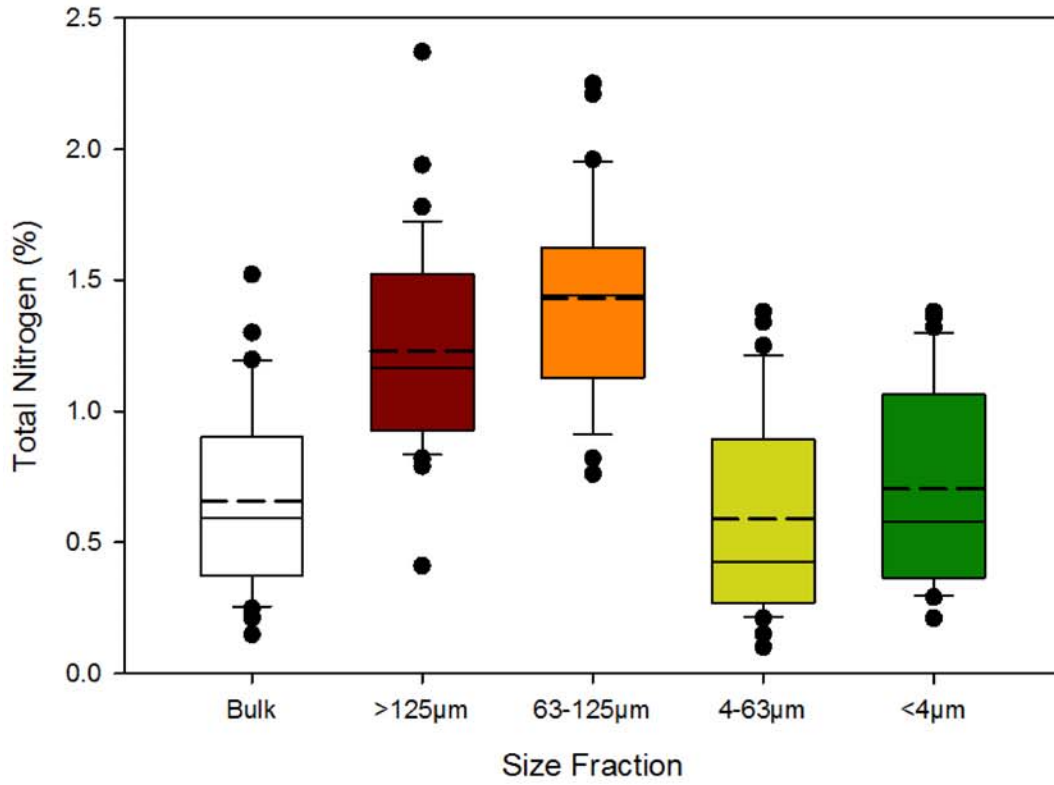


Figure B6: Box plot showing total nitrogen concentrations for bulk and size-fractionated soils from long cores examined in this study. Solid and dashed lines within the boxes are the median and means of n samples, respectively, and the closed circles are individual outliers.

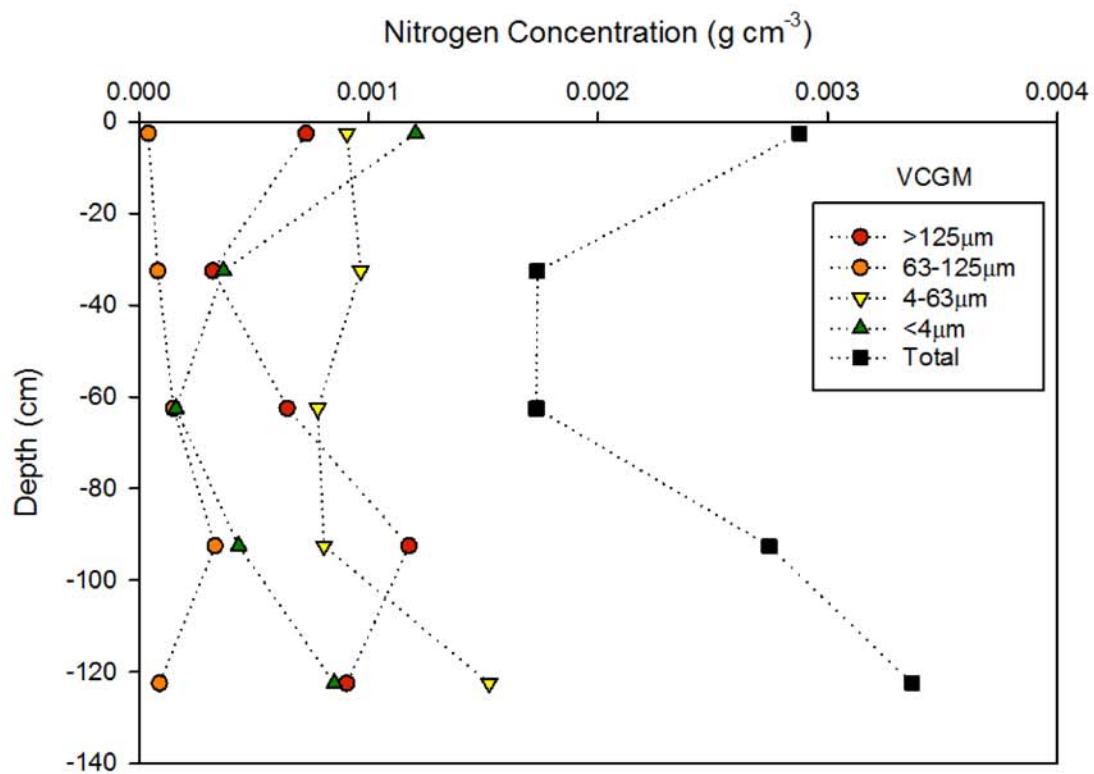


Figure B7: Down-core profiles for the Great Marsh vibracore showing variations in total nitrogen concentration and the nitrogen concentration of individual size fractions.

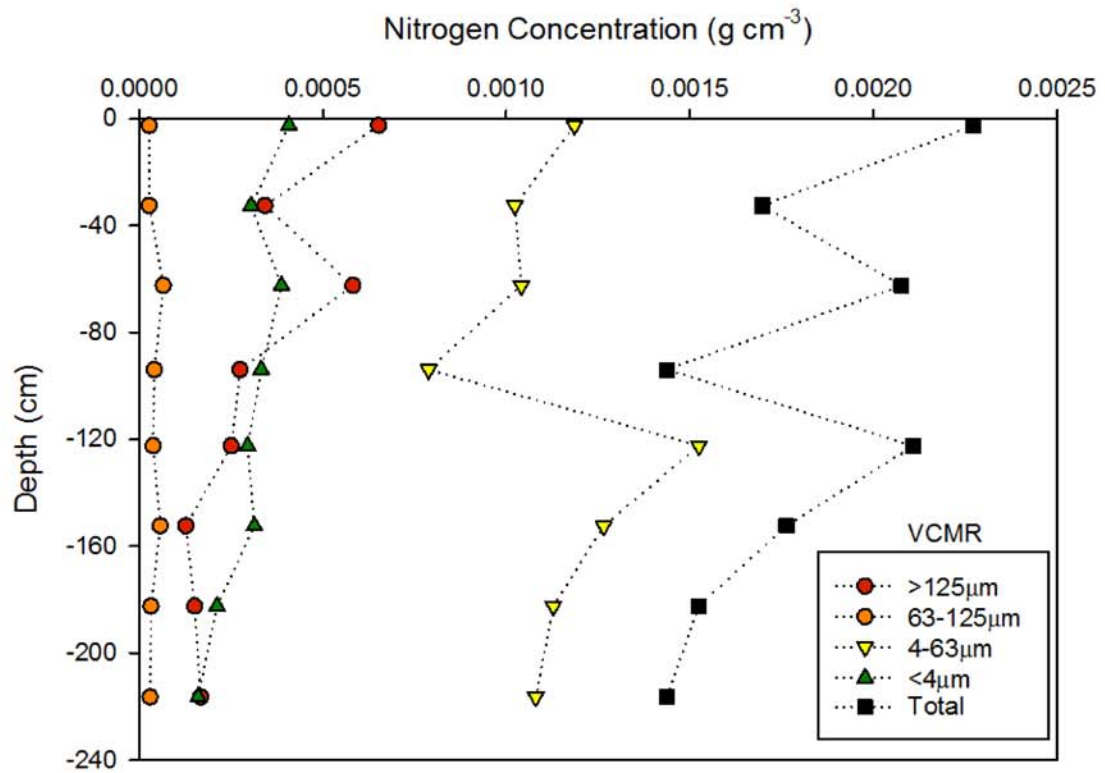


Figure B8: Down-core profiles for the Mispillion River vibracore showing variations in total nitrogen concentration and the nitrogen concentration of individual size fractions.

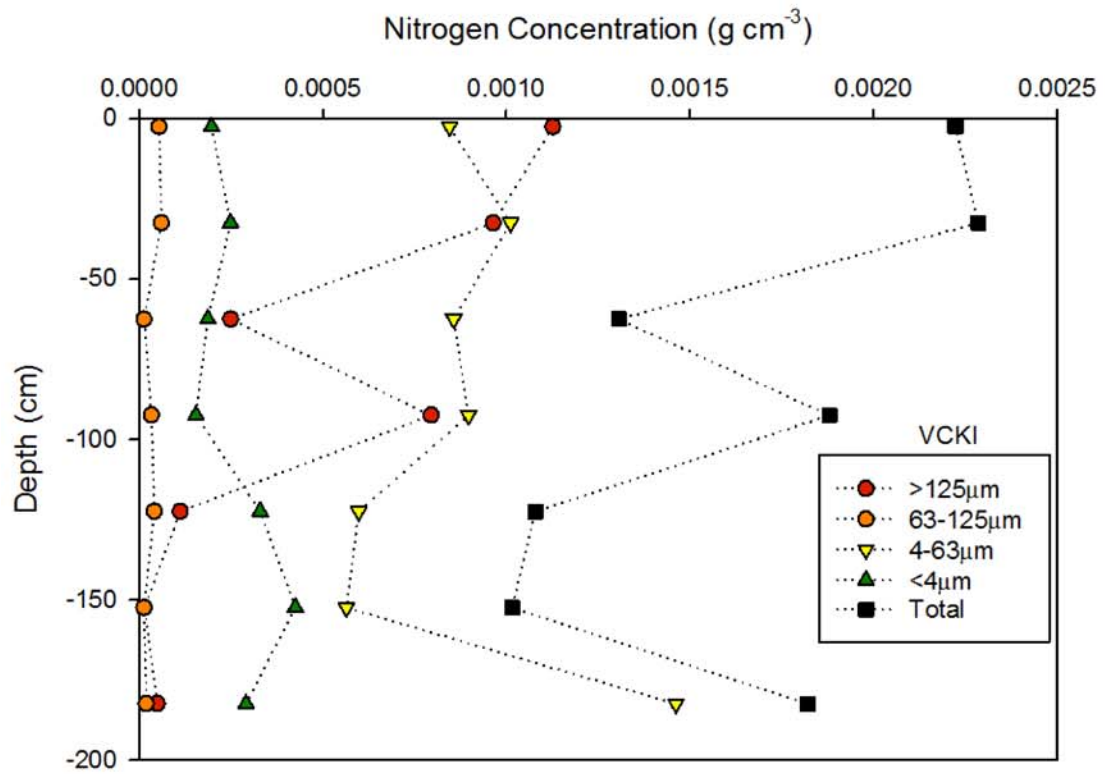


Figure B9: Down-core profiles for the Kelly Island vibracore showing variations in total nitrogen concentration and the nitrogen concentration of individual size fractions.

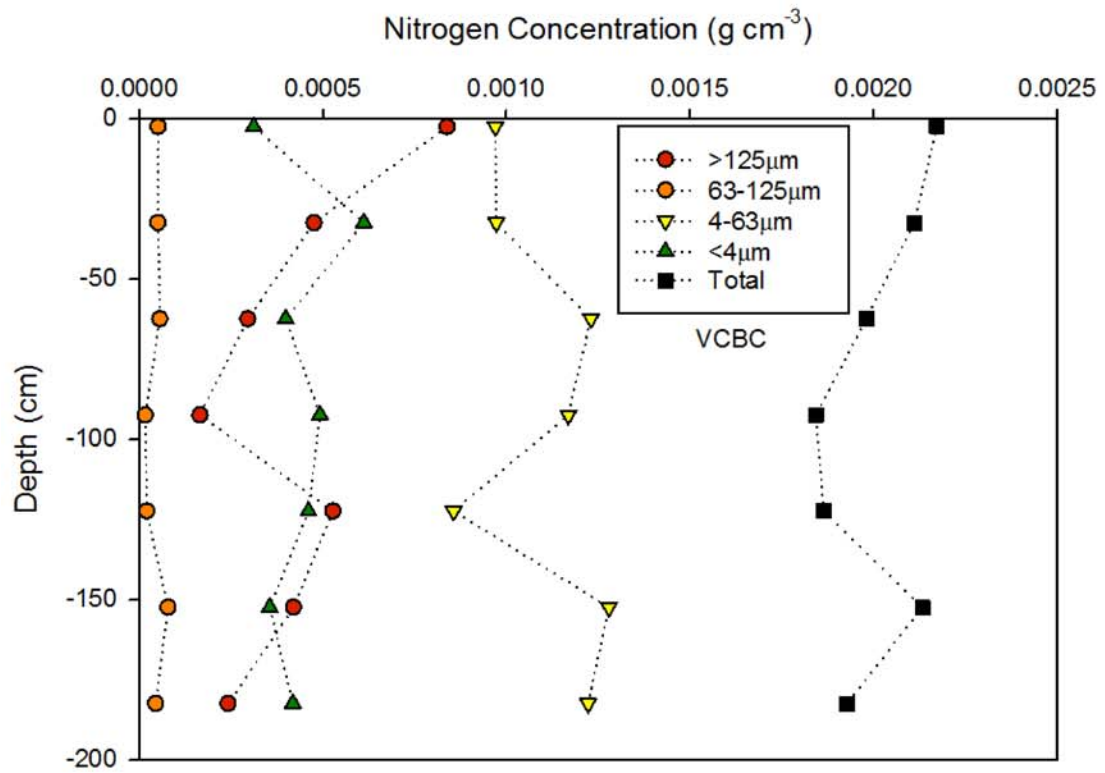


Figure B10: Down-core profiles for the Blackbird Creek vibracore showing variations in total nitrogen concentration and the nitrogen concentration of individual size fractions.

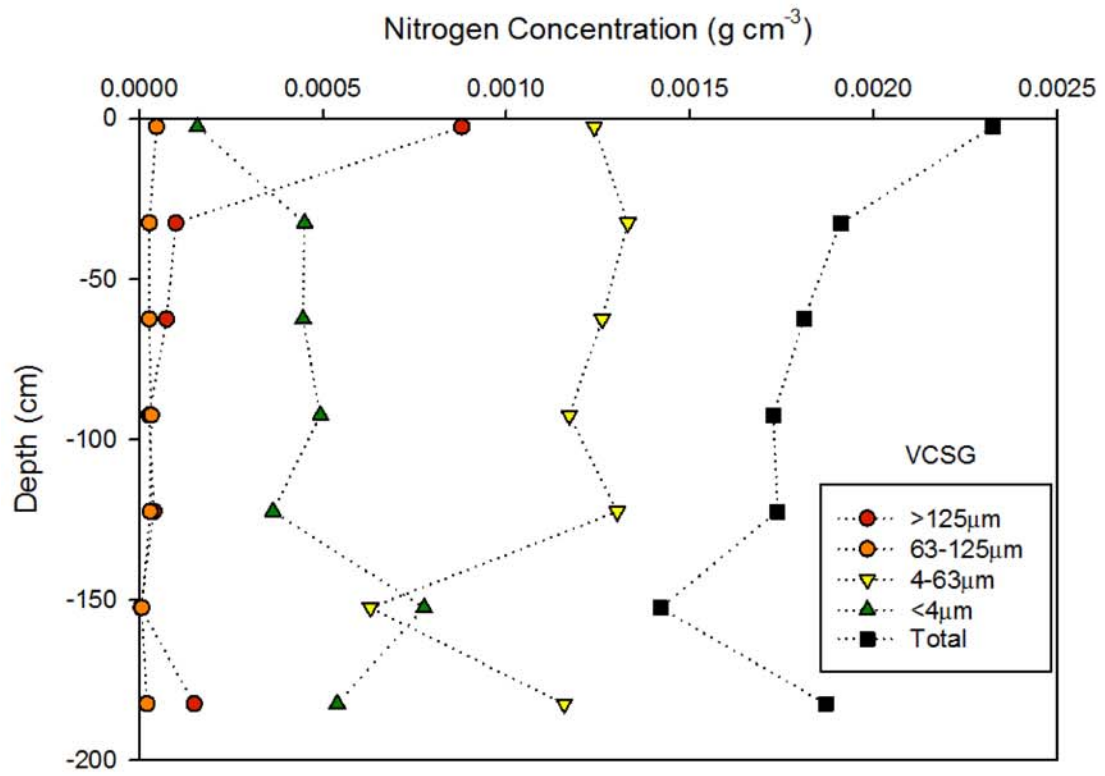


Figure B11: Down-core profiles for the St. Georges vibracore showing variations in total nitrogen concentration and the nitrogen concentration of individual size fractions.

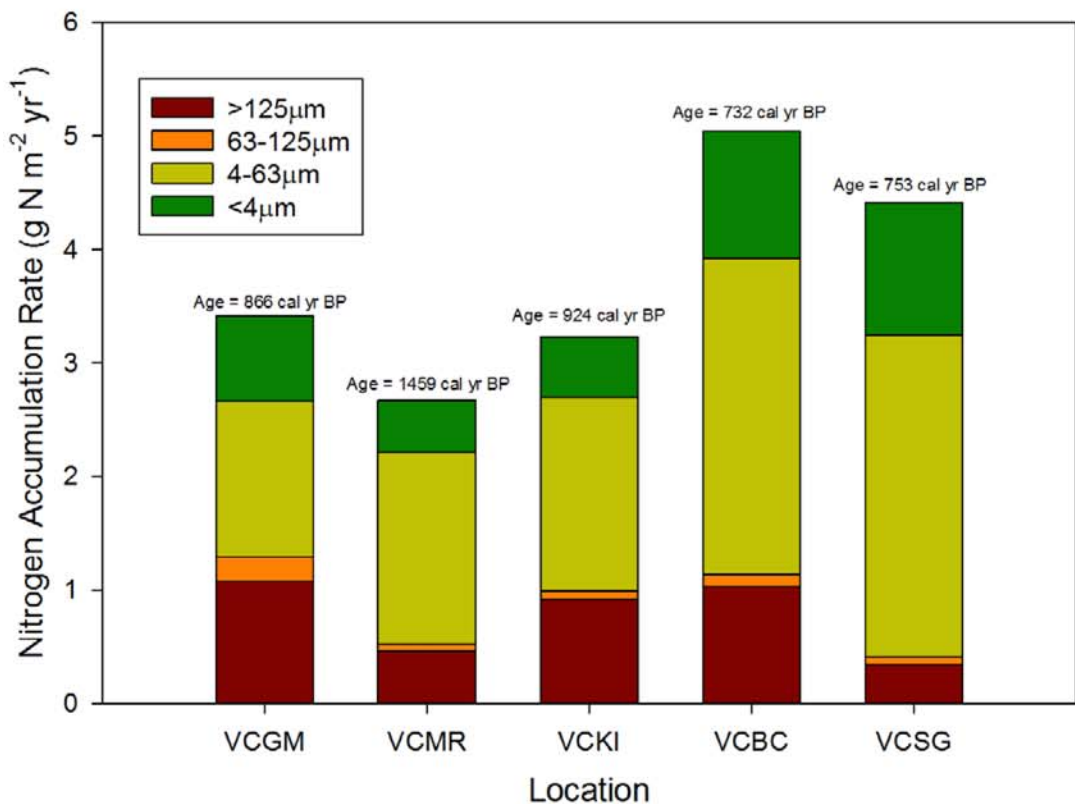


Figure B12: Stacked bar chart showing the relative contributions of the four soil size fractions to the long-term nitrogen accumulation rate determined for the five long cores. The timespan over which these rates were averaged is noted in calibrated yr B.P.

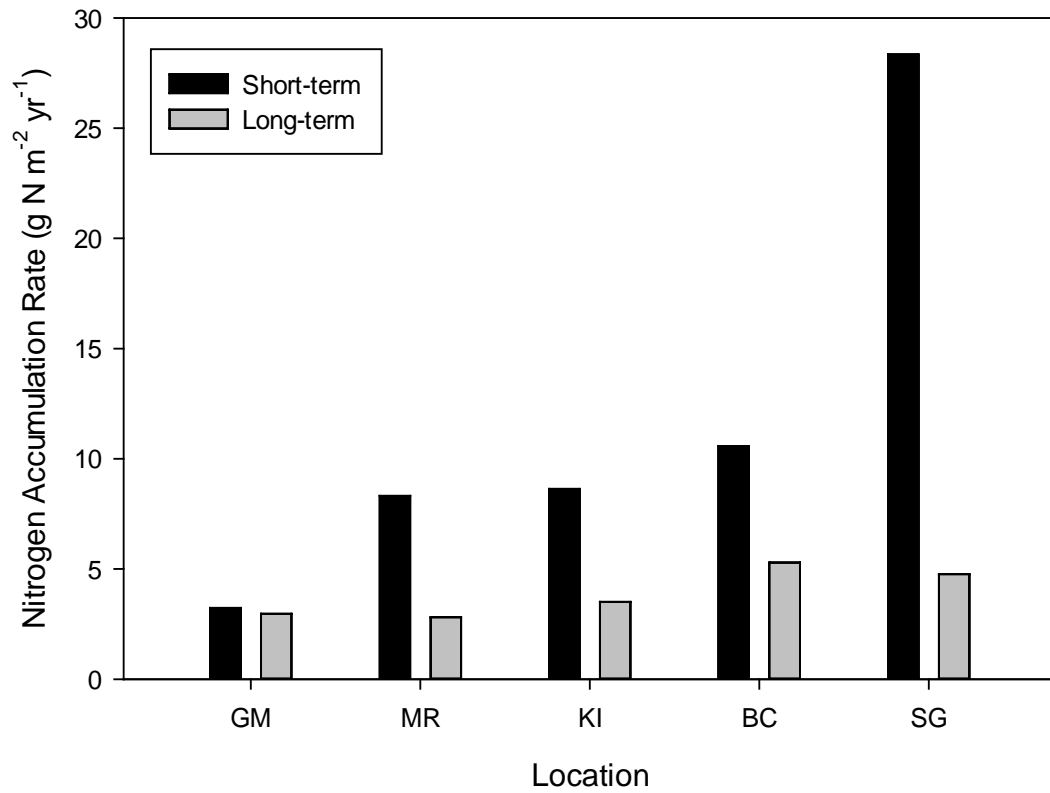


Figure B13: Comparison of short-term and long-term nitrogen accumulation rates. Black bars represent rates determined from ^{137}Cs or ^{210}Pb dating of the short cores; gray bars represent rates based on radiocarbon dating of the long cores.

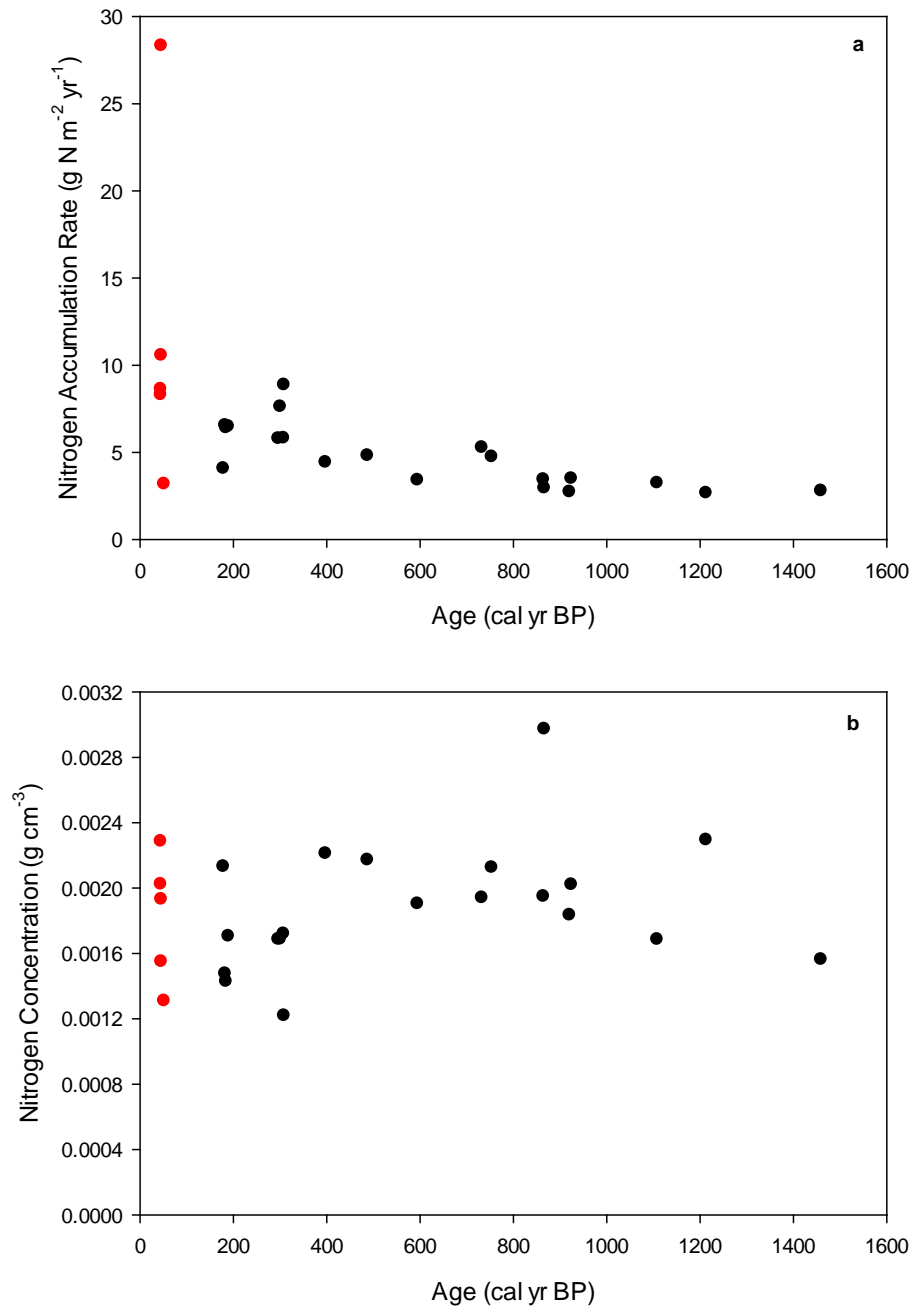


Figure B14: Scatter plots showing the dependence of a) nitrogen accumulation rate and b) nitrogen concentration on soil age (cal yr B.P.). Red and black circles denote rates for short cores and long cores collected at the same locations.